Spring 2019

Accuracy of 3D Point-Cloud and Photo-Based Models of City Street Intersections

Mariah D. Peart

ACCURACY OF 3D POINT-CLOUD AND PHOTO-BASED MODELS OF CITY STREET INTERSECTIONS

by

MARIAH PEART

(Under the Direction of Gustavo Maldonado)

ABSTRACT

From Georgia Southern University's Built Environment and Modeling lab, this study compares point positions and distance measurements completed with state-of-the-art instruments and equipment. A modern, 12-second, laser scanner, a modern unmanned aerial vehicle and a highly accurate, 1-second robotic total station were employed for this study. The latter serving as the benchmark instrument. The main objective of this quantitative comparison is to explore the accuracy and usability of a relatively large point-cloud model, as a virtual surveying tool for redesign/reconstruction purposes. This project involves the generation of large, 3D, point-cloud models of two busy and complex city street intersections. One intersection encompasses an approximate area of 300 ft × 750 ft and contains five converging elements: three streets and two railroads. It is an accident-prone location requiring redesign. The second street intersection encompasses an approximate area of 1,500 ft × 2,500 ft, containing two streets intersecting at an approximate 45-degree angle. The resulting computer model has been geo-referenced in the Georgia East State Plane Coordinate System (SPCS) using control points with coordinates established by GPS (Global Positioning System) via a rapid, network-based, Real-Time Kinematic (RTK) approach. These city street intersections are within the Blue-Mile corridor in Statesboro, GA. Along with the Statesboro City Engineers, the Blue-Mile corridor has plans to enhance and improve the traffic flow of the Blue-Mile corridor, which contains many businesses and restaurants. The final point-cloud models are to be donated to the city engineers to assist in the redesign of the intersections. A full analysis of the referred discrepancies is presented and recommendations on improving the overall current accuracies are provided.

INDEX WORDS: Remote sensing, Terrestrial LiDAR, 3D Laser scanning, Aerial photogrammetry, Close-range photogrammetry

ACCURACY OF 3D POINT-CLOUD AND PHOTO-BASED MODELS OF CITY STREET INTERSECTIONS

by

MARIAH PEART

A.S., College of Coastal Georgia, 2014

B.S., Georgia Southern University, 2017

A Thesis Submitted to the Graduate Faculty of Georgia Southern University

in Partial Fulfillment of the Requirements for the Degree

MASTER OF SCIENCE

STATESBORO, GEORGIA

ACCURACY OF 3D POINT-CLOUD AN PHOTO-BASED MOELS OF CITY STREET INTERSECTIONS

by

MARIAH PEART

Major Professor:	Gustavo Maldonado
Committee:	Marcel Maghiar
	Celine Manoosingh

Electronic Version Approved:
May 2019

DEDICATION

I would like to dedicate this thesis to my family and church family. Their prayers and encouragement have pushed me to strive for excellence in everything I do.

ACKNOWLEDGMENTS

I would like to thank the Allen E. Paulson College of Engineering and Computing for funding this research opportunity. I gratefully acknowledge all members of the Fall 2016 and Fall 2017 Senior Project Students, Spring 2019 Undergraduate Research Team along with Katarina Obermeyer, Daniel Laitano Trundle, Ananya Augustine, Tony Washington, Shawn Jackson, Drs. Maldonado, Maghiar and Martin for their hard work and contributions leading to the successful completion of this project. Also, I would like to express my sincere appreciation to Dr. Manoosingh for her advisement in the thesis research process.

TABLE OF CONTENTS

Page

LIST OF TABLES

Page

LIST OF FIGURES

Page

CHAPTER 1

INTRODUCTION

Purpose of the Study

The country's human population continues to rise as time proceeds. More areas are being developed to withstand the increasing number of residents, whether they are temporary or permanent. For example, Statesboro, GA is a smaller city that is known as a "College Town." It is the home of a large post-secondary school, Georgia Southern University. Many people come to Statesboro, GA for jobs and education. As the Fall and Spring semesters begin, the population to the city increases significantly. As an example, restaurants, grocery stores and other businesses experience high amounts of human traffic. Therefore, the city streets and roads experience heavy vehicular traffic flow in the high peak hours of the day.

City streets such as South Main Street and Fair Road are very popular to travel due to the restaurants, businesses, and especially the university campus. The city streets, mentioned previously, contain some of the busiest intersections. One city street intersection is a very complex intersection. It consists of at least three roads and two active cross-cut rail roads, as shown in Figure 1. This intersection does not contain any electronic traffic lights, only traditional stop signs. So, it is prone to many vehicular accidents. As told by a business owner, they see almost one vehicular accident per week. Another city street intersection is a very large intersection that consists of two streets with a combination of the university campus, private residence, restaurants and other businesses, as shown in Figure 2. This intersection is the first to be approached from the beginning of the Blue Mile Corridor. This corridor is one-mile-long which starts from the exit of Sweet Heart Circle and ends at Downtown Statesboro. This large intersection is the first focus for the Blue-Mile group. This group would like to improve and enhance the entire Blue-Mile corridor with the help of Statesboro's city engineers. Since both city street intersections are within the Blue-Mile corridor, the city engineers would like to redesign them for better traffic flow. Along with the desire for the Blue-Mile group to make the corridor aesthetically pleasing to the community, they would like to attract more people to visit the many businesses that Statesboro has to offer.

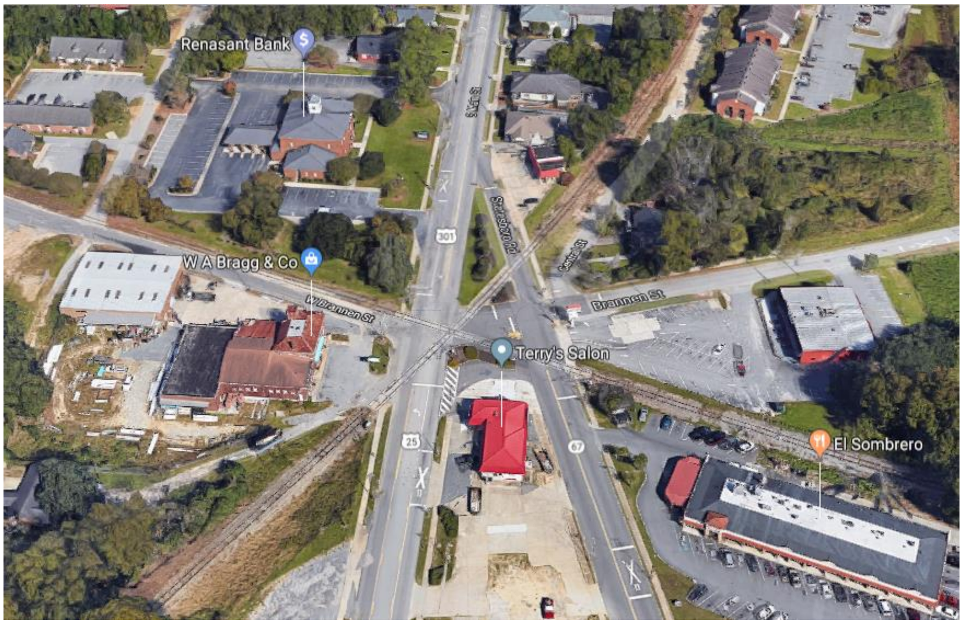

Figure 1: City Street Intersection 1 (South Main St., Fair Rd and Brannen St. with Two Cross-Cut Rail Roads)

Figure 2: City Street Intersection 2 (South Main St. and Tillman Rd)

As a graduate student, along with other teams of students from the Civil Engineering and Construction department, the Statesboro city engineers and the Blue-Mile group were approached with a presentation of the advanced technologies of 3D Laser Scanning and Close-Range Photogrammetry. With these technologies, the city engineers will be able to use a method called “Virtual Surveying or High-Definition Surveying” within 3D point-cloud and photo-based models. Virtual surveying is an advanced methodology of traditional surveying practices where it would not be necessary for an engineer or a registered land surveyor to return to the project site to obtain any additional distance measurements. This will help to keep travel expenses down in which the engineering firms or the city would be able to save costs. Yet, the traditional surveying instruments are more trustworthy to engineers and surveyors, since they are considered as “ground truth” to meet their accuracy standards. Since accuracy is very important to many engineering and surveying professionals of today’s industry, this study will investigate how close the 3D point-cloud and photo-based models are to the ground truth of real-world project sites. Also, the study will discover the discrepancy between 3D laser scanned point-cloud model and the 3D photo-based model and determine which technology would be recommended for the city engineers to use for their virtual surveying practices.

CHAPTER 2

TECHNOLOGY BACKGROUND

Remote Sensing Technologies in the Civil Engineering Industry

As time proceeds, technology continues to advance in our modern world of engineering. According to UrbanGeeks Staff, "The use of technology in Civil Engineering, which encompasses the planning, design and construction of urban environments and infrastructure projects, has been a game changer." Technologies such as laser-based and image-based scanners can be applied in various works in the Civil Engineering industry. These instruments are also known as Remote Sensing technologies. According to the United States Geological Survey agency, remote sensing is the process of detecting and monitoring the physical characteristics of an area by measuring its reflected and emitted radiation at a distance from the targeted area. This means the technology of remote sensing will allow any surface data from the earth to be collected by image-based and laser-based instruments.

There are two common types of these technologies which are called Aerial and Terrestrial. The aerial technology also known as air-borne technology collects data from a device that is mounted on an airplane or aerial vehicle. The terrestrial technology collects data from devices that are located on ground-level. Aerial Photogrammetry is an advance methodology that is commonly used by an airborne device, such as an unmanned aerial vehicle, which is commonly known as a drone. Photogrammetric image data can be collected at various ranges or distances. Image data from long-range distances can be collected by satellite devices or airplanes. Also, image data can be collected by unmanned aerial vehicles or terrestrial level devices at a closer distance. The latter is a methodology called Close-range Photogrammetry. It is a procedure of acquiring image data that is within 1,000 feet from a camera, hence the term "close-range" (2014). Laser scanning is another advance technology that has the capability of acquiring a wide range of scan data from an object's surface and shape with a non-contact, non-destructive laser beam (2019). This technology can be used as airborne or terrestrial LiDAR. With the airborne technology, a laser scanner can be mounted onto an airplane at various elevations. Inglot et. al. (2017) conducted a study to investigate a solution to effectively produce a 3D point cloud model with the use of Airborne Laser Scanning data by providing a reference point cloud model, merged with Terrestrial Laser Scanning and Low-Level Aerial Photogrammetry. Inglot et. al. (2017) suggest that merging the Terrestrial Laser Scanning and Photogrammetric point cloud models will complete any missing data points of the Airborne Laser Scanning point cloud model. This method will increase the accuracy of conducting measurements within the Airborne Laser Scanning model. Also, the authors suggest this method will be less time-consuming and more cost-efficient. The terrestrial technology is commonly used for the ground-level laser scanning method in various engineering applications.

Applications of Terrestrial Laser Scanning

Terrestrial Laser Scanning is one of the advanced technologies that is used for this study. In review of other recent research literature, it is a popular methodology for engineering applications. For example, Yu and Zhang (2017) conducted a research to determine an effective method to obtain precise spatial data from 3D laser scanning technology and traditional surveying instrument. Spatial data was acquired by the method of GPS coordinates obtained by an electronic total station, the method of GNSS surveying, photogrammetry and terrestrial 3D laser scanning. The authors analyzed the point position, side length and area of an urban building structure. All measures were obtained by spatial information given in the 3D model and the field surveying data. In conclusion, the authors suggest that the 3D model, obtained by the terrestrial laser scanning technology, was accurate enough for further engineering application. In another example, Reveiro et. al. (2013) conducted a research to validate the application of terrestrial laser scanning and photogrammetry techniques for bridge inspection procedures. These technologies were used to measure the vertical under clearance and the overall geometry of the bridge's prestressed concrete beam. The authors applied high accurate measurements with a total station as "ground truth" measurements. Since these measurements are reliable, they will be used as a base to validate the modern technologies. Applications such as the ones mentioned in the previous literature review are great examples with the use of advance technology in area of structural engineering.

Applications of Close-Range Photogrammetry

In review of other research literature from the recent years, the methodology of Close-Range Photogrammetry is another popular modern technology used in numerous applications. Structural engineering, historical documentation, topographical mapping are just a few examples to mention. Authors of various research made claims that close-range photogrammetry with aerial or terrestrial systems are less complicated to use, less-time consuming and more cost-efficient. Seibert and Teizer (2014) conducted a study to perform an evaluation of a UAV System that is built to rapidly and autonomously acquire mobile three-dimensional mapping data. The authors further explained details of the hardware and software used for 3D point-cloud modeling from the digital images, acquired. Different realistic construction environments such as a parking lot infrastructure, landfill, earthmoving during road construction, high-speed rail construction and spoil site projects were tested for an estimation of position error. An octocopter was used for the study and requires little maintenance with low operating and maintenance cost. Compared to another researcher's results of the parking lot environment case, the photogrammetric model produced an improvement of positional and height error**.** Gruszczyński et. al. (2017) conducted a study is to determine terrain relief, impacted by different height levels of vegetation, with the methods of UAV (unmanned aerial vehicle) photogrammetry and terrestrial laser scanning. From the point-cloud models, obtained from both methods, the researchers filtered the point clouds to achieve the land surface. This referenced land surface was used to determine the dense measurements (density points) by using traditional equipment such as a tacheometer and a rod-mounted reflector. The authors wanted to compare the accuracy levels, cost and effort of each method for dense land relief modeling. Kršák, B., et al. (2016) conducted a study on the usability of the UAV-based photogrammetry method in an application to documentation of geological terrain. The researchers used a modern unmanned aerial vehicle to acquire 135 aerial photos at an altitude of 35 meters. Then, a digital elevation model (DEM) was constructed with the Agisoft PhotoScan software.

With a sample size of 439 points and 10 ground control points, the authors conducted a comparison analysis using traditional surveying equipment to validate the accuracy of the point-cloud model to the actual terrain feature. Majid et al. (2017) compared UAV-based close-range photogrammetry, terrestrial-based close-range photogrammetry and terrestrial laser scanning. For this research, these technologies were used to acquire image and point-cloud data of ancient cave paintings. The researchers chose three historical caves in Malaysia to conduct this study. The ancient cave paintings were located 30 meters from the ground. The UAV system was flown to take pictures at a close distance, the digital camera was as a terrestrial technology to manually acquire photos and the terrestrial laser scanner provided point-cloud data with a non-destructive, non-contact laser beam. Also, the terrestrial laser scanner collected image data from a built-in high-resolution digital camera system. Conclusions were made that UAV-based close-range photogrammetry provided the best results in visualization of geometry and texture.

Applications of Traditional Surveying Techniques along with Modern Technology

Construction surveying, surveying engineering and geodetic surveying are common terminology to be defined as a method of measurement. In traditional surveying practices, there are different approaches to collect data. Data can vary from real-world distance and angle measurements to point position. Surveyors and engineers rely heavily on the traditional instruments such as total stations, levelers, global positioning system devices and more. Equipment such as these provide the professionals trustworthy data for various projects, such as land development, construction and maintenance inspections. Since advance technologies are being introduced in the engineering industry, the traditional technologies are used to validate the efficiency and trustworthy results for many projects. Compared to the traditional approaches, the modern methodologies can help professionals collect more data in less time (Kršák, B., et al. 2016). With results such as these, researchers suggest that the modern technologies are more-cost efficient than the traditional approaches (Siebert and Teizer, 2014; Dai et al., 2013).

In review of the other related literature, researchers have operated traditional surveying approaches to validate the potential use of the modern technologies, such as laser scanning and photogrammetry. Seibert and Teizer (2014) as previously mentioned, conducted a study to validate the photogrammetric methodology with the use of an unmanned aerial vehicle. A three-dimensional point-cloud model was generated with a corresponding software. Then, known point coordinates were obtain by a traditional total station to align the photogrammetric model in a known coordinate system. This method is known as “Indirect Geo-referencing.” The purpose of geo-refencing the model was to analyze and observer the error in position within the point-cloud model. Buffi et. al. (2017) conducted a research to validate the method of point-cloud modeling with UAV-based photogrammetry technique. Traditional topographic technologies such as the total station, global positioning system device, and terrestrial laser scanner were used to obtain "ground truth" data to validate the photogrammetry techniques. The application of these techniques were used on a structure, such as a dam. Maintenance and safety were needed for this type of structure. So the work presented, uses the photogrammetry and topographic techniques to obtain punctual, linear and surface analysis to validate the level of accuracy with use of unmanned aerial vehicles. Dai et. al. (2013) conducted a study is to compare the accuracy, quality, time efficiency and cost of modern technologies of photogrammetry, videogrammetry and time-of-flight (laser scanners). The authors believe that each application would demand a level of data accuracy and quality, but not enough information is researched in terms of cost. Also, these technologies were compared to "ground truth" point coordinates, obtained by a total station. Strach and Dronszczyk (2016) conducted a study is to verify and maintain the geometry of modern developed tram tracks in the urban transport systems. The authors use a combination of laser scanning and other surveying techniques such as a total station and GNSS satellites. These traditional surveying techniques allow the laser-scanned point cloud to orientate in any given coordinate system. The purpose of the point cloud is to provide spatial information of the transportation infrastructure, where inspections and measurement analysis can be conducted. Verifying the accuracy of the laser scanning technique needed to be verified by the reference measures of the traditional surveying instruments. The results based on the point cloud was reported as good but can be improved. The area of improvement is based on the workflow algorithms and the use of proper software. The authors used scanning targets for the laser scanning technique. These target points are hoped to be used as a reference for any surveying measurement in the transportation infrastructure. The authors also mention that coordinates' high accuracy can secure any kind of surveying task related to rail transportation. For another example, Kršák, B., et al. (2016) used traditional surveying total station to determine coordinates of sample points in the terrain feature with a polar methodology. The researchers used this approach to validate the accuracy of the point measurements within the digital elevation model process through UAV-base photogrammetry.

Standards of Accuracy

From the review of other related studies, researchers are comparing advanced three-dimensional point cloud models to real-world point positions. As time is proceeding, there are many professionals that would like to incorporate the modern approaches for better workflow. Yet, there is a constant need to validate these modern technologies through accuracy standards. Depending on the project, accuracy standards are set to determine the dependability of certain data, obtained through various approaches. Accurate data is crucial to the integrity of any project dealing with the design and construction of infrastructure or structural components. In a UAV-based photogrammetry study of point position accuracy, Kršák, B., et al. (2016) set a maximum coordinate error standard of 0.12 meters. Since this study is on city street intersection infrastructures for redesign and reconstruction, an accuracy standard was set to make a precise comparison of the modern technologies and traditional surveying practices.

CHAPTER 3

EMPLOYED INSTRUMENTS AND THEIR CAPABILITIES

Employed Instruments and Equipment

Various instruments and equipment were used for the completion of this project. For the modern laser scanning technology, the Leica C10 Scanner was operated to acquire all scan data. Along with the scanning equipment, a variety of targets were used as ground control points and constraints for the post-processing. These constraints include twin targets, six-inch black and white targets and six-inch sphere targets with supported posts and tripods. These are provided by Leica Geosystems, as well.

Figures 3-5: Employed Sphere Target, Twin Target and Black and White Target

For the modern close-range photogrammetry methodology, the DJI Mavic Pro Platinum Quadcopter unmanned aerial vehicle was operated to acquire all imagery data. For the traditional surveying approaches, the Leica TRCP 1201+ robotic total station was operated to acquire point coordinates along with a 360-degree prism reflector. Also, a survey-grade global position system device was employed to obtain the coordinates of ground control points for the purpose of aligning point-cloud models to the known Georgia East State Plane Coordinate System. The GPS device was operated by a specialist from the Georgia Southern Facilities, Services, Design & Construction Physical Plant.

Instrument Capabilities

The selected robotic total-station instrument (Figure 6) is capable of measuring with an angular accuracy of 1 second and with a reflectorless range of 1000 m. The standard deviation of its measuring errors (accuracies), for distances less than 500 m, is 2 mm + 2 ppm * distance. This accuracy decreases to 4 mm + 2 ppm * distance for distances larger than 500 m. This motorized instrument presents a robust centralized dual-axis compensator with setting accuracy of 0.5 seconds from zenith (Table 1). As it was the case in the selected scanner, this compensator enhances the capability of this instrument to substantially minimize angular errors caused by tilting of the vertical axis.

Figure 6: Leica TCRP 1201+ Robotic Total Station and 360-degree Prism Reflector

Table 1: One-Second Robotic Total Station Specifications (Adapted from Maldonado et al, 2015)

Item	**1-Second Robotic Total Station**
Principle Type:	Combined, Pulse and Phase-Shift Based
Range	**Reflectorless: 1000 m**. (Using one standard prism, under light haze with visibility of 20 km, Range = 3,000 m)
Accuracy of Single Measurement	**Distance, Reflectorless Mode**: Std. Dev. = ± [**2 mm** + **2 ppm** × (Dist. **< 500 m**)] Std. Dev. = ± [4 mm + 2 ppm × (Dist. **> 500 m**)]
	Distance, Reflector Mode: Std. Dev. = ± [1 mm + 1.5 ppm × (Dist. **< 3000 m**)]
Angular Accuracies (Standard Deviation)	Horizontal Angle = **1 sec**
	Vertical Angle = **1 sec**
Inclination Sensor	Centralized Dual-Axis Compensator, with **0.5-sec** accuracy.
Data collection Speed	Approximately, 1-3 points per minute

The Leica C10 Scanner (Figure 7) is employed for scan data acquisition on a supported tripod, at ground-level (terrestrial-level). Along with the scanner, sphere targets, black and white targets and twin targets are used in the field to later stitch the scan data into a single model. According to the manufacturer (Table 2), the employed laser-based scanner is characterized by its long range, 300 m at 90% albedo (134 m at 18% albedo), ultra-fine scanning capabilities and its survey-grade accuracy. It captures spatial XYZ coordinates at a maximum rate of 50,000 points per second. The instrument presents an ample field of view with a full 360° horizontal coverage and a vertical-angle range of 270°. The standard deviation of its measuring errors (accuracies), within a 50 m range, are ≤ 6 mm and ≤ 4 mm for positions and distances, respectively. Its horizontal and vertical angular resolution, at one standard deviation, is 60 μ rad (12 seconds). It presents dual axis compensators for precise automatic leveling of its vertical axis within 1-second resolution from zenith. This feature considerably reduces angular errors due to tilting of the vertical axis. This scanner also contains an integrated, auto-adjusting, high-resolution digital camera. For ready comparison, Table 2 presents a summary of the main characteristics of the laser scanning instrument employed in this study.

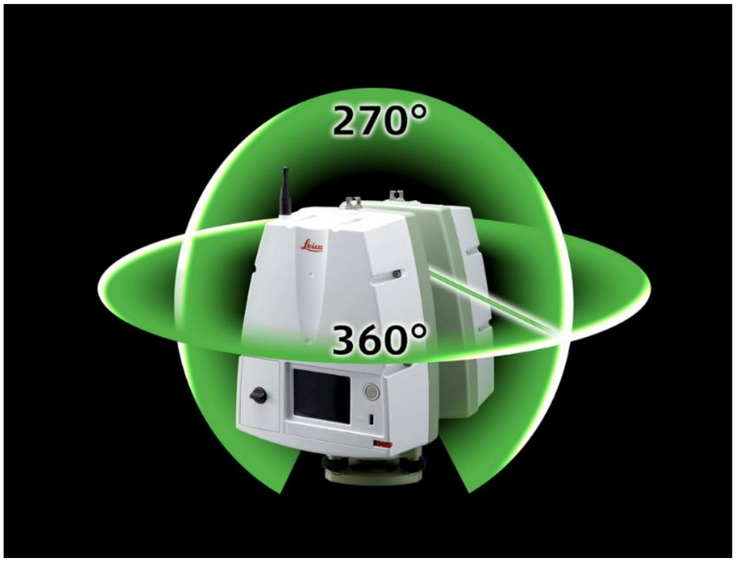

Figure 7: Leica C10 Scanner and Employed Operation

Table 2: Leica C10 Scanner Specifications (Adapted from Maldonado et al, 2015)

Item	**Laser-Based Scanning Instrument**
Type:	Pulse (time of flight)
Range	300 m @ 90%; 134 m @ 18% albedo (minimum range 0.1 m)
Accuracy of single measurement	Within 1-to-50-meter range: Position = 6 mm Distance = 4 mm (Both one sigma)
Angular Accuracies	Horizontal Angle = 12 sec Vertical Angle = 12 sec
Inclination Sensor	Dual-Axis Compensator, with 1.5-sec accuracy.
Scan rate	Up to 50,000 points/sec, maximum instantaneous rate
Dual-axis compensator	Selectable on/off, resolution 1”, dynamic range +/- 5’, accuracy 1.5”

The Mavic Pro Platinum Quadcopter (Figure 8) is an unmanned aerial vehicle that contains a built-in 12-megapixel camera to acquire image data of the second study area (city street intersection of South Main Street and Tillman Road). The camera has two vision systems (forward and downward). For case study 3, the downward vision system was employed. Also, this UAV has an obstacle sensory range for precision measurement and detectability. For precise measurements, the UAV should be flown in a range between 2 ft to 49 ft. The detectable range for image data is between 49 ft to 98 ft. For this case study, the quadcopter was flown within the detectable range. In Appendix A, Tables A.1-A.4 present a summary of the main characteristics of the UAV employed in this study.

Figure 8: Mavic Pro Platinum Quadcopter

Operated Software

Cyclone is Leica’s corresponding post-processing software employed to register (stitch) all scans into a final virtual 3D point cloud model. Agisoft PhotoScan is the software employed to reconstruct 3D photo-based point cloud, dense cloud and digital elevation models by stitching UAV image data that contains matching points. Microsoft Excel is a common data analysis software with many capabilities. This software was employed to calculate distance measurements, discrepancies of coordinates and distances, along with statistical output (Minimum, Maximum, Mean, Standard Deviation and Root-Mean-Square) for comparative results. Also, this software was employed to create the tables and graphs that are presented in the three case studies.

CHAPTER 4

CASE STUDY 1: ACCURACY OF NON-GEOREFERENCED, GEOREFERENCED AND VISUALLY ALIGNED 3D POINT CLOUDS

Objective of this Study

The objective of this study is to determine measurement and point location discrepancies of various registration approaches to construct a 3D point-cloud model. These models were obtained with a modern 3D laser scanning instrument for the redesign purposes of a multiplex city street intersection, located in Statesboro, Georgia. This study, also, investigates the accuracy of using a survey-grade GPS (Global Positioning System) device against the modern laser scanning instrument. Geo-referencing is the method of aligning a virtual point-cloud model to a real-world geographical coordinate system. When geo-referencing a 3D point cloud model, the GPS coordinates of the specified control points hold a responsibility to the level of accuracy in comparison to the "ground truth" of the real-world topography. These coordinates are obtained from a state plane coordinate system for true position values within the 3D point cloud model. GPS devices use an RTK (Real-Time Kinematic) approach which acquires multiple GPS satellites to measure the precision of a position. RTK methods are used for applications with the need of higher accuracies (Real-Time Kinematic (RTK)). The devices measure the radial distances from the satellite systems, user range error. Then, these devices calculated the accuracy of the position in comparison to the "ground truth" ("GPS Accuracy"). When applying this study to an actual infrastructure for city engineers, a standard of accuracy must be followed. For this case study, a measured error of 1 centimeter is considered as a standard of accuracy.

Methodology

For the study area, a set of seven control point locations were determined. These control points were mapped to cover all directions for the 3D point-cloud model (Figure 9). The purpose the control points is to align their positions to a known GPS system. The GPS coordinates were acquired with a traditional survey-grade GPS device by the Georgia Southern Facilities, Services, Design & Construction Physical Plant. The personnel followed a Real-time Kinematic approach to acquire each coordinate of the Georgia East State Plane Coordinate System. Approximately, 15 seconds was the time duration to acquire the GPS coordinate at each location.

Figure 9: GPS Coordinates of Selected Control Points (Provided by the Georgia Southern Physical Plant)

Along with setting control points, target point locations were determined, as well. The purpose of setting these target locations is to be sure the scanning instrument can acquire at least three targets per scan, recommended by the Leica Cyclone software. These targets will act as constraints to aid the software to register (stitch) each neighboring scan to produce the 3D point-cloud model. Targets such as the twin target, sphere targets and black & white targets were employed for this study.

Since the study was approximately 600 ft by 400 ft in size, 18 individual scans were completed to cover the entire spatial area. A set of instructions from a protocol (Appendix B) was followed. The duration of each scan was approximately 20 minutes. Each scan includes scan data acquisition with the non-destructive laser beam and image data acquisition from the built-in camera. Depending on light exposure of the scanned area, the duration of each scan can vary.

Then, all 18 scans were imported into Leica's Cyclone software. This software holds the capability to construct and analyze 3D point-cloud models by co-registering each scan in the same coordinate system. A set of instructions was followed to complete the post-processing (Appendix C). The method of target-to-target Registration was employed to construct the 3D point-model. Within the registration, a statistical report of each constraint (target) is provided. Each constraint (target) of every scan has a calculated error measurement. The software employs an algorithm to calculate the level of error in each scan. Since an accuracy standard was established for this technique, a set of targets from different scans were disabled within the registration. The remaining scan targets were enabled, which produced an overall error of 1 cm (0.033 ft). Once the registration is complete, the 3D point-cloud was produced with over 240 million points. Each of the scanned points attained their own XYZ coordinate, allowing the first scan station (location) to be referred as the origin. This is considered as a "non-georeferenced" point-cloud model.

Constraint ID	ScanWorld	ScanWorld	Type	Status	Weight	Error	Error Vector
T9	Station-005: S...	Station-008: S...	Coincident: Vertex - Vertex	Off	1.0000	0.012 m	(-0.002, 0.005, -0.011) m
T5	Station-004: S...	Station-011: S...	Coincident: Vertex - Vertex	Off	1.0000	0.012 m	(-0.001, -0.001, -0.012) m
T3	Station-001: S...	Station-005: S...	Coincident: Vertex - Vertex	Off	1.0000	0.012 m	(-0.002, -0.011, -0.002) m
T9	Station-011: S...	Station-012: S...	Coincident: Vertex - Vertex	Off	1.0000	0.012 m	(-0.002, 0.001, 0.011) m
T17	Station-003: S...	Station-006: S...	Coincident: Vertex - Vertex	Off	1.0000	0.012 m	(0.003, -0.011, -0.003) m
T9	Station-004: S...	Station-006: S...	Coincident: Vertex - Vertex	Off	1.0000	0.012 m	(-0.005, -0.007, 0.008) m
T9	Station-003: S...	Station-011: S...	Coincident: Vertex - Vertex	Off	1.0000	0.011 m	(0.000, 0.003, -0.011) m
T5	Station-003: S...	Station-018: S...	Coincident: Vertex - Vertex	Off	1.0000	0.011 m	(-0.003, 0.000, 0.011) m
T9	Station-001: S...	Station-011: S...	Coincident: Vertex - Vertex	Off	1.0000	0.011 m	(0.001, 0.002, -0.011) m
T11	Station-011: S...	Station-013: S...	Coincident: Vertex - Vertex	Off	1.0000	0.011 m	(0.004, -0.003, 0.010) m
T19	Station-013: S...	Station-014: S...	Coincident: Vertex - Vertex	On	1.0000	0.010 m	(0.002, 0.000, 0.010) m
T9	Station-006: S...	Station-008: S...	Coincident: Vertex - Vertex	On	1.0000	0.010 m	(0.002, 0.006, -0.008) m
T5	Station-003: S...	Station-012: S...	Coincident: Vertex - Vertex	On	1.0000	0.010 m	(0.007, -0.003, -0.007) m
T16	Station-003: S...	Station-018: S...	Coincident: Vertex - Vertex	On	1.0000	0.010 m	(0.000, 0.001, 0.010) m
T9	Station-005: S...	Station-015: S...	Coincident: Vertex - Vertex	On	1.0000	0.010 m	(-0.001, 0.006, -0.008) m

Figure 10: Sample of Statistical Report of Constraints for Non-georeferenced, Target-to-Target Registration

Since GPS coordinates were acquired at each control point, a set of procedures were followed to import them into the Leica software (Appendix D). With these GPS coordinates, the registration of the non-georeferenced point-cloud was aligned to fit the position of each control point in the known Georgia East SPCS. The Cyclone software employs an algorithm to adjust error between the control points and the non-georeferenced point-cloud. A statistical report for all seven constraints is presented in the registration (Figure 11). With no targets disabled, the overall error is displayed as 31 mm. Once, the registration is complete, a new point-cloud model is constructed (Figure 12). This is now called a "geo-referenced" point-cloud model.

Constraint ID	ScanWorld	ScanWorld	Type	Status	Weight	Error	Error Vector
T5	ScanWorld [R...	Control Points ...	Coincident: Vertex - Vertex	On	1.0000	0.031 m	(-0.020, 0.021, 0.010) m
T1	ScanWorld [R...	Control Points ...	Coincident: Vertex - Vertex	On	1.0000	0.022 m	(-0.011, -0.018, -0.007) m
T21	ScanWorld [R...	Control Points ...	Coincident: Vertex - Vertex	On	1.0000	0.019 m	(0.001, -0.014, -0.012) m
T9	ScanWorld [R...	Control Points ...	Coincident: Vertex - Vertex	On	1.0000	0.016 m	(0.013, 0.008, 0.004) m
T19	ScanWorld [R...	Control Points ...	Coincident: Vertex - Vertex	On	1.0000	0.014 m	(0.004, -0.012, -0.005) m
T11	ScanWorld [R...	Control Points ...	Coincident: Vertex - Vertex	On	1.0000	0.014 m	(0.010, 0.007, 0.005) m
T3	ScanWorld [R...	Control Points ...	Coincident: Vertex - Vertex	On	1.0000	0.010 m	(0.003, 0.008, 0.005) m

Figure 11: Statistical Report of Constraints for Geo-referenced, Target-to-Target Registration

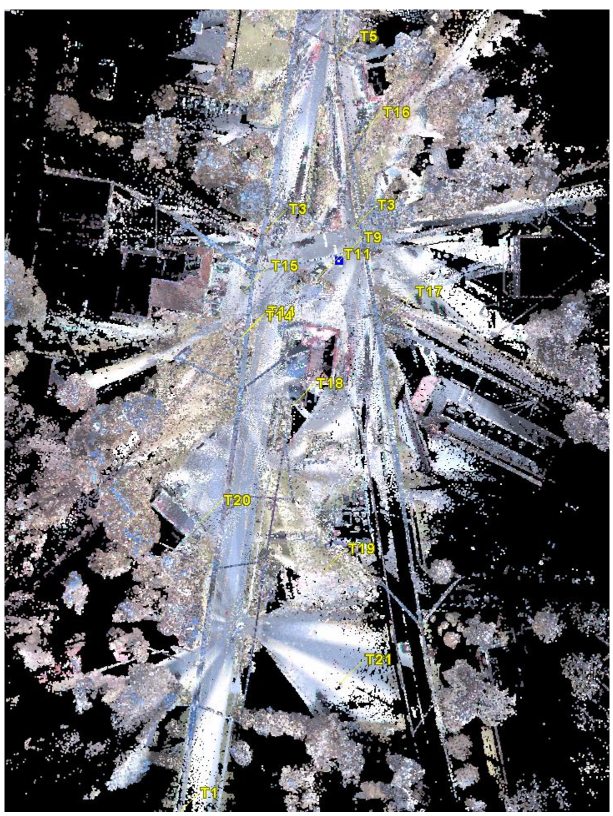

Figure 12 (a): Aerial View of City Street Intersection 1 Point Cloud Model

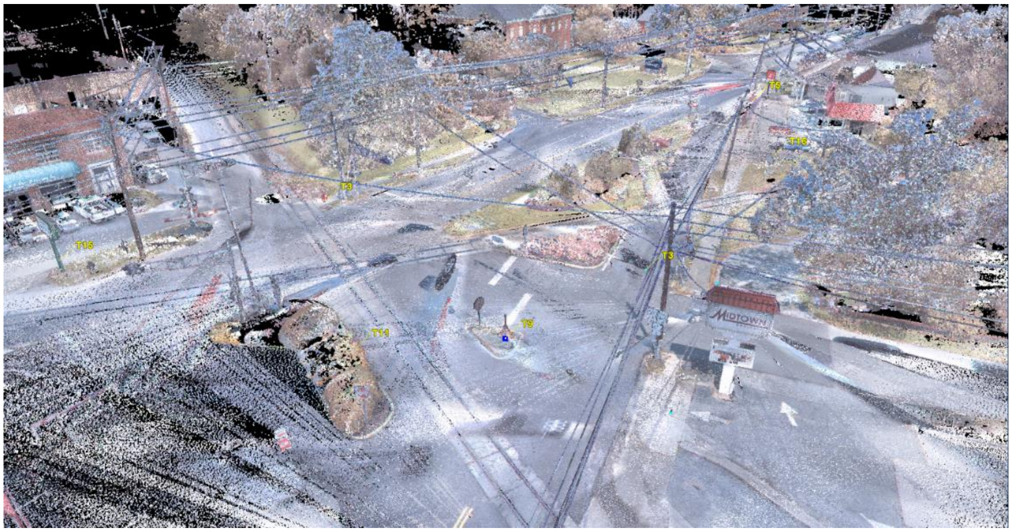

Figure 12 (b): Aerial View of City Street Intersection 1 Point Cloud Model

Compared to the target-to-target registration, a different method was employed called visual alignment. In the same Cyclone software, this type of registration is a procedure where two separate scans with similar geographical features are aligned horizontally in aerial view and vertically in side view (See Figures 13-14).

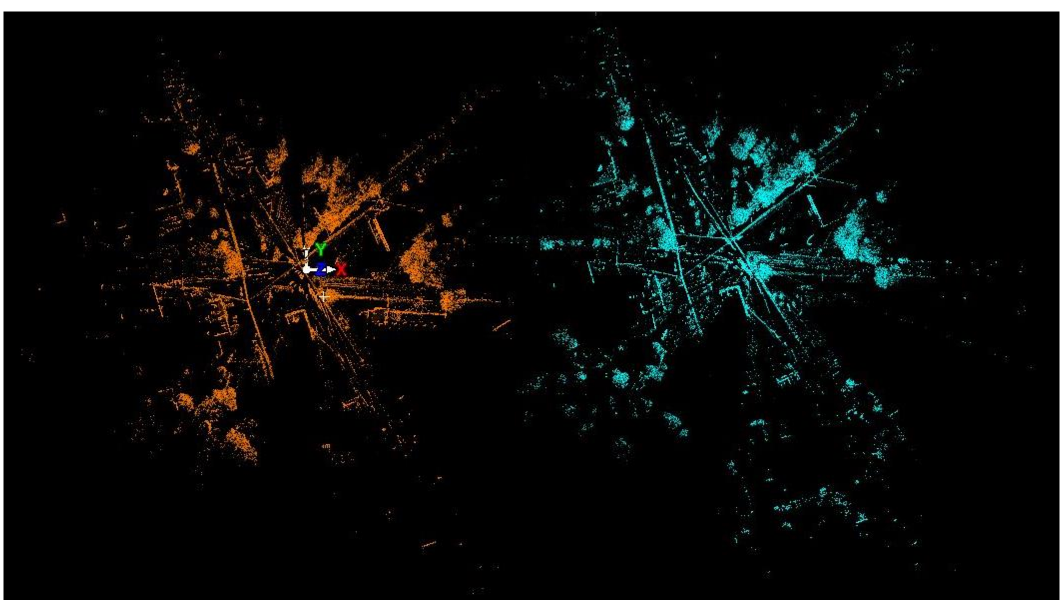

Figures 13 (a): Top View of Horizontal Visual Alignment Registration (Separate Scans)

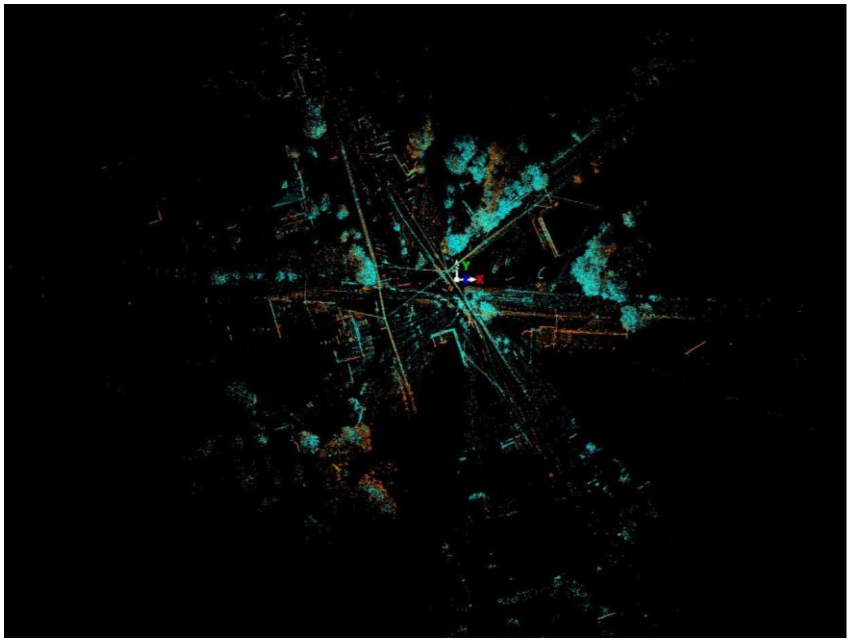

Figures 13 (b): Top View of Horizontal Visual Alignment Registration

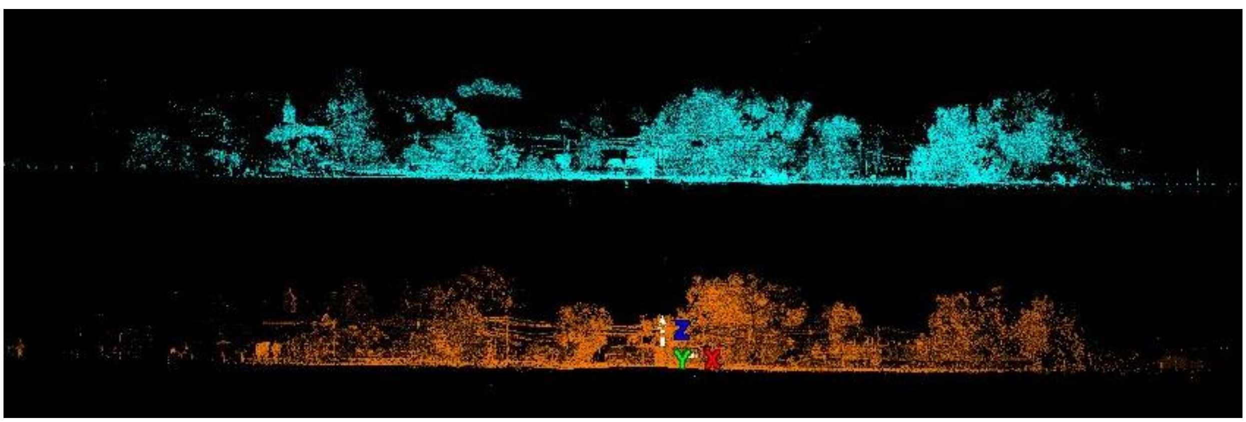

Figure 14 (a): Side View of Elevation Visual Alignment Registration (Separate Scans)

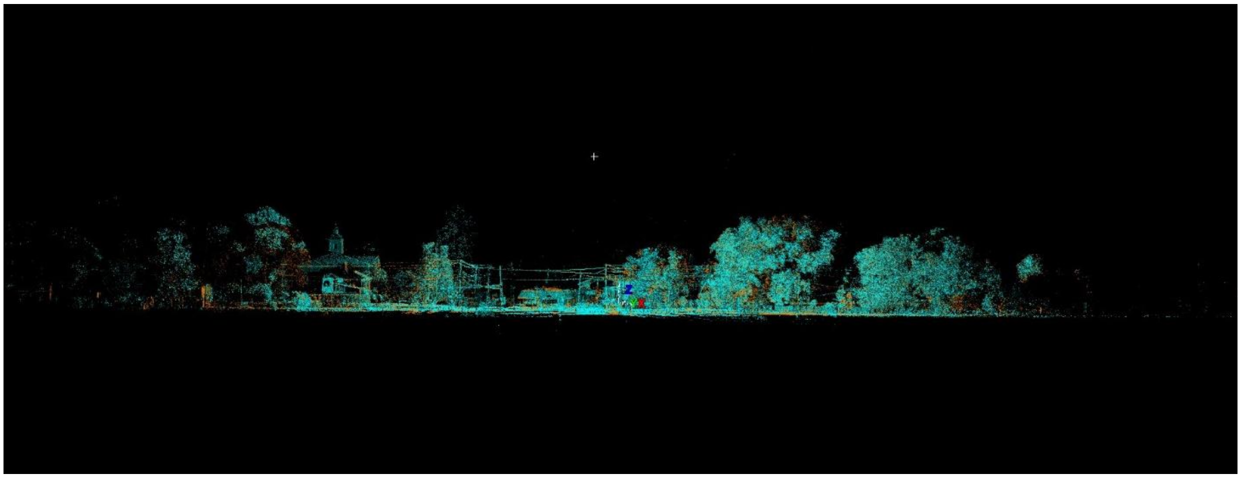

Figure 14 (b): Side View of Elevation Visual Alignment Registration

Once the visual alignment procedure is complete, the software runs an algorithm to calculate the number of aligned points and the measured error of those scans. The higher several scan points are aligned, the better outcome for the measured error between each scan. All 18 scans were employed to complete this registration method. Then, the software displays a statistical report of the measured error of each cloud constraint (Figure 15). The overall error was presented as 7 mm (0.02 ft or 0.28 inches). Once, the registration was complete, then the 3D point-cloud model was constructed. From observation, some target locations appeared as multiple positions due to the alignment error, as shown in Figure 8. Since these multiple errors are visible, the point-cloud model will not be aligned to a known geographical coordinate system. So, this model will remain as “non-georeferenced.”

ScanWorlds' Constraints | Constraint List | ModelSpaces

Constraint ID	ScanWorld	ScanWorld	Type	Status	Weight	Error	Error Vector	Group Error	Group Error Vector	Group
Cloud/Mes...	Station-006: S...	Station-017: S...	Cloud: Cloud/Mesh - Cloud...	On	1.0000	0.001 m	aligned [0.013 m]	0.001 m	aligned [0.013 m]	Group 1
Cloud/Mes...	Station-005: S...	Station-006: S...	Cloud: Cloud/Mesh - Cloud...	On	1.0000	0.001 m	aligned [0.011 m]	0.001 m	aligned [0.011 m]	Group 1
Cloud/Mes...	Station-002: S...	Station-018: S...	Cloud: Cloud/Mesh - Cloud...	On	1.0000	0.001 m	aligned [0.020 m]	0.001 m	aligned [0.020 m]	Group 1
Cloud/Mes...	Station-006: S...	Station-007: S...	Cloud: Cloud/Mesh - Cloud...	On	1.0000	0.001 m	aligned [0.015 m]	0.001 m	aligned [0.015 m]	Group 1
Cloud/Mes...	Station-003: S...	Station-004: S...	Cloud: Cloud/Mesh - Cloud...	On	1.0000	0.001 m	aligned [0.020 m]	0.001 m	aligned [0.020 m]	Group 1
Cloud/Mes...	Station-002: S...	Station-003: S...	Cloud: Cloud/Mesh - Cloud...	On	1.0000	0.001 m	aligned [0.016 m]	0.001 m	aligned [0.016 m]	Group 1
Cloud/Mes...	Station-001: S...	Station-010: S...	Cloud: Cloud/Mesh - Cloud...	On	1.0000	0.002 m	aligned [0.026 m]	0.002 m	aligned [0.026 m]	Group 1
Cloud/Mes...	Station-008: S...	Station-009: S...	Cloud: Cloud/Mesh - Cloud...	On	1.0000	0.002 m	aligned [0.019 m]	0.002 m	aligned [0.019 m]	Group 1
Cloud/Mes...	Station-002: S...	Station-012: S...	Cloud: Cloud/Mesh - Cloud...	On	1.0000	0.002 m	aligned [0.019 m]	0.002 m	aligned [0.019 m]	Group 1
Cloud/Mes...	Station-004: S...	Station-005: S...	Cloud: Cloud/Mesh - Cloud...	On	1.0000	0.003 m	aligned [0.016 m]	0.003 m	aligned [0.016 m]	Group 1
Cloud/Mes...	Station-007: S...	Station-015: S...	Cloud: Cloud/Mesh - Cloud...	On	1.0000	0.003 m	aligned [0.013 m]	0.003 m	aligned [0.013 m]	Group 1
Cloud/Mes...	Station-007: S...	Station-008: S...	Cloud: Cloud/Mesh - Cloud...	On	1.0000	0.004 m	aligned [0.022 m]	0.004 m	aligned [0.022 m]	Group 1
Cloud/Mes...	Station-013: S...	Station-014: S...	Cloud: Cloud/Mesh - Cloud...	On	1.0000	0.004 m	aligned [0.025 m]	0.004 m	aligned [0.025 m]	Group 1
Cloud/Mes...	Station-015: S...	Station-016: S...	Cloud: Cloud/Mesh - Cloud...	On	1.0000	0.004 m	aligned [0.020 m]	0.004 m	aligned [0.020 m]	Group 1
Cloud/Mes...	Station-009: S...	Station-013: S...	Cloud: Cloud/Mesh - Cloud...	On	1.0000	0.004 m	aligned [0.024 m]	0.004 m	aligned [0.024 m]	Group 1
Cloud/Mes...	Station-002: S...	Station-001: S...	Cloud: Cloud/Mesh - Cloud...	On	1.0000	0.005 m	aligned [0.029 m]	0.005 m	aligned [0.029 m]	Group 1
Cloud/Mes...	Station-001: S...	Station-011: S...	Cloud: Cloud/Mesh - Cloud...	On	1.0000	0.007 m	aligned [0.015 m]	0.007 m	aligned [0.015 m]	Group 1

Figure 15: Statistical Report of Constraints for Visual Alignment Registration

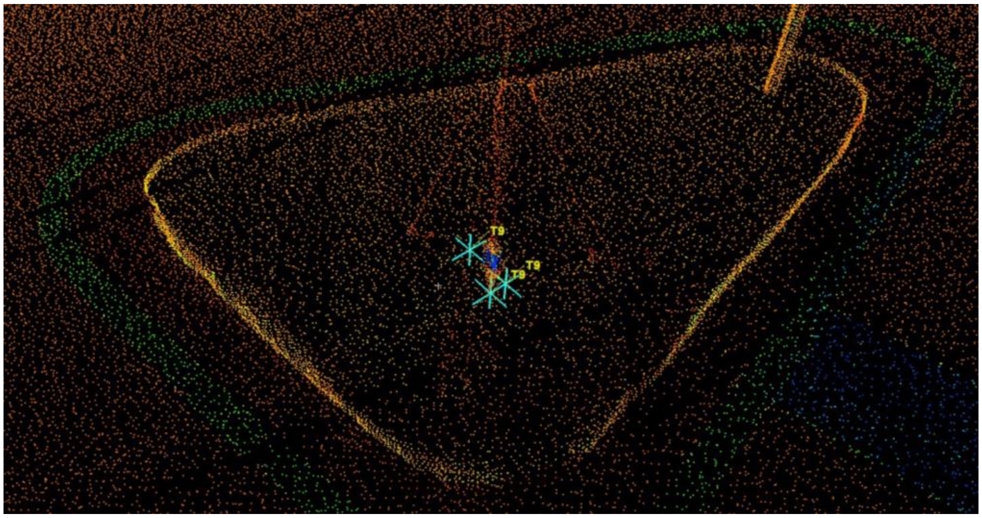

Figure 16: Multiple Targets of Control Point T9 in Visually Aligned Point-cloud Model

For each registration method, point-cloud models of more than 240 million points were produced. With this data, unnecessary points such as solar beams, passing vehicles and pedestrians were captured in the model. A set of procedures (Appendix C) was followed to remove the "traffic noise" from the model. Filtering these points will help further the data analysis process.

To conduct a proper accuracy analysis between registration methods, a set of 38 sample points were selected from the point-cloud model. These scan data points were chosen from each direction of the model. These points were strategically selected from vertices of stop signs, business signs, buildings, etc. The XYZ (Northing, Easting and Elevation) coordinates of each point were recorded and analyzed. Since each sample of all registration methods are of the same location, the discrepancy of each direction coordinate was analyzed. Then, each registration sample set of points were calculated to obtain distance measurement of different centers (T9, N1, N2, N3, S4 and S6).

CHAPTER 5

CASE STUDY 2: ACCURACY OF POINT-CLOUD MODEL VERSUS TRADITIONAL SURVEYING INSTRUMENT

Objective of this Study

The objective of this study is to validate the modern technology of terrestrial laser scanning in comparison to the traditional methodology of survey-grade instruments. The terrestrial laser scanning methodology was used to produce a 3D point-cloud model of the multiplex city street intersection that consists of at least three roads and two active, cross-cut railroads (same as Case Study 1, as seen in Figure 1). The traditional survey-grade instrument that will be employed is the accurate, one-second robotic total station. This total station will serve as a benchmark instrument. The city engineers would like to redesign the geometry of this intersection for better traffic flow, in the future. Along, with the use of an accurate robotic total station, serving as a "ground truth" against the virtual point-cloud, a discrepancy analysis of XYZ coordinates and distance measurements will be conducted to validate the terrestrial laser scanning technology.

Methodology

Like Case Study 1, a set of seven control point locations were determined throughout the study area. These control points were mapped to cover all directions for the 3D point-cloud model. The purpose the control points is to align their positions to a known GPS system. The GPS coordinates were acquired with a traditional survey-grade GPS device by the Georgia Southern Facilities, Services, Design & Construction Physical Plant. The personnel followed a rapid Real-time Kinematic approach to acquire each coordinate of the Georgia East State Plane Coordinate System. Approximately, 15 seconds was the time duration to acquire the GPS coordinate at each location.

Along with setting control points, target point locations were determined, as well. The purpose of setting these target locations is to assure the scanning instrument can acquire at least three targets per scan, recommended by the Leica Cyclone software. These targets will act as constraints to aid the software to register (stitch) each neighboring scan to produce the 3D point-cloud model. Targets such as the twin target, sphere targets and black & white targets were employed for this study.

Since the study was approximately 600 ft by 400 ft in size, 18 individual scans were completed to cover the entire spatial area. A set of instructions from a laser scanning protocol (Appendix B) was followed. The duration of each scan was approximately 20 minutes. Each scan includes scan data acquisition with the non-destructive laser beam and image data acquisition from the built-in camera. Depending on light exposure of the scanned area, the duration of each scan can vary.

All 18 scans were imported into Leica's Cyclone software. This software holds the capability to construct and analyze 3D point-cloud models by co-registering each scan in the same coordinate system. A set of instructions was followed to complete the post-processing (Appendix C). The method of target-to-target registration was employed to construct the 3D point-cloud model. Within the registration, a constraint list is provided (Figure 10). Each constraint (target) of every scan has a calculated error measurement. The software employs an algorithm to calculate the level of error of each scan. Since an accuracy standard of one centimeter was set for this technique, a set of targets from different scans were disabled. The remaining scan targets were enabled, which produced an overall error of 1 cm.

Since GPS coordinates were acquired at each ground control point, a set of procedures were followed to import them into the Leica software (Appendix D). With these GPS coordinates, the registration of the non-georeferenced point-cloud was aligned to fit the position of each control point. The Cyclone software employs an algorithm to adjust error between the control points and the non-georeferenced point-cloud. The software provided a statistical constraint list report (as shown in Figure 11), and the overall error displayed as 31 mm. Once, the registration is complete, a new georeferenced point-cloud model is constructed (Figure 17).

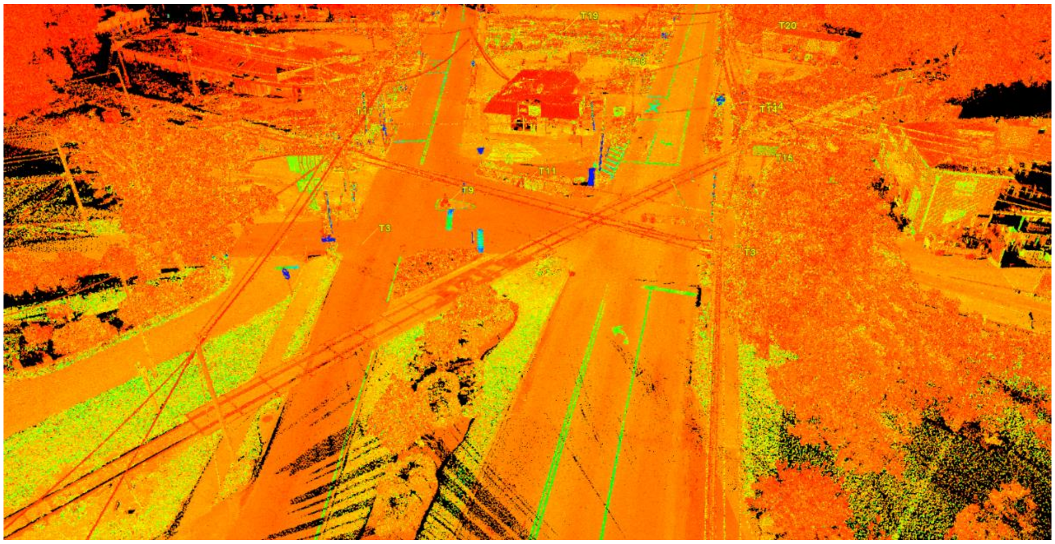

Figure 17: High Intensity Aerial View of City Street Intersection 1 Point-Cloud Model

For each registration method, point-cloud models of more than 240 million points were produced. With this data, unnecessary points such as solar beams, passing vehicles and pedestrians were captured in the model. A set of procedures (Appendix C) was followed to remove the "traffic noise" from the model. Filtering these points will help the furthering of the data analysis process.

To conduct an appropriate discrepancy analysis of point locations and distance measurements, a set of 38 sample points were selected from the point-cloud model. All points were purposely selected from a target located in the center of the city street intersection, target T9. The scan data points were chosen from each direction of the central target within the model. These points were strategically selected from vertices of stop signs, business signs, buildings, etc. Since target T9 (one of the control points) was centrally located, the accurate benchmark instrument, robotic total station, was positioned at that target location in the field-site. A set of procedures were followed from the protocol in Appendix E. Then, all 38 point coordinates were selected based on the point-cloud coordinate of target T9, since it was observed to be exact compared to the GPS coordinate of the same location. In the analysis, the discrepancy of each northing, easting and elevation coordinate was calculated. Then, the distance measurements of each sample point were calculated from target T9, along with five additional centers, by using the following distance formula for 3D spaces.

Distance Formula:

$$Distance = \sqrt{(\Delta Northing)^2 + (\Delta Easting)^2 + (\Delta Elevation)^2}$$

CHAPTER 6

CASE STUDY 3: ACCURACY OF POINT-CLOUD AND PHOTO BASED MODELS VERSUS TRADITIONAL SURVEYING INSTRUMENT

Objective of this Study

Statesboro, Georgia has a complex intersection at South Main Street and Tillman Road. The intersection has a total of two roads intersecting at an approximate 45° angle (Figure 2). It frequently experiences high volumes of traffic and is a part of the Blue-Mile Corridor. The Blue Mile group plans to participate with the redesign and improvement of this one-mile corridor along South Main Street. The objective of this study is to explore the usability of the advanced technologies of aerial close-range photogrammetry and terrestrial 3D laser scanning. To validate the accuracy of these technologies, an accurate traditional surveying instrument will be employed as a "ground truth" benchmark. From the results, the 3D virtual world model, containing more accurate data, will be donated to the Blue-Mile group and to the City of Statesboro, for the future redesign of this corridor.

Methodology

Control points were established in the field. Similar to Case Study 1 and Case Study 2, these control points were set in each direction of the study area (Figure 18). The eight control point locations were chosen to be employed for future geo-referencing. Along with the control points, five additional target locations were established to be constraints for each neighboring scan. All targets at each constraint location, were six-inch sphere targets. These sphere targets allow the operator to properly acquire them with the 3D scanner. Compared to the other Leica targets, these sphere targets give a benefit for the workflow to be less time-consuming in the scanning procedure.

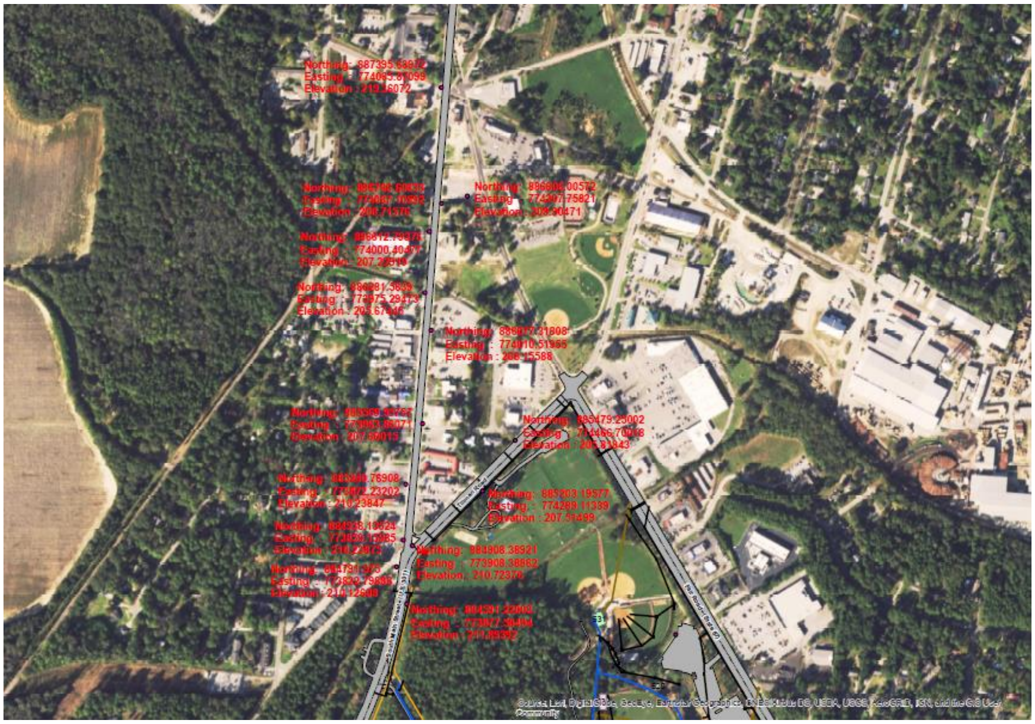

Figure 18: GPS Coordinates of each Ground Control Point for City Street Intersection 2 (Provided by Georgia Southern Physical Plant)

The scanner was stationed at a location, chosen by the personnel, where it acquires at least three targets (recommended by Leica Cyclone software), in a clear line of site. Each scan will have a reference about the XYZ axes, when there are enough constraints for the registration process. The 3D scanner sends out a non-destructive laser beam covering 270 degrees of vertical space and 360 degrees of horizontal space (Figure 7). Then, the scanner was moved to different locations until data collection was completed, covering the entire area of interest. For every scan station (location), the scanner spent a duration of approximately 6 minutes to collect scan data and approximately 6-8 minutes to collect imagery data for the red-green-blue color acquisition for the model visualization. Duration of each scan varies due to light exposure. So, the more exposure the scanner has the less time it takes to acquire the point and image data.

A total of 47 scans were completed in the field and imported in the corresponding Leica Cyclone software. The software provided a statistical report of calculated errors for every target in each scan (Figure 19). Following the same tolerance of error or accuracy standard in Case Study 1 and Case Study 2, all targets with an error measurement of more than one centimeter (0.033 ft) were disabled from the list of constraints within the registration. This procedure allowed the overall accuracy of the registration to be one centimeter maximum. Once the registration was completed, approximately 350 million points were generated for the entire construction of the non-georeferenced point-cloud model (Figure 20).

At each control point, GPS coordinates were obtained within the Georgia East State Plane Coordinate System. These known geographical coordinates were employed to georeferenced the point cloud model. GPS coordinates were acquired by the Physical Plant Facility at Georgia Southern University. The personnel employed a GPS receiver to attain the coordinates through a rapid Real-time Kinematic approach, like cases 1 and 2. Each coordinate was acquired in a duration of approximately 15 seconds. Following a set of procedures in Leica Cyclone (Appendix D), all eight GPS coordinates were imported, and the previously constructed point-cloud model was georeferenced to the known Georgia East State Plane Coordinate System. In the laser-scanned point-cloud, a sample of georeferenced points were selected to obtain their coordinates directly from the finalized 3D model.

ScanWorlds' Constraints | Constraint List | ModelSpaces

Constraint ID	ScanWorld	ScanWorld	Type	Status	Weight	Error	Error Vector
GL7	GNAT GPS C...	ScanWorld [R...	Coincident: Vertex - Vertex	Off	1.0000	0.057 m	(0.014, 0.029, 0.047) m
GL8	GNAT GPS C...	ScanWorld [R...	Coincident: Vertex - Vertex	On	1.0000	0.026 m	(0.005, -0.008, 0.024) m
GL9	GNAT GPS C...	ScanWorld [R...	Coincident: Vertex - Vertex	On	1.0000	0.024 m	(-0.002, 0.022, -0.008) m
GL10	GNAT GPS C...	ScanWorld [R...	Coincident: Vertex - Vertex	Off	1.0000	0.032 m	(0.010, 0.030, 0.006) m
T1	GNAT GPS C...	ScanWorld [R...	Coincident: Vertex - Vertex	On	1.0000	0.021 m	(0.008, 0.010, -0.016) m
GL4	GNAT GPS C...	ScanWorld [R...	Coincident: Vertex - Vertex	Off	1.0000	0.037 m	(-0.002, -0.008, -0.036) m
GL1	GNAT GPS C...	ScanWorld [R...	Coincident: Vertex - Vertex	On	1.0000	0.020 m	(0.005, -0.018, -0.005) m
GL2	GNAT GPS C...	ScanWorld [R...	Coincident: Vertex - Vertex	On	1.0000	0.016 m	(-0.004, -0.015, 0.003) m
GL3	GNAT GPS C...	ScanWorld [R...	Coincident: Vertex - Vertex	On	1.0000	0.012 m	(0.005, -0.010, -0.002) m
GL5	GNAT GPS C...	ScanWorld [R...	Coincident: Vertex - Vertex	On	1.0000	0.013 m	(-0.012, -0.004, 0.001) m
GL6	GNAT GPS C...	ScanWorld [R...	Coincident: Vertex - Vertex	On	1.0000	0.023 m	(-0.005, 0.023, 0.003) m

Figure 19: Constraint List of Error Measurements for Geo-referenced, Laser-Scanned, Point-Cloud Model Target-to-Target Registration

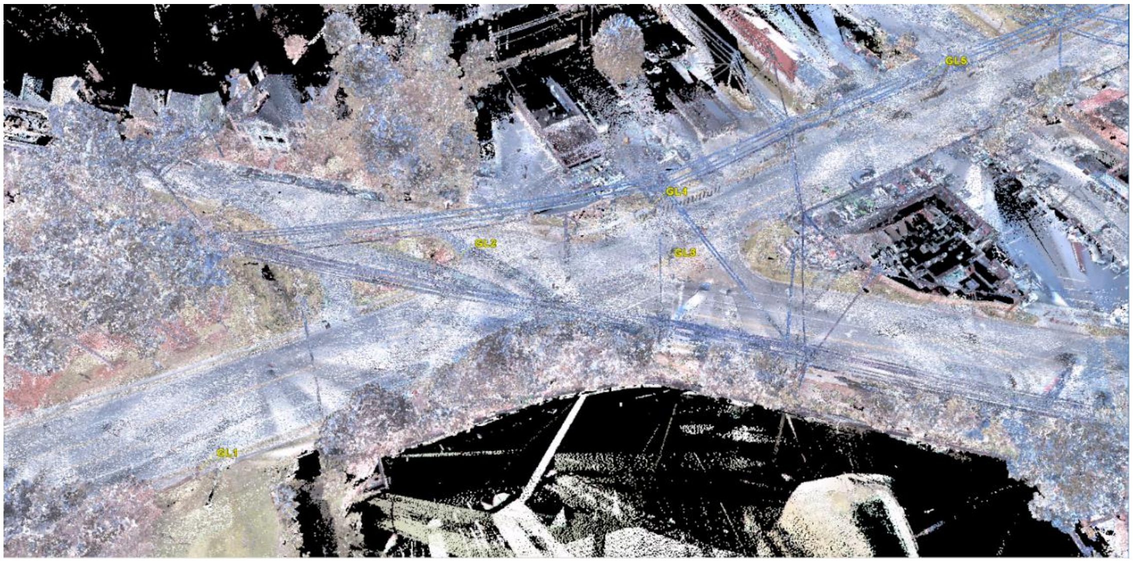

Figure 20 (a): Aerial View of Geo-Referenced Point-Cloud Model of City Intersection 2

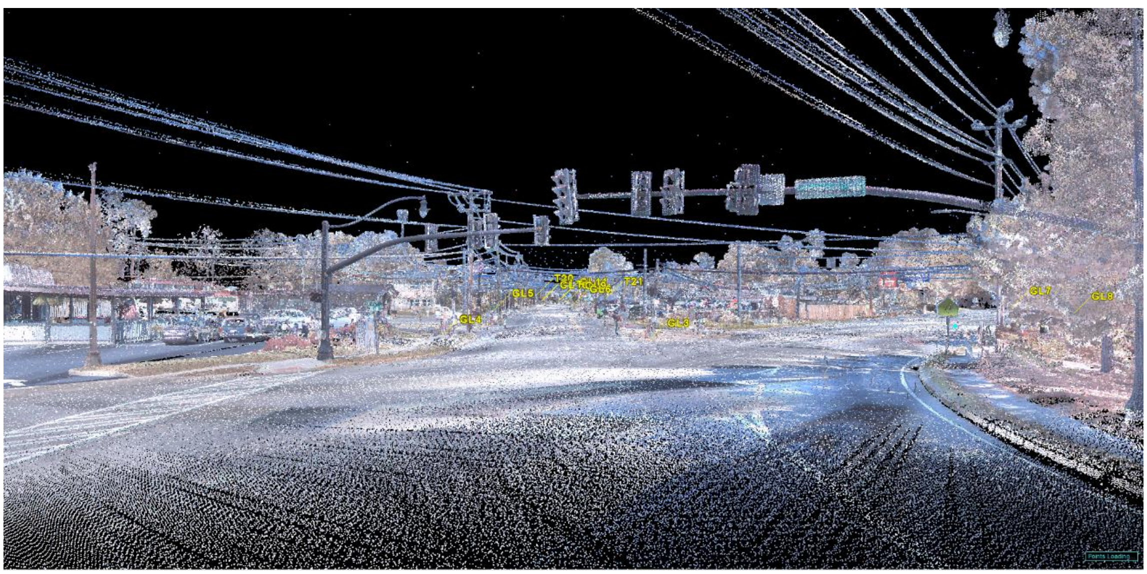

Figure 20 (b): Perspective View of Geo-Referenced Point-Cloud Model of City Intersection 2

For the close-range photogrammetric approach, the DJI Mavic Platinum Pro unmanned aerial vehicle was flown over two sidewalks within the field-site at an elevation of approximately 22 m (72 ft), by a certified ground pilot operator. This elevation height was well within the detectable obstacle sensory range of 30 m (98 ft). The airborne camera was oriented as a downward vision system to the ground level for accurate image acquisition. Over 1200 images were attained from the field. Each neighboring image contained at least a 60% side overlap and 80% of forward overlap (Useful Tips on Image Capture: How to Get an Image Dataset that Meets PhotoScan Requirements?), as shown in Figure 21.

(a) (b) (c)

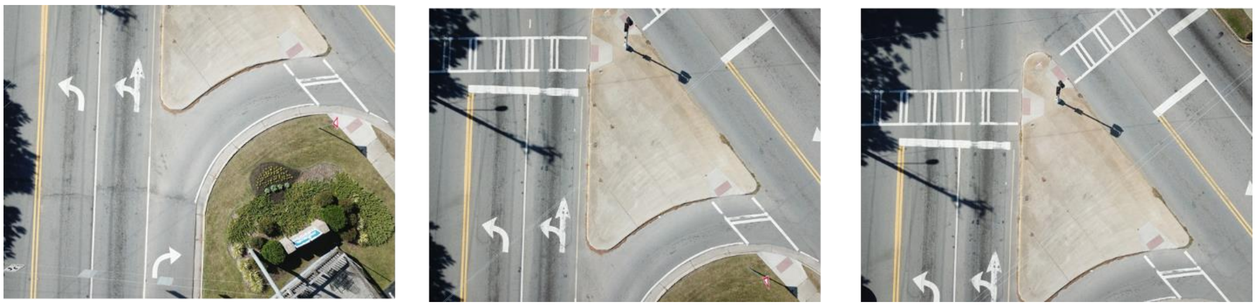

Figures 21 (a)-(c): Example of neighboring images taken with the recommended percentage of overlap.

The duration of the entire imagery acquisition was approximately one hour and 45 minutes. The photos were imported into a computer and filtered for a proper 3D construction. Like the trimming process in a laser-scanned point-cloud model, photos with any passing vehicles on the city street were eliminated. Then, the remaining sub-set of 1200+ photos were imported into the Agisoft PhotoScan software. A set of procedures (Appendix F) were followed for the 3D photo-based model construction, Figure 22.

Figure 22 (a): Aerial View of 3D Dense-Cloud Photo-Based Model of City Intersection 2

Figure 22 (b): Perspective View of 3D Dense-Cloud Photo-Based Model of City Intersection 2

For the photogrammetric point cloud, a set of five ground control points were marked with virtual flags in each image, where the point is visible (Figure 23). Once all points were marked, then the five GPS coordinates were imported into PhotoScan to geo-reference the photo-based model. A sub-set of 30 sample points were virtually marked with the same procedures as the control points (Appendix F).

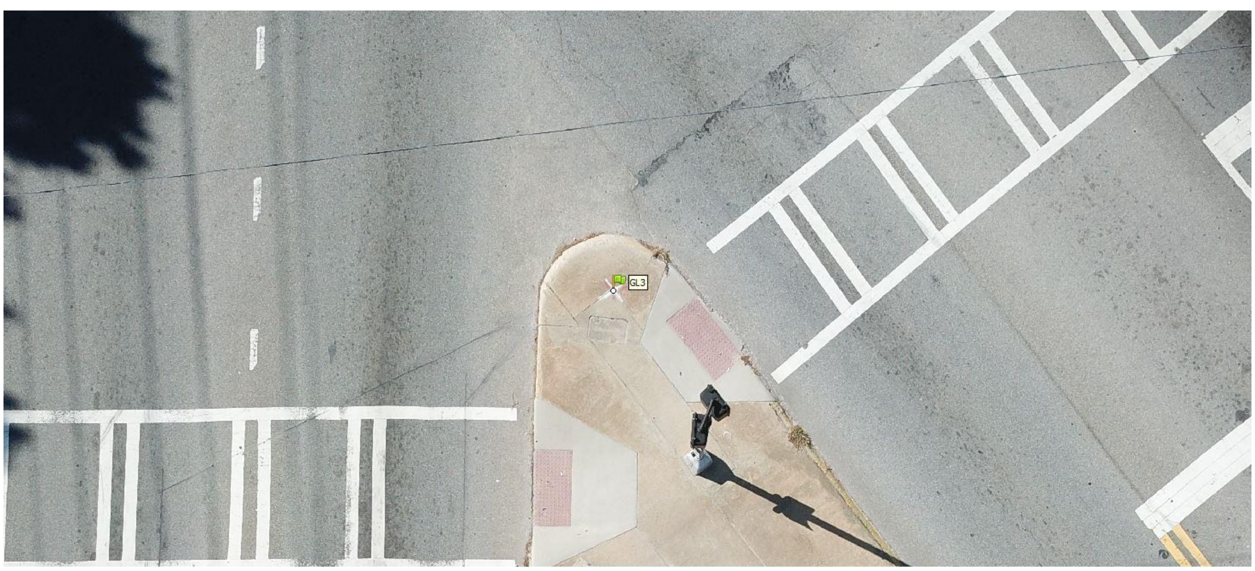

Figure 23: Marker Placement for Sample Point/Ground Control Point for Photo-Based Model of City Intersection 2

Like Case Study 1 and Case Study 2, a set of 52 points were strategically selected from the 3D laser scanned point-cloud model. 255 indirect distances were obtained for the laser-scanned point cloud through the distance expression for 3D spaces (as mentioned in Chapter 4). For the traditional surveying application, the accurate one-second robotic total station, employed as a benchmark instrument, was set up at the central control point, GL3. A 360-reflector prism was used as a benchmark for a known back sight coordinate to set the appropriate coordinate system for the robotic total station. Then, a sample of 52-point coordinates was attained with a reflectorless laser beam. Similar to the previous study area, vertices of building roofs, road markings, electrical poles, and more were employed as sample points (see Figure 23). A set of procedures were followed to complete this point acquisition process (Appendix E).

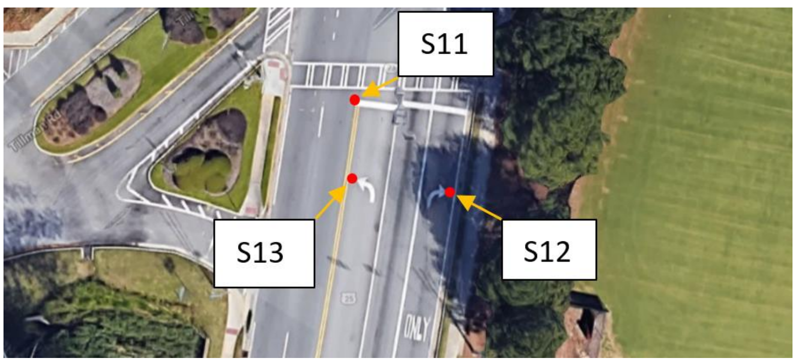

Figure 24: Set of Employed Sample Points for City Intersection 2

In the PhotoScan software, scale bars were established to calculate distances within the. Scale bars are target based and calibrated to support highly accurate measurement of 3D data (Cultural Heritage Imaging 2015). In the accuracy settings, the scale bar was set to a default accuracy of one millimeter (Figure 25). Yet, it is recommended the scale bar accuracy should be set to 0.0001 meters (Figure 26) if the operator is using a physical scale bar in the field (Cultural Heritage Imaging, 2015).

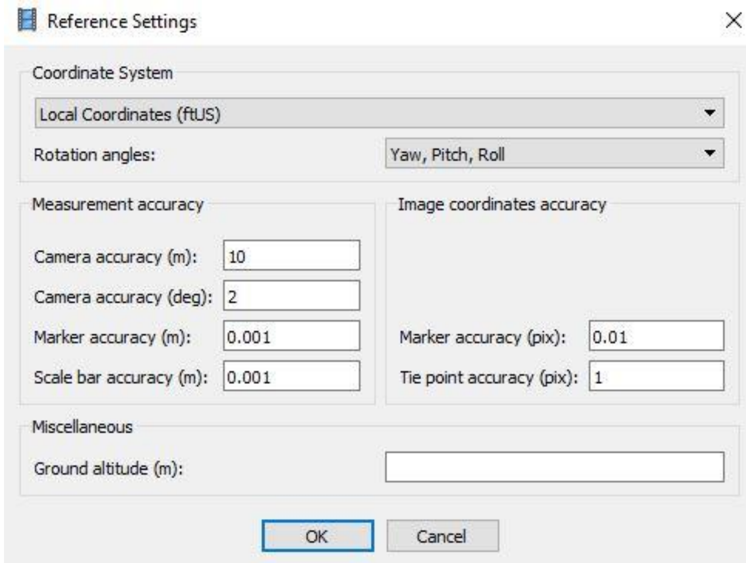

Figure 25: Default Accuracy Settings used for Photo-Based Model of City Intersection 2

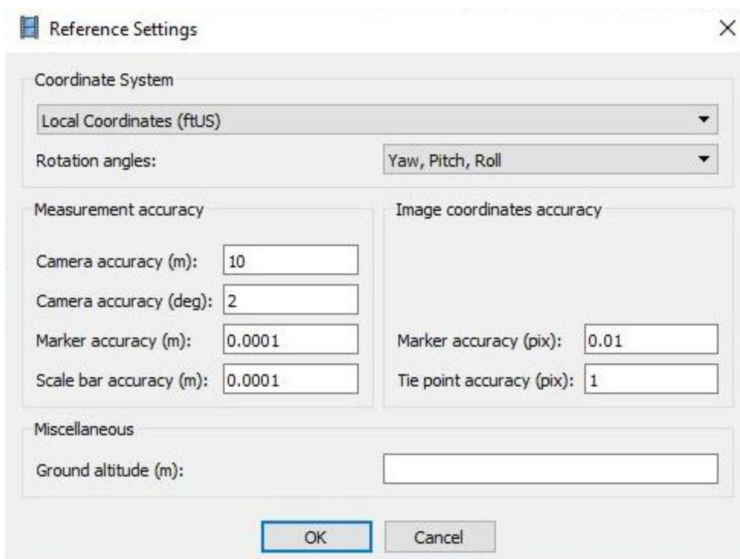

Figure 26: Example of Accuracy Settings Recommended by the Cultural Heritage Imaging

Two virtual scale bars, in Agisoft PhotoScan, were employed for the measurement process, though four scale bars are recommended by Cultural Heritage Imaging (2015). One virtual scale bar was measured from the northern-most ground control point (GL5) to the southern-most ground control point (GL1). Another virtual scale bar was measured from the eastern-most ground control point (GL8) to the western-most ground control point (GL2). Since the ground control points contained known GPS coordinates, the distance formula for 3D spaces was employed to calculate the known scale bar measurement (see Chapter 4). The known measured distances within each scale bar were inserted into the PhotoScan software. These virtual scale bars set the sample points, within the model at the appropriate setting for measurement. Then, five center points (GL1, GL2, GL3, GL5 and GL8) were chosen to measure distances to the other 30 sample points. Additionally, sample point N12 was chosen to measure 29 sample points. A set of scale bars from each "center point" to the sample point were used for this procedure, as shown in Figure 27. A total of 179 direct distance measurements were estimated via the PhotoScan software. Then, the camera alignment for each image was optimized by setting the parameters in Figure 28. The optimization will help minimize the estimated error in point coordinates and distances within the software.

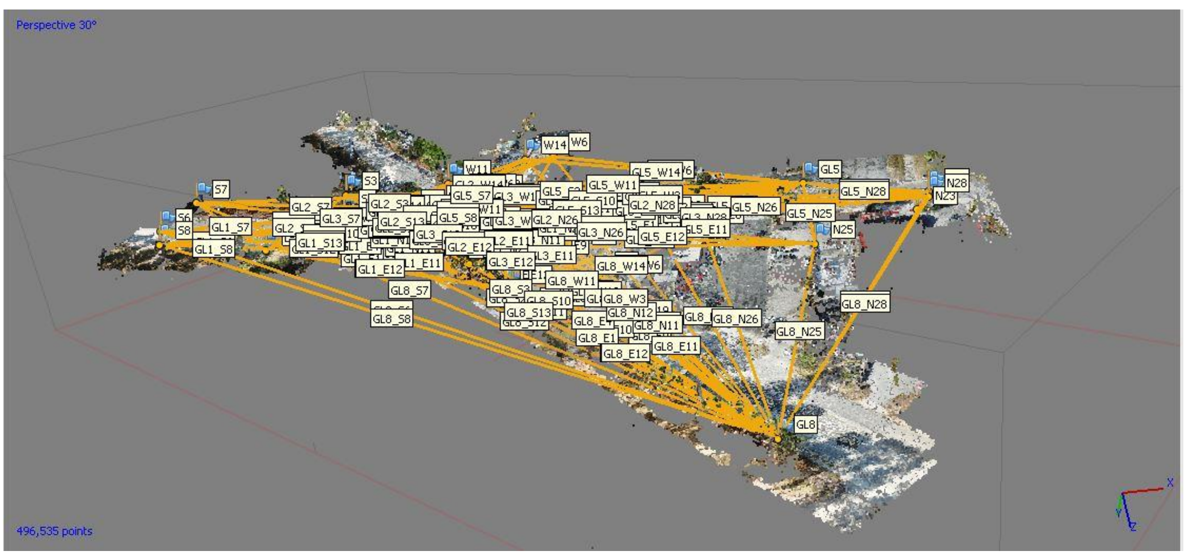

Figure 27: Distances Measured in PhotoScan for Photo-Based Model of City Intersection 2

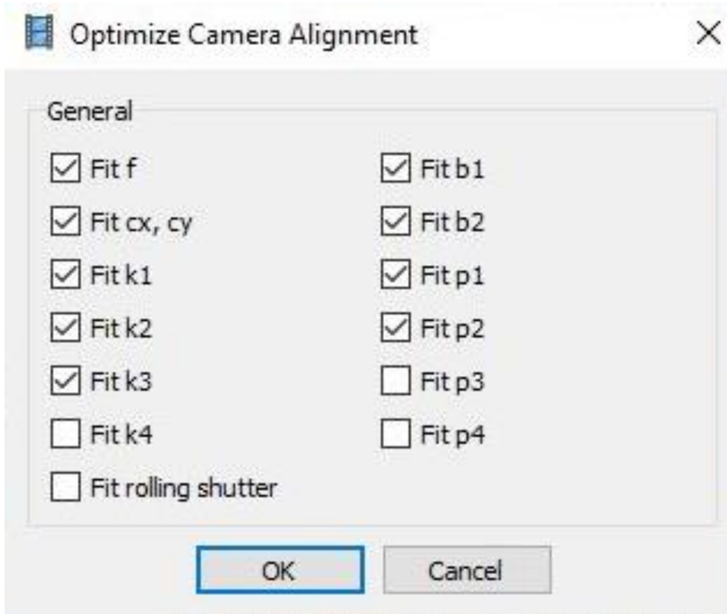

Figure 28: Example of Optimize Camera Alignment Settings used for Photo-Based Model of City Intersection 2

CHAPTER 7

RESULTS

Case Study 1

After co-registering (stitching) all 18 individual scans, the resulting non-georeferenced point-cloud model presented an overall error of 0.033 ft (i.e., 0.4 inches) or 10 mm. However, the geo-referencing procedure increased this overall error to 0.101 ft (i.e., 1.2 inches) or 31 mm. This is because each geo-referencing control point was acquired via a rapid RTK approach, stationing the GPS instrument for about 15 seconds on each of them. This resulted in errors in their position coordinates, approximately ±1 inch in the horizontal components and ±2 inches in the vertical component. Consequently, after geo-referencing, the inherent or minimum relative position error in this study is 0.10 ft or 31 mm.

A discrepancy analysis was performed to compare the point-cloud data measurements against the calculated distance measurements of the accurate one-second total station as a benchmark. The non-georeferenced model consisted of its own XYZ coordinate, so the position of each sample point could not be analyzed for comparison against the coordinates attained by the accurate one-second total station. However, the geo-referenced point-cloud model was employed to compare the coordinates obtained via laser-scanned point-cloud to the accurate total station for any present outliers. Two sample points were presented as outliers (E8 and S5). After the outliers were removed, a total of 211 distances were calculated from six centers.

After completing the distance discrepancy, the non-georeferenced point-cloud model presented 0.08 ft of a mean discrepancy with a -0.01% of a relative discrepancy in all 211 distance measurements. The standard deviation of all distances resulted as 0.07 ft with 0.06% of a relative discrepancy. From all distances measured, approximately 68% of the sample points consisted of a discrepancy of fewer than 0.10 ft (1.20 inches), as shown in Table 3. Also, the overall discrepancy for all 211 distances was displayed as 0.30 ft (3.60 inches), as shown in Figure 29.

Table 3 (a): Distance Discrepancy Analysis for Non-Georeferenced Point-cloud Model

<table>
<tr><th>NONGEO</th><th>Distance Measured (RTS,ft)</th><th>Discrepancy (ft)</th><th>Relative Discrepancy %</th><th>Absolute Discrepancy (ft)</th></tr>
<tr><td>Min =</td><td>11.384</td><td>-0.353</td><td>-0.402</td><td>0.001</td></tr>
<tr><td>Max =</td><td>717.298</td><td>0.291</td><td>0.293</td><td>0.353</td></tr>
<tr><td>Mean =</td><td></td><td>-0.038</td><td>-0.012</td><td>0.081</td></tr>
<tr><td>Std Dev =</td><td></td><td>0.099</td><td>0.059</td><td>0.068</td></tr>
<tr><td>Median =</td><td></td><td>-0.033</td><td>-0.011</td><td>0.061
Median of |Discr|</td></tr>
</table>

Table 3 (b): Distance Discrepancy Analysis for Non-Georeferenced Point-cloud Model

<table>
<tr><th>Sum & %</th><th>Sum & %</th><th>Sum & %</th><th>Sum & %</th><th>Sum & %</th><th>Sum & %</th><th>Sum & %</th><th>Sum & %</th><th>Sum & %</th></tr>
<tr><td>23</td><td>57</td><td>83</td><td>105</td><td>144</td><td>175</td><td>200</td><td>205</td><td>208</td></tr>
<tr><td>10.9%</td><td>27.0%</td><td>39.3%</td><td>49.8%</td><td>68.2%</td><td>82.9%</td><td>94.8%</td><td>97.2%</td><td>98.6%</td></tr>
<tr><td>Points with |Discr|<0.01</td><td>Points with |Discr|<0.03</td><td>Points with |Discr|<0.05</td><td>Points with |Discr|<Median</td><td>Points with |Discr|<0.10</td><td>Points with |Discr|<0.15</td><td>Points with |Discr|<0.20</td><td>Points with |Discr|<0.25</td><td>Points with |Discr|<0.30</td></tr>
<tr><td>0.010 ft</td><td>0.030 ft</td><td>0.050 ft</td><td>0.061 ft</td><td>0.100 ft</td><td>0.150 ft</td><td>0.200 ft</td><td>0.250 ft</td><td>0.300 ft</td></tr>
</table>

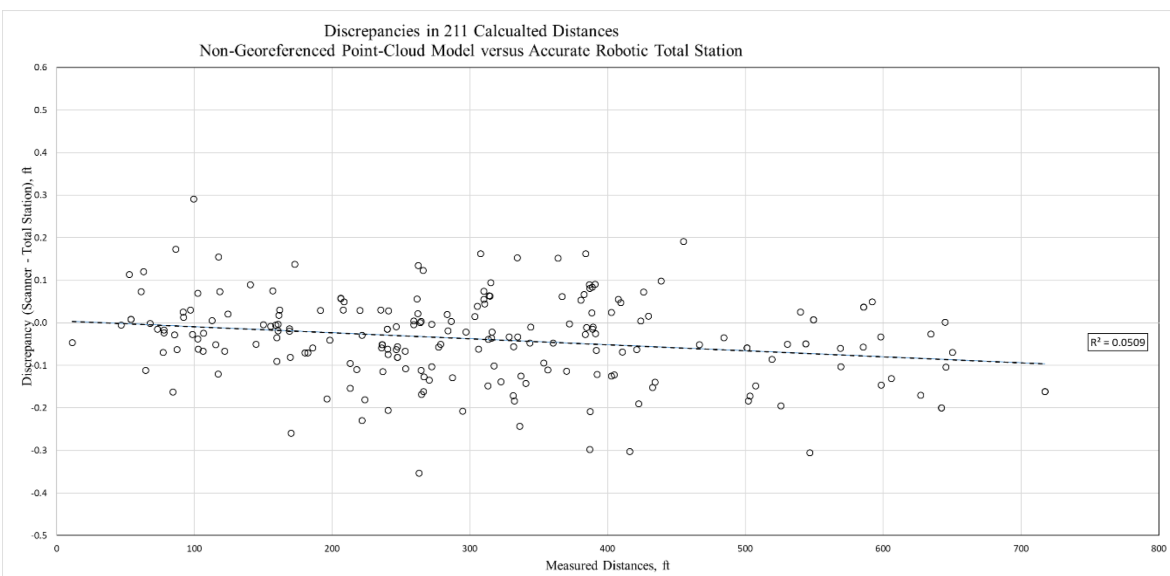

Figure 29: Graph – Discrepancies in 211 Calculated Distances Non-Georeferenced Point-Cloud Model versus Accurate Robotic Total Station

After the point-cloud model was geo-referenced, the sample of 211 distance measurements presented a mean discrepancy of 0.09 ft with a relative discrepancy of -0.02% against the accurate robotic total station. The standard deviation of 0.07 ft (0.075% relative standard deviation) was presented in the results of this case. From all distances measured, approximately 65% of the sample points consisted of a discrepancy of fewer than 0.10 ft (1.2 inches), as shown in Table 4.

Table 4 (a): Distance Discrepancy Analysis for Geo-Referenced Point-cloud Model

<table>
<tr><th>GEOREF</th><th>Distance Measured (RTS,ft)</th><th>Discrepancy (ft)</th><th>Relative Discrepancy %</th><th>Absolute Discrepancy (ft)</th></tr>
<tr><td>Min =</td><td>11.384</td><td>-0.353</td><td>-0.738</td><td>0.002</td></tr>
<tr><td>Max =</td><td>717.298</td><td>0.292</td><td>0.294</td><td>0.353</td></tr>
<tr><td>Mean =</td><td></td><td>-0.047</td><td>-0.017</td><td>0.088</td></tr>
<tr><td>Std Dev =</td><td></td><td>0.100</td><td>0.075</td><td>0.067</td></tr>
<tr><td>Median =</td><td></td><td>-0.050</td><td>-0.018</td><td>0.073
Median of |Discr|</td></tr>
</table>

Table 4 (b): Distance Discrepancy Analysis for Geo-Referenced Point-cloud Model

<table>
<tr><th>Sum & %</th><th>Sum & %</th><th>Sum & %</th><th>Sum & %</th><th>Sum & %</th><th>Sum & %</th><th>Sum & %</th><th>Sum & %</th><th>Sum & %</th></tr>
<tr><td>17</td><td>41</td><td>68</td><td>105</td><td>137</td><td>174</td><td>200</td><td>205</td><td>207</td></tr>
<tr><td>8%</td><td>19%</td><td>32%</td><td>50%</td><td>65%</td><td>82%</td><td>95%</td><td>97%</td><td>98%</td></tr>
<tr><td>Points with |Discr|<0.01</td><td>Points with |Discr|<0.03</td><td>Points with |Discr|<0.05</td><td>Points with |Discr|<Median</td><td>Points with |Discr|<0.10</td><td>Points with |Discr|<0.15</td><td>Points with |Discr|<0.20</td><td>Points with |Discr|<0.25</td><td>Points with |Discr|<0.30</td></tr>
<tr><td>0.010 ft</td><td>0.030 ft</td><td>0.050 ft</td><td>0.073 ft</td><td>0.100 ft</td><td>0.150 ft</td><td>0.200 ft</td><td>0.250 ft</td><td>0.300 ft</td></tr>
</table>

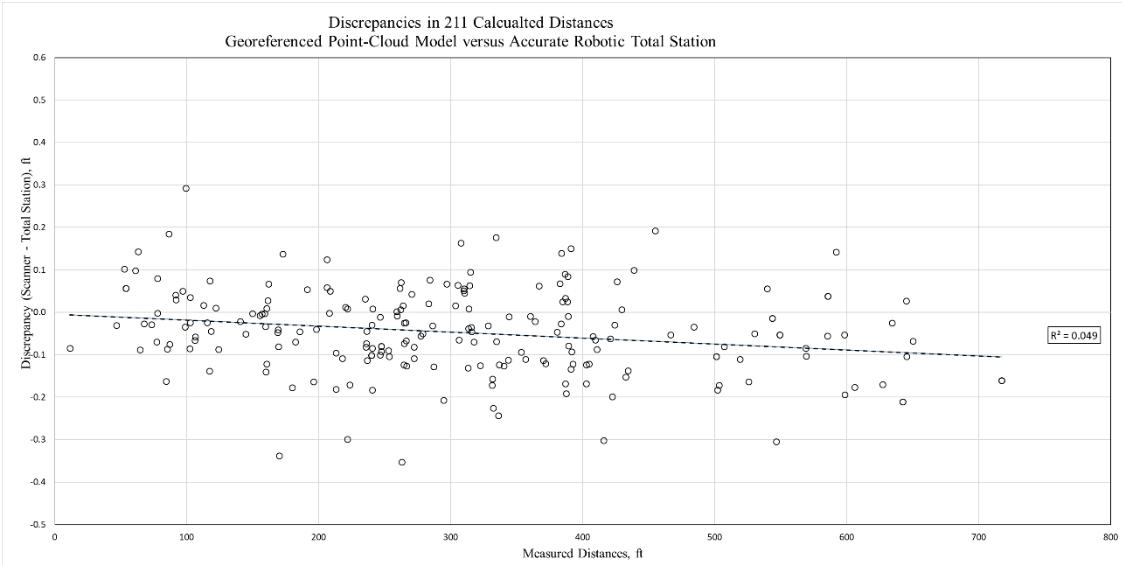

Figure 30: Graph – Discrepancies in 211 Calculated Distances Georeferenced Point-Cloud Model versus Accurate Robotic Total Station

After visually aligning all 18 scans, the point-cloud model produced an overall error of 7 mm (0.023 ft) with a minimum error of 1 mm (0.003 ft) (Figure 15). Though the visual alignment registration displayed a smaller overall error than the previous registrations, the resulting point-cloud model presented targets with multiple positions (see Figure 16). These multiple target positions restricted the point-cloud model from the geo-reference procedure to a known geographical state plane coordinate system. As mentioned previously, the non-georeferenced model consists of its own XYZ coordinate system, since the first scan station (location) is set as the origin (X=0, Y=0, Z=0). Therefore, the position of each sample point cannot be analyzed for comparison against the coordinates obtained by the one-second robotic total station.

Distance measurements were calculated using the distance formula (Chapter 4) from six centers in the visually aligned non-georeferenced point-cloud model. A mean discrepancy of 0.11 ft (1.36 inches) with a relative discrepancy of -0.01% was reported for all distances. Also, a standard deviation of 0.11 ft (1.34 inches) with a 0.07% relative standard deviation was presented in the results for this case. From all distances measured, approximately 58% of the sample points consisted of a discrepancy of fewer than 0.10 ft (1.2 inches), as shown in Table 5.

Table 5 (a): Distance Discrepancy Analysis for Visually Aligned Point-cloud Model

VISUAL ALIGN	Distance Measured (RTS,ft)	Discrepancy (ft)	Relative Discrepancy %	Absolute Discrepancy (ft)
Min =	11.384	-0.463	-0.492	0.001
Max =	717.298	0.553	0.310	0.553
Mean =		-0.036	-0.008	0.113
Std Dev =		0.155	0.074	0.112
Median =		-0.040	-0.015	0.079
				Median of |Discr|

Table 5 (b): Distance Discrepancy Analysis for Visually Aligned Point-cloud Model

Sum & %	Sum & %	Sum & %	Sum & %	Sum & %	Sum & %	Sum & %	Sum & %	Sum & %
12	49	76	105	122	157	178	188	193
6%	23%	36%	50%	58%	74%	84%	89%	91%
Points with |Discr|<0.01	**Points with |Discr|<0.03**	**Points with |Discr|<0.05**	**Points with |Discr|<Median**	**Points with |Discr|<0.10**	**Points with |Discr|<0.15**	**Points with |Discr|<0.20**	**Points with |Discr|<0.25**	**Points with |Discr|<0.30**
0.010	0.030	0.050	0.079	0.100	0.150	0.200	0.250	0.300
ft	ft	ft	ft	ft	ft	ft	ft	ft

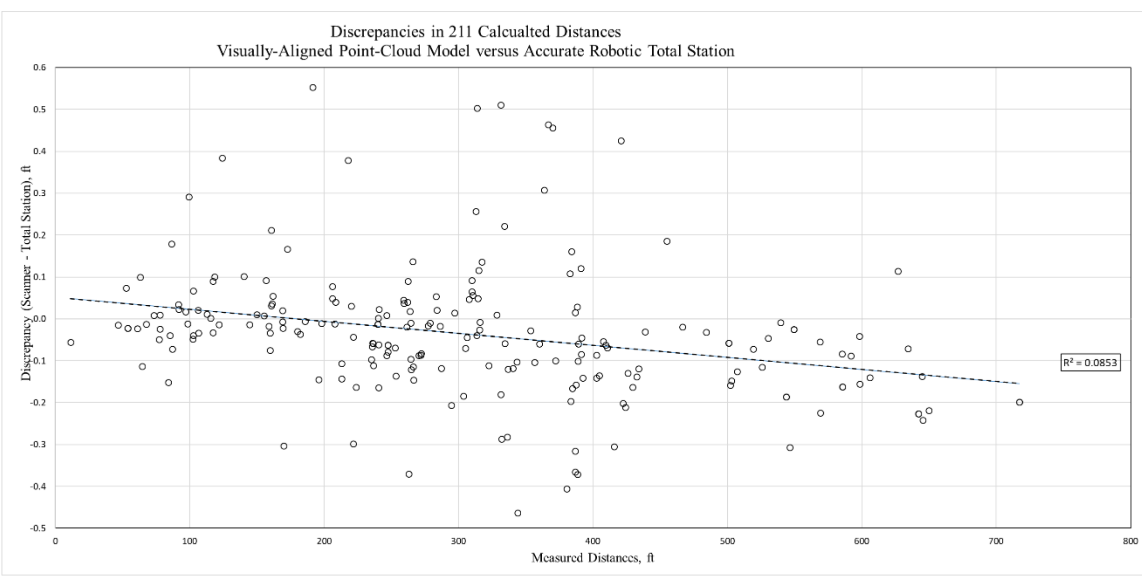

Figure 31: Graph - Discrepancies in 211 Calculated Distances Visually-Aligned Point-Cloud Model versus Accurate Robotic Total Station

Case Study 2

Coordinate discrepancies were calculated for all selected 38 points by subtracting the coordinates acquired by the robotic total station from those captured by the scanning instrument. They are listed in Table 6 where two inconsistent outliers are observed, E8 and S5. They have component discrepancies of 0.45 ft and 0.44 ft (5.40 inches and 5.28 inches), respectively. It was realized that those two points represented data erroneously collected in the field and, consequently, they were removed from the present study which was completed with the remaining 36 surrounding points. The ranges of these discrepancies (max and min values), their mean values, root mean square (RMS) values and standard deviations are summarized in Table 7. It can be observed that all three RMS values and their associated standard deviations range in magnitude from 0.03 ft to 0.26 ft (or from 0.6 inches to 1.1 inches). That is, about 15 mm to 27 mm each of them. This one-sigma error is consistent with the inherent error in this study.

Table 6: Discrepancy in 38 Coordinates (Laser Scanner versus Total Station)

Discrepancy in Coordinates (Laser Scanner vs. Total Station)									
Sample Size	**Point Label**	**Diff. in Northing (ft)**	**Diff. in Easting (ft)**	**Diff. in Elevation (ft)**	**Sample Size**	**Point Label**	**Diff. in Northing (ft)**	**Diff. in Easting (ft)**	**Diff. in Elevation (ft)**
1	**N1**	-0.100	0.093	0.072	20	**S3**	-0.027	-0.078	-0.060
2	**N2**	-0.037	-0.007	-0.036	21	**S4**	0.065	-0.076	0.049
3	**N3**	0.009	0.024	-0.017	~~22~~	~~**S5**~~	~~0.122~~	~~-0.443~~	~~0.069~~
4	**N4**	-0.123	0.007	-0.013	23	**S6**	-0.067	-0.196	-0.013
5	**N5**	-0.111	-0.081	0.024	24	**S7**	-0.083	-0.082	-0.021
6	**N6**	0.004	0.031	-0.012	25	**S8**	0.139	-0.101	0.016
7	**N7**	0.123	-0.061	-0.136	26	**W1**	0.054	-0.046	-0.016
8	**N8**	0.018	0.031	-0.005	27	**W2**	-0.007	-0.059	-0.024
9	**E1**	-0.155	-0.041	0.001	28	**W3**	0.028	0.138	-0.096
10	**E2**	-0.009	-0.078	-0.066	29	**W4**	0.204	-0.095	0.055
11	**E3**	-0.133	-0.005	-0.089	30	**W5**	0.143	0.026	0.031
12	**E4**	-0.072	-0.056	0.028	31	**W6**	0.266	0.221	0.079
13	**E5**	-0.051	-0.026	0.015	32	**W7**	-0.012	-0.028	-0.012
14	**E6**	-0.021	-0.066	-0.007	33	**W8**	-0.001	0.023	-0.022
15	**E7**	-0.018	-0.022	-0.016	34	**S9**	-0.023	-0.049	-0.015
~~16~~	~~**E8**~~	~~-0.450~~	~~0.189~~	~~0.006~~	35	**S10**	0.007	-0.118	-0.041
17	**E9**	-0.005	-0.067	-0.121	36	**N9**	-0.022	0.040	-0.052
18	**S1**	0.039	-0.072	-0.025	37	**N10**	0.102	-0.012	-0.002
19	**S2**	-0.033	-0.058	0.003	38	**S11**	0.148	-0.120	-0.071

Table 7: Statistical Analysis of 36 Absolute Coordinate Discrepancies

	|Diff.| in Northing (ft)	|Diff.| in Easting (ft)	|Diff.| in Elevation (ft)
Min =	0.001	0.005	0.001
Max =	0.266	0.221	0.136
Mean =	0.068	0.065	0.038
Std Dev. =	0.063	0.048	0.034
RMS =	0.093	0.081	0.051

The measured coordinates of the selected center points (T9, N1, N2, N3, S4, and S6) are listed in Table 8. From each of these center points, a total of 35 distances (except 36 for T9) were calculated twice: (i) using coordinates obtained within the point-cloud model and (ii) by employing coordinates captured by the total-station instrument. This resulted in 211 different distances ranging from approximately 11 to 717 feet. Again, the corresponding discrepancies were calculated by subtracting the total-station distances from the scanned ones. Each major row of Table 8 shows results for a set of distances corresponding to a unique center point.

Table 8: Analysis of Discrepancies in 211 Measured Distances

Selected Center Point	Employed Instrum. to acquire coords.	Coordinates of Center Point and their discrepancies: Northing (ft)	Easting (ft)	Elev. (ft)	ANALYSIS of DISCREPANCIES in 211 MEASURED DISTANCES: Discrepancy in Center Location, (ft)	# of Measured Distances	Max Discrep. (ft)	Min Discrep. (ft)	Mean Discrep. (ft)	RMS Discrep. (ft)	Std Dev Discrep. (ft)
T9	Scanner	887364.647	774166.884	219.084	0.000	36	0.185	-0.171	-0.024	0.083	0.079
	Total-Sta	887364.647	774166.884	219.084							
	Discrep.	0.000	0.000	0.000							
N3	Scanner	887579.637	774210.387	238.017	0.031	35	0.095	-0.299	-0.013	0.084	0.084
	Total-Sta	887579.628	774210.363	238.034							
	Discrep.	0.009	0.024	-0.017							
N2	Scanner	887531.928	774185.520	234.337	0.052	35	0.143	-0.338	-0.050	0.103	0.090
	Total-Sta	887531.965	774185.527	234.373							
	Discrep.	-0.037	-0.007	-0.036							
S4	Scanner	887030.972	774187.330	226.530	0.111	35	0.176	-0.210	-0.063	0.108	0.088
	Total-Sta	887030.907	774187.406	226.481							
	Discrep.	0.065	-0.076	0.049							
N1	Scanner	887634.145	773970.997	267.386	0.154	35	-0.046	-0.353	-0.148	0.165	0.073
	Total-Sta	887634.245	773970.904	267.314							
	Discrep.	-0.100	0.093	0.072							
S6	Scanner	887002.325	774307.979	228.228	0.208	35	0.292	-0.170	0.016	0.098	0.097
	Total-Sta	887002.392	774308.175	228.241							
	Discrep.	-0.067	-0.196	-0.013							

Those rows are ordered by increased discrepancies in the location of their center points. This order shows some correlation with the column containing the RMS value of the associated discrepancies. All calculated discrepancies were plotted in Figure 32, where it can be observed that 63% of them (133) are in the ±0.1-foot range (approximately ±1 inch). Also, approximately 95% of the distances are within the ±0.2-foot range. That is, the majority of the distances have a discrepancy within the inherent error of the model which is related to the geo-referencing control points.

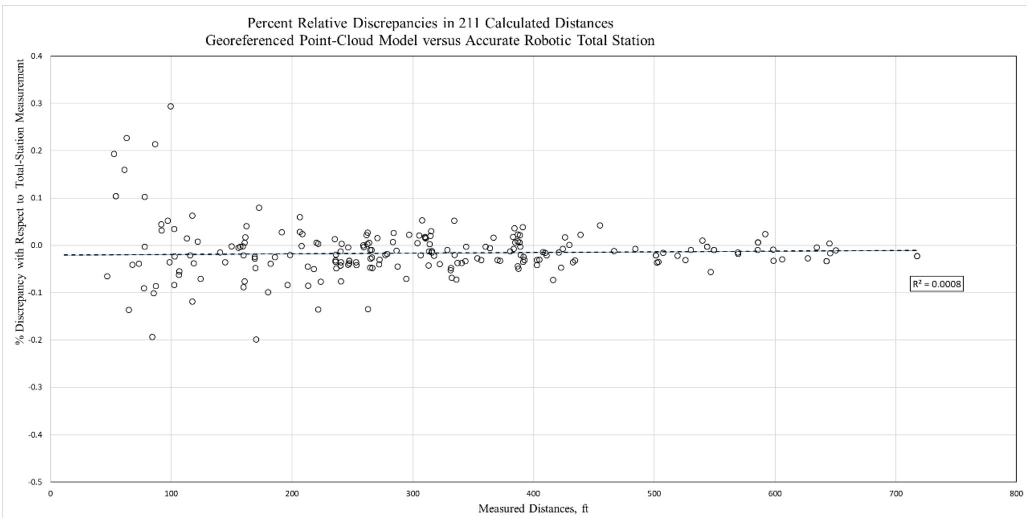

Figure 32: Graph – Percent Relative Discrepancies in 211 Calculated Distances Georeferenced Point-Cloud Model vs. Accurate-Robotic Total Station

Case Study 3

Laser Scanning versus Robotic Total Station

After co-registering (stitching) all 45 individual scans, the resulting non-georeferenced point-cloud model presented an overall error of 0.03 ft (i.e., 0.40 inches) or 10 mm. However, the geo-referencing procedure increased this overall error to 0.085 ft (i.e., 1.02 inches) or 26 mm. This is because each geo-referenced control point was acquired via a rapid RTK approach, stationing the GPS instrument for only about 15 seconds on each of them, similar to the previous study area. This resulted in errors in their position coordinates, approximately from 0.012 inches to 0.048 inches in the horizontal components and about 0.012

inches in the vertical component. Consequently, after geo-referencing, the inherent or minimum relative position error in this study is 0.085 ft or 26 mm.

Coordinate discrepancies were calculated for all selected 52 points by subtracting the coordinates acquired by the robotic total station from those captured by the scanning instrument. They are listed in Table 9 where five inconsistent outliers are observed, N7, N13, E12, S11, and S12. They have component discrepancies between 0.22 ft and 0.45 ft (2.64 inches to 5.40 inches), respectively. It was realized that those five points represented data erroneously collected in the field and, consequently, they were removed from the present study which was completed with the remaining 47 surrounding points. The ranges of these discrepancies (max and min values), their mean values, root mean square (RMS) values and standard deviations are summarized in Table 10. It can be observed that all three RMS values and their associated standard deviations range in magnitude from 0.03 ft to 0.23 ft (or from 0.36 inches to 2.76 inches). That is, about 9 mm to 70 mm each of them. This range in values is more than one-sigma of error, statistically. Yet it does include the inherent error in this study. Since the three RMS values range in a magnitude of 61 mm to 70 mm, removing more discrepancies as outliers may reduce the overall error and be more consistent with the inherent error of this study.

The measured coordinates of the selected center points (GL3, W10, N6, E8, N18, and S6) are listed in Table 11. From each of these center points, a total of 46 distances (except 47 for GL3) were calculated twice: (i) using coordinates obtained within the point-cloud model and (ii) by employing coordinates captured by the total-station instrument. This resulted in 277 different distances ranging from approximately 3 to 932 feet. Again, the corresponding discrepancies were calculated by subtracting the total-station distances from the scanned ones. Each major row of Table 11 shows results for a set of distances corresponding to a unique center point. Those rows are ordered by increased discrepancies in the location of their center points. This order shows some correlation with the column containing the RMS value of the associated discrepancies. All calculated discrepancies were plotted in Figure 33, where it can be observed that 86% of them (238) are in the ±0.10-foot range, with none exceeding the ±0.20-foot range. That is, the majority of the distances have a discrepancy within the inherent error of the model which is related to the geo-referenced control points.

Table 9: Discrepancy in 52 Coordinates (Laser Scanner versus Robotic Total Station)

Discrepancy in Coordinates (Laser Scanner vs. Total Station)									
Sample Size	**Point Labels**	**Diff. in Northing (ft)**	**Diff. in Easting (ft)**	**Diff. in Elevation (ft)**	**Sample Size**	**Point Labels**	**Diff. in Northing (ft)**	**Diff. in Easting (ft)**	**Diff. in Elevation (ft)**
1	**N1**	-0.051	-0.014	-0.038	27	**E6**	-0.019	-0.001	0.061
2	**N2**	-0.041	-0.031	0.043	28	**E7**	-0.06	0.004	0.096
3	**N5**	-0.115	0.044	-0.003	29	**E8**	0.058	0.015	0.022
4	**N6**	-0.02	-0.002	0.058	30	**E9**	0	0.034	-0.03
~~5~~	~~**N7**~~	~~-0.217~~	~~-0.058~~	~~-0.014~~	31	**E10**	-0.021	0.007	-0.012
6	**N8**	-0.03	-0.047	0.025	32	**E11**	0.067	0.147	-0.05
7	**N10**	0.025	0.125	-0.038	~~33~~	~~**E12**~~	~~0.003~~	~~0.238~~	~~-0.034~~
8	**N11**	-0.044	-0.003	0.062	34	**S1**	0.104	0.052	0.115
9	**N12**	0.024	-0.01	0.078	35	**S2**	-0.148	-0.005	0.021
~~10~~	~~**N13**~~	~~-0.275~~	~~-0.05~~	~~0.061~~	36	**S3**	-0.167	0.108	0
11	**N14**	-0.045	-0.071	0.03	37	**S4**	-0.13	-0.045	0.01
12	**N15**	-0.021	-0.001	0	38	**S6**	0.005	0.079	0.016
13	**N16**	-0.156	-0.005	-0.012	39	**S7**	-0.068	0.096	-0.012
14	**N17**	-0.024	-0.014	0.006	40	**S8**	0.044	0.047	0.003
15	**N18**	-0.04	-0.047	-0.032	41	**S10**	0.051	0.018	0.001
16	**N19**	-0.061	0.01	-0.017	~~42~~	~~**S11**~~	~~-0.21~~	~~0.154~~	~~-0.032~~
17	**N21**	-0.108	-0.045	-0.04	~~43~~	~~**S12**~~	~~-0.477~~	~~-0.03~~	~~-0.053~~
18	**N24**	-0.059	-0.062	-0.049	44	**S13**	-0.07	0.073	-0.054
19	**N25**	-0.024	0.007	-0.022	45	**W1**	-0.052	0.038	0.09
20	**N26**	0.006	-0.005	-0.034	46	**W3**	-0.012	0.021	0.133
21	**N28**	-0.017	-0.038	-0.07	47	**W4**	-0.071	0.193	0.037
22	**E1**	-0.024	-0.002	0.024	48	**W6**	-0.017	-0.038	0.073
23	**E2**	-0.008	0.137	0.028	49	**W9**	-0.054	0.01	0.043
24	**E3**	0.054	-0.008	0.015	50	**W10**	0	-0.008	0.046
25	**E4**	-0.037	0.018	0.077	51	**W11**	-0.112	-0.03	0.073
26	**E5**	-0.002	0.008	0.122	52	**W14**	-0.064	0.031	-0.062

Table 10: Statistical Analysis of 47 Absolute Coordinate Discrepancies

	|Diff.| in Northing (ft)	**|Diff.| in Easting (ft)**	**|Diff.| in Elevation (ft)**
Min =	0.000	0.001	0.000
Max =	0.167	0.193	0.133
Mean =	**0.052**	**0.039**	**0.042**
Std Dev. =	**0.042**	**0.043**	**0.033**
RMS =	**0.066**	**0.058**	**0.053**

Table 11: An1alysis of Discrepancies in 277 Measured Distances (Selected Center Points)

Selected Center Point	Employed Instrum. to acquire coords.	Coordinates of Center Point and their discrepancies			ANALYSIS of DISCREPANCIES in 277 MEASURED DISTANCES						
		Northing (ft)	Easting (ft)	Elev. (ft)	Discrepancy in Center Location, (ft)	# of Measured Distances	Min Discrep. (ft)	Max Discrep. (ft)	Mean Discrep. (ft)	Std Dev Discrep. (ft)	RMS Discrep. (ft)
GL3	Scanner	884908.373	773908.397	210.720	0.019	47	-0.184	0.148	-0.001	0.070	0.034
	Total-Sta	884908.389	773908.389	210.724							
	Discrep.	-0.016	0.008	-0.004							
W10	Scanner	885050.666	773832.028	222.047	0.047	46	0.036	-0.112	0.159	0.024	0.063
	Total-Sta	885050.666	773832.036	222.001							
	Discrep.	0.000	-0.008	0.046							
N6	Scanner	885034.139	773831.564	224.979	0.061	46	-0.109	0.155	0.013	0.057	0.114
	Total-Sta	885034.159	773831.566	224.921							
	Discrep.	-0.020	-0.002	0.058							
E8	Scanner	885237.521	774175.871	230.057	0.064	46	-0.082	0.192	0.059	0.059	0.243
	Total-Sta	885237.463	774175.856	230.035							
	Discrep.	0.058	0.015	0.022							
N18	Scanner	885360.182	773963.995	223.229	0.070	46	-0.158	0.098	-0.013	0.052	0.116
	Total-Sta	885360.222	773964.042	223.261							
	Discrep.	-0.040	-0.047	-0.032							
S6	Scanner	884436.193	773842.571	235.271	0.081	46	-0.058	-0.174	0.097	-0.046	0.057
	Total-Sta	884436.188	773842.492	235.255							
	Discrep.	0.005	0.079	0.016							

Table 12 (a): Discrepancy Analysis of 277 Measured Distances in Georeferenced Point-Cloud Model

<table>
<tr><th></th><th>Distance Measured (RTS, ft)</th><th>Discrepancy (ft)</th><th>Relative Discrepancy (%)</th><th>Absolute Discrepancy (ft)</th></tr>
<tr><td>Min =</td><td>2.699</td><td>-0.184</td><td>-1.121</td><td>0.000</td></tr>
<tr><td>Max =</td><td>932.320</td><td>0.192</td><td>0.301</td><td>0.192</td></tr>
<tr><td>Mean =</td><td></td><td>0.006</td><td>0.001</td><td>0.053</td></tr>
<tr><td>Std Dev =</td><td></td><td>0.068</td><td>0.083</td><td>0.043</td></tr>
<tr><td>Median =</td><td></td><td>0.005</td><td>0.002</td><td>0.045
Median of |Discr|</td></tr>
</table>

Table 12 (b): Discrepancy Analysis of 277 Measured Distances in Georeferenced Point-Cloud Model

<table>
<tr><th>Sum & %</th><th>Sum & %</th><th>Sum & %</th><th>Sum & %</th><th>Sum & %</th><th>Sum & %</th><th>Sum & %</th><th>Sum & %</th></tr>
<tr><td>68</td><td>126</td><td>136</td><td>176</td><td>211</td><td>238</td><td>266</td><td>277</td></tr>
<tr><td>24.5%</td><td>45.5%</td><td>49.1%</td><td>63.5%</td><td>76.2%</td><td>85.9%</td><td>96.0%</td><td>100.0%</td></tr>
<tr><td>Points with |Discr|<0.02</td><td>Points with |Discr|<0.04</td><td>Points with |Discr|<Median</td><td>Points with |Discr|<0.06</td><td>Points with |Discr|<0.08</td><td>Points with |Discr|<0.10</td><td>Points with |Discr|<0.15</td><td>Points with |Discr|<0.20</td></tr>
<tr><td>0.020 ft</td><td>0.040 ft</td><td>0.045 ft</td><td>0.060 ft</td><td>0.080 ft</td><td>0.100 ft</td><td>0.150 ft</td><td>0.200 ft</td></tr>
</table>

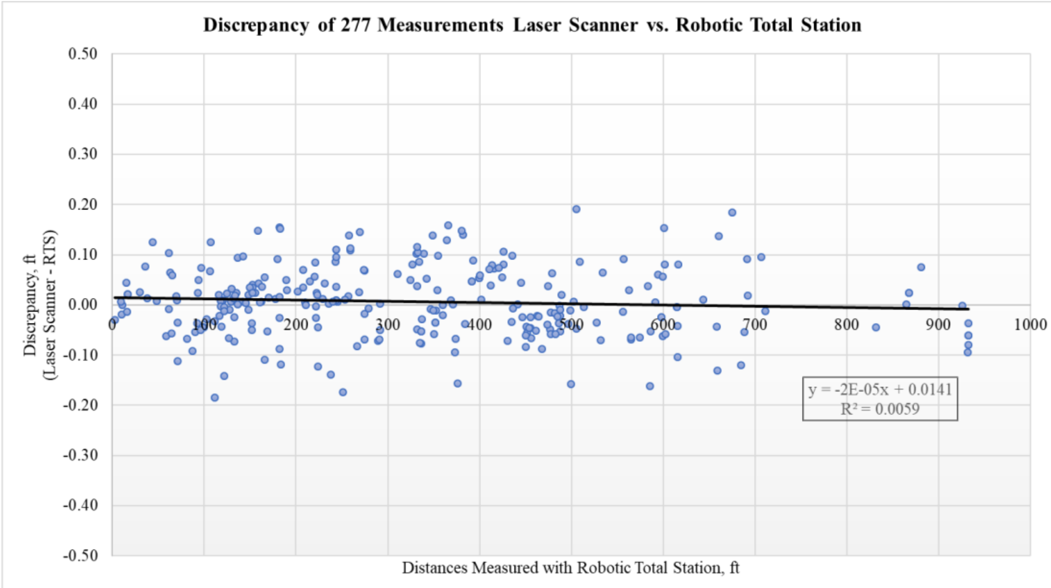

Figure 33: Graph – Discrepancy of 277 Measurements (Laser Scanner versus Robotic Total Station)

Aerial Close-Range Photogrammetry versus Robotic Total Station

Results for the aerial close-range photogrammetry approach in comparison to the accurate robotic total station are referred to in Appendix G. As shown in Table G.1, the discrepancies of northing and easting coordinates are consistent. However, the discrepancies of the elevation coordinates are inconsistent and very large. For example, the elevation discrepancy at point label S3 is 56.505 ft below the exact real-world position. A discrepancy of this magnitude is not ideal for accurate virtual surveying practices.

Though the results are not desirable for this case study, another study of a similar approach was conducted recently with different results. While assisting an undergraduate research team, they were able to employ the same Mavic Pro Quadcopter and obtain image data of a business building structure and construct a 3D photo-based model. The quadcopter was flown in a set path at an approximate height of 70 ft, with the downward vision camera system, above the topography which included the building structure. Then, the quadcopter was flown approximately 50 ft away from the building structure while the built-in camera acquired images at a 30° angle from the forward vision camera system. Approximately 140 images were employed to construct the 3D photo-based model, as seen in Figure 34. The photo-based model was geo-referenced with four known ground control points. The coordinates of these ground control points were obtained through a sophisticated closed-traverse procedure with the accurate one-second robotic total station. Then, a discrepancy analysis was performed against the accurate, one-second robotic total station.

Figure 34: Photo-Based Model of Building Structure and Topography

Coordinate discrepancies were calculated for all selected 47 points by subtracting the coordinates acquired by the robotic total station from those captured and marked with the photogrammetry method. They are listed in Table 13 where no outliers were discarded from this sample size. The ranges of these discrepancies (max and min values), their mean values, root mean square (RMS) values and standard deviations are summarized in Table 14. It can be observed that all three RMS values and their associated standard deviations range in magnitude from 0.07 ft to 0.15 ft (or from 0.84 inches to 1.8 inches). That is, about 23 mm to 46 mm each of them.

The measured coordinates of the selected center points (T01, L2, L34, L25, L32, and L24) are listed in Table 15. From each of these center points, a total of 46 distances (except 47 for T01) were calculated twice: (i) using coordinates obtained within the photo-based model and (ii) by employing coordinates captured by the total-station instrument. This resulted in 277 distances ranging from approximately 3 to 183 feet. Again, the corresponding discrepancies were calculated by subtracting the total-station distances from the scanned ones. Each major row of Table 15 shows results for a set of distances corresponding to a unique center point.

Table 13: Discrepancy in 47 Coordinates (Photogrammetry versus Robotic Total Station)

Discrepancy in Coordinates (UAV vs. Total Station)									
Sample Size	**Point Label**	**Diff. in Northing (ft)**	**Diff. in Easting (ft)**	**Diff. in Elevation (ft)**	**Sample Size**	**Point Label**	**Diff. in Northing (ft)**	**Diff. in Easting (ft)**	**Diff. in Elevation (ft)**
1	**L2**	-0.245	-0.021	-0.027	**25**	**L42**	0.053	-0.019	-0.056
2	**L4**	-0.147	0.035	-0.051	**26**	**L43**	-0.024	-0.123	0.009
3	**L6**	0.033	-0.033	-0.184	**27**	**L44**	0.062	0.122	-0.114
4	**L7**	-0.028	0.019	-0.143	**28**	**L47**	0.200	0.119	-0.772
5	**L8**	0.038	-0.101	-0.192	**29**	**L48**	-0.077	0.013	-0.090
6	**L9**	0.041	-0.085	-0.186	**30**	**L49**	0.205	0.109	-0.680
7	**L11**	0.117	-0.099	-0.104	**31**	**L50**	-0.199	0.104	-0.215
8	**L12**	0.171	-0.147	-0.155	**32**	**F15**	-0.087	-0.052	-0.079
9	**L13**	0.010	-0.002	0.060	**33**	**F16**	-0.133	-0.163	-0.116
10	**L15**	0.081	-0.034	-0.046	**34**	**F17**	-0.001	-0.063	0.012
11	**L16**	0.076	0.038	0.059	**35**	**F18**	0.015	-0.219	-0.272
12	**L20**	-0.110	0.021	0.110	**36**	**F19**	-0.056	-0.276	-0.170
13	**L21**	-0.080	-0.309	-0.244	**37**	**F20**	0.038	-0.211	-0.242
14	**L24**	0.053	-0.128	0.067	**38**	**F24**	-0.088	0.124	0.013
15	**L25**	-0.125	-0.043	-0.186	**39**	**F25**	-0.039	0.222	0.003
16	**L26**	-0.045	-0.158	-0.263	**40**	**F26**	-0.050	0.246	0.036
17	**L27**	0.033	-0.335	0.051	**41**	**F27**	0.062	0.166	0.101
18	**L28**	-0.142	-0.124	-0.335	**42**	**F28**	0.001	0.015	0.035
19	**L30**	-0.127	-0.165	-0.214	**43**	**F29**	0.071	0.078	0.050
20	**L31**	-0.055	-0.163	-0.041	**44**	**F30**	0.385	0.294	0.013
21	**L33**	-0.090	-0.149	-0.225	**45**	**F31**	-0.024	0.211	0.028
22	**L34**	-0.062	-0.072	-0.092	**46**	**F32**	-0.063	0.252	0.088
23	**L36**	0.191	-0.094	0.010	**47**	**F33**	-0.061	0.411	-0.051
24	**L38**	0.001	-0.104	-0.064					

Table 14: Statistical Analysis of 47 Absolute Coordinate Discrepancies

	|Diff.| in Northing (ft)	**|Diff.| in Easting (ft)**	**|Diff.| in Elevation (ft)**
Min =	0.001	0.002	0.003
Max =	0.385	0.411	0.772
Mean =	0.087	0.130	0.135
Std Dev. =	0.074	0.095	0.150
RMS =	0.114	0.161	0.202

Table 15: Analysis of Discrepancies in 277 Photogrammetric Measured Distances (Selected Center Points)

Selected Center Point	Employed Instrum. to acquire coords.	Coordinates of Center Points and their dicrepancies			ANALYSIS of DISCREPANCIES in 277 MEASURED DISTANCES						
		Northing (ft)	Easting (ft)	Elevation (ft)	Discrepancy in Center Location (ft)	# of Measured Distances	Abs. Min Discrep. (ft)	Abs. Max Discrep. (ft)	Abs. Mean Discrep. (ft)	Std Dev. Discrep. (ft)	RMS Discrep. (ft)
L34	UAV	707.483	366.052	235.359	0.132	46	0.003	0.319	0.106	0.134	0.134
	Total-Sta	707.545	366.124	235.451							
	Discrep.	-0.062	-0.072	-0.092							
F24	UAV	626.294	387.608	225.551	0.153	46	0.001	0.431	0.102	0.108	0.131
	Total-Sta	626.382	387.484	225.538							
	Discrep.	-0.088	0.124	0.013							
L25	UAV	748.412	400.581	237.327	0.228	46	0.001	0.357	0.124	0.139	0.153
	Total-Sta	748.537	400.624	237.513							
	Discrep.	-0.125	-0.043	-0.186							
T01	UAV	599.951	400.241	225.360	0.233	47	0.000	0.383	0.099	0.112	0.134
	Total-Sta	599.990	400.015	225.398							
	Discrep.	-0.039	0.226	-0.038							
L2	UAV	647.758	368.420	240.574	0.247	46	0.019	0.527	0.174	0.127	0.197
	Total-Sta	648.003	368.441	240.601							
	Discrep.	-0.245	-0.021	-0.027							
F32	UAV	622.758	461.534	223.496	0.274	46	0.003	0.448	0.206	0.113	0.234
	Total-Sta	622.821	461.282	223.408							
	Discrep.	-0.063	0.252	0.088							

Those rows were ordered by increased discrepancies in the location of their center points. This order shows some correlation with the column containing the RMS value of the associated discrepancies. All calculated discrepancies were plotted in Figure 35, where it can be observed that 50% of them (138) are in the ±0.1-foot range (approximately ±1 inch). Also, approximately 75% of the distances are within the ±0.2-foot range (Table 16). That is, the majority of the distances have a discrepancy that is not within the inherent error of the model which is related to the geo-referenced control points. However, at least half of the sample size has a discrepancy that is within the desired accuracy tolerance of ±1 inch.

Table 16 (a): Discrepancy Analysis of 277 Measured Distances in Traverse-Georeferenced Photo-Based Model

	Distance Measured (RTS, ft)	Discrepancy (ft)	Relative Discrepancy %	Absolute Discrepancy (ft)
Min =	2.938	-0.357	-3.314	0.000
Max =	183.479	0.527	3.043	0.527
Mean =		0.073	0.079	0.135
Std Dev. =		0.151	0.371	0.100
Median =		0.085	0.087	0.108
				Median of |Discr|

Table 16 (b): Discrepancy Analysis of 277 Measured Distances in Traverse-Georeferenced Photo-Based Model

Sum & %	Sum & %	Sum & %	Sum & %	Sum & %	Sum & %	Sum & %	Sum & %	Sum & %
13	26	60	93	138	207	257	272	277
4.7%	9.4%	21.7%	33.6%	49.8%	74.7%	92.8%	98.2%	100.0%
Points with |Discr|<0.010	**Points with |Discr|<0.020**	**Points with |Discr|<0.050**	**Points with |Discr|<0.080**	**Points with |Discr|<Median**	**Points with |Discr|<0.200**	**Points with |Discr|<0.300**	**Points with |Discr|<0.400**	**Points with |Discr|<0.530**
0.010 ft	0.020 ft	0.050 ft	0.080 ft	0.108 ft	0.200 ft	0.300 ft	0.400 ft	0.530 ft

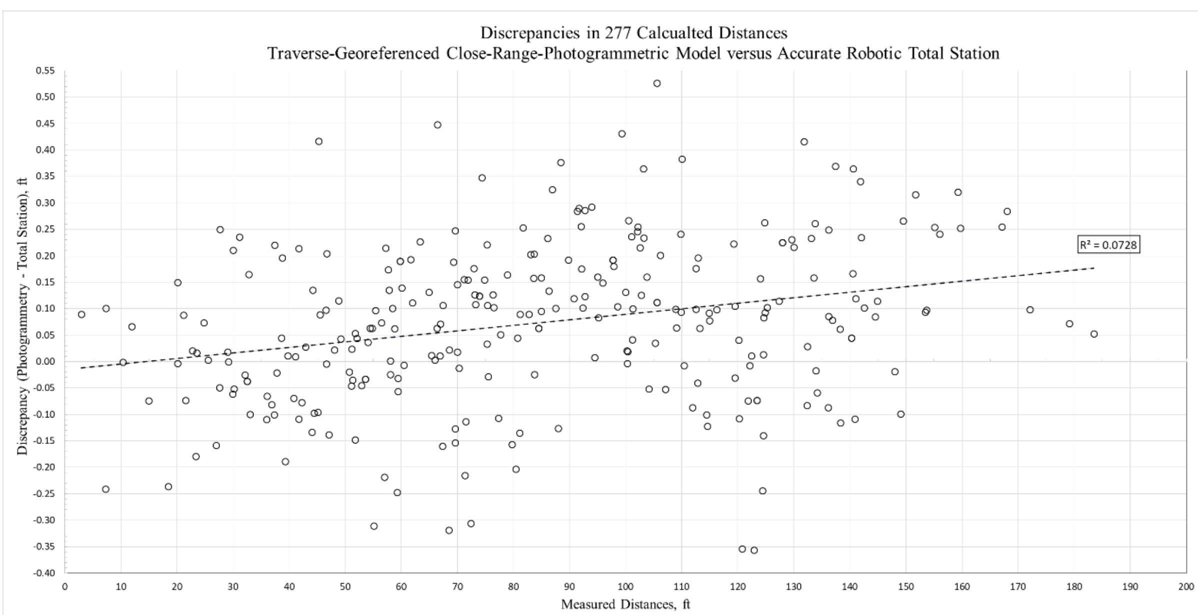

Figure 35: Graph – Discrepancies in 277 Calculated Distances Transverse-Georeferenced Close-Range Photogrammetric Model versus Accurate Robotic Total Station

CHAPTER 8

CONCLUSIONS

Case Study 1

In this study, three resulting point-cloud models were constructed with two types of registration methods, target-to-target and visual alignment. One of the point-cloud models were geo-referenced by employing GPS coordinates of seven control points. The non-georeferenced point cloud registered by the target-to-target method produced an overall error of 0 ft to 0.03 ft (≈ 0.4 in.) or 10 mm (Table 17). The georeferenced point cloud registered by the target-to-target method produced an overall error of 0.033 ft (≈ 0.4 inches) to 0.10 ft (≈ 1.2 in.) or 31 mm. The non-georeferenced point cloud registered by the visual alignment method produced an overall error of 0.003 ft (0.04 inches) or 1 mm to 0.02 ft (≈ 0.3 in.) or 7 mm. In this work, these errors are referred to as the inherent errors of the model. Point positions of the non-georeferenced point-cloud models, compared to the accurate benchmark instrument, were not analyzed due to the difference in coordinate systems within the model and the known Georgia East SPCS. Yet, distance measurements were employed to compare the three point-cloud registrations. All 211 distances ranged between approximately 11 ft to 717 ft. For the target-to-target, non-georeferenced point-cloud, most of the discrepancies (68.2%), compared to the total station, were within 0.10 foot-range (1.2 inches). It was observed that approximately 27% of the 211 discrepancies were within the inherent error of this point-cloud. Also, the visually aligned non-georeferenced point-cloud had approximately 57.8% of discrepancies, compared to the total station, that were within the 0.10 foot-range (1.2 inches). It was observed that approximately 19% of these discrepancies were within the inherent error of this point-cloud. The target-to-target georeferenced point-cloud model had most discrepancies (64.9%) within the 0.10 foot-range (1.2 inches), in which these discrepancies were within the inherent error of this point-cloud. As shown in Figure 36, a comparison of the absolute-valued discrepancies based on the percentage of the distances with fewer absolute discrepancies was created for observation. Half of the 211 distances measured consisted of absolute discrepancies that were approximately 0.06 ft (0.72 inches) in the target-to-target, non-georeferenced registration, 0.07 ft (0.84 inches) in the target-to-target, geo-referenced registration and 0.08 ft (0.96 inches) in the visually-aligned non-georeferenced point-cloud. Each registration, represented in the graph, shows a similar trend line. When more distances are included in the study, then more absolute discrepancies will appear. Notice the target-to-target, non-georeferenced and georeferenced registrations have close percentages of distances with absolute discrepancies, starting at approximately 82% of the distances with an absolute discrepancy of 0.15 ft (1.80 inches). The visually-aligned, non-georeferenced registration displayed a lower percentage of distances with a similar value of absolute discrepancies, compared to the target-to-target registrations. Overall, with the sample of the distances measured with each registration method, the target-to-target georeferenced point cloud produces discrepancies within the ±1-inch tolerance for redesign/construction work of the city street intersection.

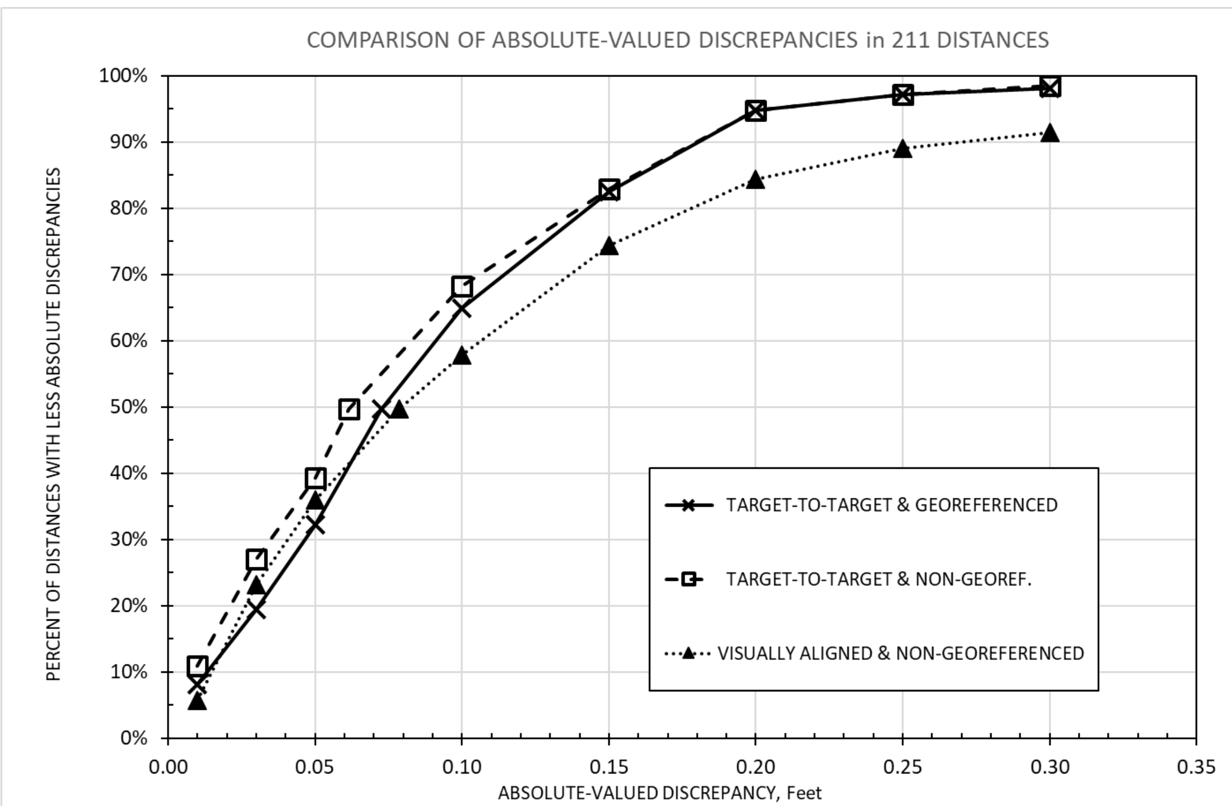

Figure 36: Graph – Comparison of Absolute-Valued Discrepancies in 211 Distances

Table 17: Comparison of Case Study 1 Results (Software Error versus Calculated Discrepancy to the Robotic Total Station)

Comparison of Inherent Software Error vs. Calculated Distance Discrepancy to R.T.S.			
Non-Georeferenced (Target-to-Target) Point-Cloud Model			
	(ft)	**(in)**	**(mm)**
Inherent Software Error	0.033	0.394	**10**
Calculated Overall Distance Discrepancy	0.081	0.972	**25**
Georeferenced (Target-to-Target) Point-Cloud Model			
	(ft)	**(in)**	**(mm)**
Inherent Software Error	0.102	1.220	**31**
Calculated Overall Distance Discrepancy	0.088	1.056	**27**
Non-Georeferenced (Visually Aligned) Point-Cloud Model			
	(ft)	**(in)**	**(mm)**
Inherent Software Error	0.023	0.276	**7**
Calculated Overall Distance Discrepancy	0.113	1.356	**34**

Case Study 2

In this study, the resulting point-cloud model was geo-referenced by employing GPS coordinates of seven control points. They corresponded to scanned targets T1, T3, T5, T9, T11, T19, and T21. These coordinates were acquired at the beginning of the study via a rapid, network-based, RTK scheme that increased the overall error of the virtual model, from 0.033 ft (≈ 0.4 in.) or 10 mm to 0.101 ft (≈ 1.2 in.) or 31 mm (Table 18). In this work, this error is referred to as the inherent error of the model. The resulting spatial coordinates of numerous points in the selected intersection area, do not substantially differ if they were captured by either a laser-based, one-second, survey-grade, robotic, total station or from the model produced by a less accurate, twelve-second, laser scanner. Same as Case Study 1, After considering 36 points widely distributed within the modeled area (i.e., discarding 2 outliers), the standard deviations of the discrepancies in point positions almost coincide with their associated RMS values: RMS_{North}=0.09 ft, RMS_{East}=0.08 ft, and RMS_{Elev}=0.05 ft. That is, the standard deviations of those discrepancies range from

0.6 to 1.1 inches (or from 15 to 28 mm) in the considered intersection area. This is consistent with the inherent or minimum relative position error in this study, 0.101 ft or 31 mm (Table 18).

Regarding the discrepancies in distances, the coordinates of the referred 36 points were employed to calculate numerous distances between themselves and six points that served as centers (T9, N1, N2, N3, S4, and S6). A total of 211 distances, ranging from 11 feet and to 717 feet, were determined in this fashion, within the modeled intersection. Overall, most of them (65%) showed discrepancies within the ±0.10-foot range (±1.2 inches), i.e. within the inherent error of the point-cloud model incorporated by the GPS-based control points. 175 discrepancies, out of the 211 (83%), remained within the ±0.15-foot range (±1.8 inches) and 199 (94%) are within the ±0.20-foot range (±2.4 inches). Additionally, it is observed that the discrepancies of measured distances are not correlated to the magnitudes of those distances. The R-Squared value for these two variables is very low ($R^2 \approx 0.044$). However, Figure 30 shows a tendency with a negative slope as distances increase. Since total-station distances are subtracted from point-cloud-model distances, this could indicate that the resulting model tends to slightly underestimate distances as they increase in magnitude.

Finally, from a practical point of view, if the design/construction of an intersection, similar in size to the selected one, requires working within one-inch accuracy, the procedure presented in this study is close to that requirement, but some distances may not be within that tolerance. Geo-referencing control points with low accuracy contributed to the observed discrepancies. Since the non-georeferenced model had a lower overall error (3 times smaller), it would have produced more accurate relative distances. If geo-referencing was necessary for design/construction purposes, acquiring highly accurate coordinates for the geo-referencing control points would be recommended. This could reduce the magnitude of the inherent error 3 times with respect to the value observed in this study. In other words, if the coordinates of the geo-referencing control points were obtained with an accuracy of ±0.033 ft (±10 mm), it is expected that most virtual distances, extracted from the point-cloud model, will not defer in more than ±1 inch (±25 mm) from accurate field measurements completed with a survey-grade total station.

Table 18: Comparison of Case Study 2 Results (Software Error versus Calculated Discrepancy to the Robotic Total Station)

Comparison of Inherent Software Error vs. Calculated Point and Distance Discrepancy to R.T.S.				
Georeferenced (Target-to-Target) Point-Cloud Model				
		(ft)	**(in)**	**(mm)**
Inherent Software Error		0.102	1.220	**31**
Point Discrepancy	**Northing**	0.068	0.820	**21**
	Easting	0.065	0.778	**20**
	Elevation	0.038	0.454	**12**
Distance Discrepancy		0.088	1.056	**27**

Case Study 3

For the laser scanning technology, 47 points were widely distributed within the modeled area (i.e., discarding 5 outliers). The standard deviations of the discrepancies in point positions almost coincide with their associated RMS values: RMS_{North}=0.18 ft, RMS_{East}=0.13 ft, and RMS_{Elev}=0.13 ft. That is, the standard deviations of those discrepancies range from 0.05 to 0.06 ft (or from 15 to 18 mm) in the considered intersection area. These statistical values are consistent with the inherent or minimum relative position error in this study, 0.085 ft or 26 mm, as shown in Table 19. Also, approximately 77% of the sample size in distance measurements were within the overall point-cloud error that was produced by the corresponding laser scanning software.

In Appendix G, a conclusion is explained on the overall results of the photogrammetry methodology for City Street Intersection 2. However, 47 points were widely distributed in the photo-based model of the building structure and topography study area. With no outliers discarded from this study, the standard deviations of the discrepancies in point positions did coincide with their associated RMS values: RMS_{North}=0.11 ft, RMS_{East}=0.16 ft, and RMS_{Elev}=0.20 ft. That is, the standard deviations of those discrepancies range from 0.11 to 0.17 ft (or from 34 to 52 mm) in the 3D modeled structure and infrastructure areas.

However, the discrepancies were inconsistent with the inherent error for the 47 point coordinates which was 0.001 ft (0.013 inches) or 4 mm, as shown in Table 19. Also, the inherent error for the 277 measured distances was 0.008 ft (0.091 inches) or 28 mm (Table 19). Though most position and distance discrepancies were not within the inherent PhotoScan software error, these discrepancies were more accurate than the results from Appendix G. Since the desired field discrepancy is one inch for this study, the methodology employed for the building structure, surrounding infrastructure and topography displayed a remarkable improvement for the aerial close-range photogrammetry technology. Yet for the comparison of the modern employed technologies, the 3D Terrestrial LiDAR is more appropriate for this particular study. To assist the Blue-Mile group and the Statesboro city engineers, laser scanning technology produces more reliable information for redesigning a city street infrastructure with virtual surveying methods.

Table 19: Comparison of Case Study 3 with Improved Results (Inherent Software Error versus Calculated Point and Distance Discrepancy to Robotic Total Station)

Inherent Software Error vs. Calculated Point and Distance Discrepancy to R.T.S.				
Geo-referenced (Target-to-Target) Point-Cloud Model (City Street Infrastructure)				
		(ft)	**(in)**	**(mm)**
Inherent Software Error		**0.085**	**1.024**	**26**
Point Discrepancy	**Northing**	0.052	0.624	16
	Easting	0.039	0.468	12
	Elevation	0.042	0.504	13
Distance Discrepancy		0.053	0.636	16
Traversed-Georeferenced Photo-Based Model (Building Structure and Parking Lot Infrastructure)				
		(ft)	**(in)**	**(mm)**
Inherent Software Point Error		**0.001**	**0.013**	**4**
Point Discrepancy	**Northing**	0.087	1.045	27
	Easting	0.130	1.554	39
	Elevation	0.135	1.621	41
Inherent Software Distance Error		**0.008**	**0.091**	**28**
Distance Discrepancy		0.135	1.620	41

Improvements for Study

In close-range photogrammetry, data collection from unmanned aerial vehicles reduces the amount of time in the field, which is cost efficient compared to terrestrial laser scanning. Yet, post-processing data with PhotoScan is more tedious, time-consuming and less accurate than the laser-scanner software, Leica Cyclone. From the results, laser scanning is confirmed to be a validated method of measuring 277 distances within a virtual world model. On the other hand, the employed, close-range photogrammetry technique from an approximate altitude of 72 ft (22 meters), using a 12 Megapixel camera, produced considerably larger errors (Appendix G). However, UAV flight altitude can be decreased within the recommended obstacle sensory range for precision measurement (Table A.3). For example, the improved aerial photogrammetry study displayed better results when the distance between the surface of the building structure and the built-in camera was approximately 50 ft (which was close to the recommended obstacle sensory range). Also, increasing the camera resolution will produce a better post-process to acquire points within the image data. Unmanned aerial vehicles are improving as time proceeds since these technologies are employed in more applications.

Also, terrestrial laser scanning technology has improved since the Built Environment and Modeling lab of Georgia Southern University purchased the Leica C10 Scan Station. Now, newer laser scanners now have the capability to acquire more scan data within a less time duration, at a longer range. Also, field targets (i.e. HDS Sphere targets) that are employed for point-cloud constraints in the Cyclone software have become larger in size. These larger sphere targets help the scanner operator to acquire them easily in the field which helps to reduce the discrepancy at the center of the target point. With these improved technologies in today's market, surveying and engineering professionals can consider them to be applied in most of their engineering applications. Certain standards of accuracy are to be followed in particular applications, such as the presented case studies. Methods to produce a 3D point-cloud model can affect the accuracy of the desired data. However, the method of geo-referencing a 3D laser-scanned point-cloud model with GPS coordinates, acquired through the RTK approach, does not defer the data that is required to be within or close to the accuracy standard which is set by the surveyor or engineering professional for redesign/construction purposes.

REFERENCES

"3D Scanning Technology — Hard Work That Looks Like 'Magic.'" *Laser Design Inc*, CyberOptics Corporation, 2019, www.laserdesign.com/what-is-3d-scanning.

Agisoft. PhotoScan. (2017). [WWW document]. URL http://www.agisoft.com

Buffi, Giulia, et al. "Survey of the Ridracoli Dam: UAV–based photogrammetry and traditional topographic techniques in the inspection of vertical structures." *Geomatics, Natural Hazards and Risk* 8.2 (2017): 1562-1579.

Cultural Heritage Imaging. "Guidelines for Calibrated Scale Bar Placement and Processing." *Cultural Heritage Imaging*, 2015, www.agisoft.com/pdf/tips_and_tricks/CHI_Calibrated_Scale_Bar_Placement_and_Processing.pdf.

Dai, Fei, et al. "Comparison of image-based and time-of-flight-based technologies for three-dimensional reconstruction of infrastructure." *Journal of construction engineering and management* 139.1 (2012): 69-79.

"DJI Mavic Pro Platinum – Specs, Tutorials & Guides – DJI." *DJI Official*, 2019, www.dji.com/mavic-pro-platinum/info#specs.

"GPS Accuracy." *GPS.gov: GPS Accuracy*, National Coordination Office for Space-Based Positioning, Navigation, and Timing, 2017, www.gps.gov/systems/gps/performance/accuracy/.

Gruszczyński, Wojciech, Wojciech Matwij, and Paweł Ćwiąkała. "Comparison of low-altitude UAV photogrammetry with terrestrial laser scanning as data-source methods for terrain covered in low vegetation." *ISPRS Journal of Photogrammetry and Remote Sensing* 126 (2017): 168-179.

Inglot, Adam, and Paweł Tysiąc. "Airborne Laser Scanning Point Cloud Update by Used of the Terrestrial Laser Scanning and the Low-Level Aerial Photogrammetry." *Geodetic Congress (BGC Geomatics), 2017 Baltic*. IEEE, 2017.

Kršák, B., et al. "Use of low-cost UAV photogrammetry to analyze the accuracy of a digital elevation model in a case study." *Measurement* 91 (2016): 276-287.

Leica Geosystems (2010), Leica ScanStation C10, User and System Field Manuals, Version 1.0.

Majid, Z., et al. "Three-dimensional mapping of an ancient cave paintings using close-range photogrammetry and terrestrial laser scanning technologies." *ISPRS-International Archives of the Photogrammetry, Remote Sensing and Spatial Information Sciences* (2017): 453-457.

Maldonado, G. O., Maghiar, M., Jackson N. M., Garrett, D. M. and Givens K. E. (2015). Comparison of Building Measurements Acquired via Laser-Based Scanner and Modern Total Station. 51st ASC Annual International Conference Proceedings.

"Real-Time Kinematic (RTK)." NovAtel, Hexagon Positioning Intelligence, www.novatel.com/an-introduction-to-gnss/chapter-5-resolving-errors/real-time-kinematic-rtk/.

Riveiro, Belén, et al. "Validation of terrestrial laser scanning and photogrammetry techniques for the measurement of vertical underclearance and beam geometry in structural inspection of bridges." *Measurement* 46.1 (2013): 784-794.

Siebert, Sebastian, and Jochen Teizer. "Mobile 3D mapping for surveying earthwork projects using an Unmanned Aerial Vehicle (UAV) system." *Automation in Construction* 41 (2014): 1-14.

Strach, Michał, and Piotr Dronszczyk. "Comprehensive 3D Measurements of Tram Tracks in the Tunnel Using the Combination of Laser Scanning Technology and Traditional TPS/GPS Surveying." *Transportation Research Procedia*, vol. 14, Jan. 2016, pp. 1940–1949. *EBSCOhost*, doi:10.1016/j.trpro.2016.05.161.

"State of: Close-Range Photogrammetry." XyHt, Flatdog Media, 25 June 2014, www.xyht.com/lidarimaging/state-of-close-range-photogrammetry/.

UrbanGeekz Staff. "5 Advanced Technologies Used in Civil Engineering." *UrbanGeekz*, 30 Jan. 2018, urbangeekz.com/2018/01/5-advanced-technologies-used-in-civil-engineering/.

Useful Tips on Image Capture: How to Get an Image Dataset That Meets PhotoScan Requirements? Agisoft PhotoScan, www.agisoft.com/pdf/tips_and_tricks/Image%20Capture%20Tips%20-%20Equipment%20and%20Shooting%20Scenarios.pdf.

"What Is Remote Sensing and What Is It Used for?" *USGS Science for a Changing World*, www.usgs.gov/faqs/what-remote-sensing-and-what-it-used?qt-news_science_products=7#qt-news_science_products.

Yu, Xueqin, and Tao Zhang. "Application of terrestrial 3D laser scanning technology in spatial information acquisition of urban buildings." *Image, Vision and Computing (ICIVC), 2017 2nd International Conference on*. IEEE, 2017.

APPENDIX A

DJI MAVIC PRO PLATINUM QUADCOPTER SPECIFICATIONS

Table A.1 DJI Mavic Pro Aircraft Specifications (Adapted from DJI Official, 2019)

AIRCRAFT	
Folded	H83mm x W83mm x L198mm
Diagonal Size (Propellers Excluded)	335 mm
Weight (Battery & Propellers Included)	1.62 lbs (734 g) (exclude gimbal cover)
	1.64 lbs (743 g) (include gimbal cover)
Max Ascent Speed	16.4 ft/s (5 m/s) in Sport mode
Max Descent Speed	9.8 ft/s (3 m/s)
Max Speed	40 mph (65 kph) in Sport mode without wind
Max Service Ceiling Above Sea Level	16404 feet (5000 m)
Max Flight Time	30 minutes (no wind at a consistent 15.5 mph (25 kph))
Max Hovering Time	27 minutes (no wind)
ESC(Electronic Speed Controller)	FOC
Max Total Travel Distance (One Full Battery, No Wind)	9.3 mi (15 km, no wind)
Operating Temperature Range	32° to 104° F (0° to 40° C)
Satellite Positioning Systems	GPS / GLONASS
Hover Accuracy Range	Vertical: +/- 0.1 m (when Vision Positioning is active) or +/-0.5 m
	Horizontal: +/- 0.3 m (when Vision Positioning is active) or +/-1.5 m
Operating Frequency	FCC: 2.4-2.4835GHz; 5.150-5.250 GHz; 5.725-5.850 GHz
	CE: 2.4-2.4835GHz; 5.725-5.850 GHz
	SRRC： 2.4-2.4835 GHz;5.725-5.850 GHz
Transmitter Power (EIRP)	2.4GHz FCC:<=26 dBm; CE: <=20 dBm; SRRC:<=20 dBm; MIC:<=18 dBm
	5.2 GHz FCC:<=23 dBm
	5.8 GHz FCC:<=23 dBm; CE <=13 dBm; SRRC: <=23 dBm; MIC: -

Table A.2: DJI Mavic Pro Camera Specifications (Adapted from DJI Official, 2019)

CAMERA	
Sensor	1/2.3” (CMOS), Effective pixels:12.35 M (Total pixels:12.71M)
Lens	FOV 78.8° 26 mm (35 mm format equivalent) f/2.2
	Distortion < 1.5% Focus from 0.5 m to ∞
ISO Range	video: 100-3200
	photo: 100-1600
Electronic Shutter Speed	8s -1/8000 s
Image Size	4000×3000
Still Photography Modes	Single shot
	Burst shooting: 3/5/7 frames
	Auto Exposure Bracketing (AEB): 3/5 bracketed frames at 0.7 EV Bias
	Interval
Video Recording Modes	C4K: 4096×2160 24p
	4K: 3840×2160 24/25/30p
	2.7K: 2720x1530 24/25/30p
	FHD: 1920×1080 24/25/30/48/50/60/96p
	HD: 1280×720 24/25/30/48/50/60/120p
Max Video Bitrate	60 Mbps
Supported File Systems	FAT32 (≤ 32 GB); exFAT (> 32 GB)
Photo	JPEG, DNG
Video	MP4, MOV (MPEG-4 AVC/H.264)
Supported SD Cards	Micro SD™
	Max capacity: 128 GB. Class 10 or UHS-1 rating required
Operating Temperature Range	32° to 104° F (0° to 40° C)

Table A.3: DJI Mavic Pro Vision System Specifications (Adapted from DJI Official, 2019)

VISION SYSTEM	
Vision System	Forward Vision System
	Downward Vision System
Obstacle Sensory Range	Precision measurement range: 2 ft (0.7 m) to 49 ft (15 m) Detectable range: 49 ft (15 m) to 98 ft (30 m)
Operating Environment	Surface with clear pattern and adequate lighting (lux > 15)
Velocity Range	≤22.4 mph (36 kph) at 6.6 ft (2 m) above ground
Altitude Range	1 - 43 feet (0.3 - 13 m)
Operating Range	1 - 43 feet (0.3 - 13 m)

Table A.4: DJI Mavic Pro Gimbal Specifications (Adapted from DJI Official, 2019)

GIMBAL	
Controllable Range	Pitch: -90° to +30°
	Roll: 0° or 90° (Horizontally and vertically)
Stabilization	3-axis (pitch, roll, yaw)

APPENDIX B

LASER SCANNING PROTOCOL

Free Scanning with Targets using Leica ScanStation C10

Quick Reference Manual for scanning without a laptop

Student Training Manual

Developed By Jerome Clendenen

Typical Scanner and Target Setup

Scan Resolution Settings

Resolution Setting	Point Spacing at 100 meters	Point spread increase per meter of distance from the scanner	Max range of recorded point	Time to complete a scan	Estimated Number of Scans per hour including target acquisition
Low	.20m Or 20cm	.002m Or 2mm	100 meter	1 minute 50 seconds	5-6
Medium	.10m Or 10cm	.001m Or 1mm	100 meter	6 minutes 55 seconds	3-4
High	.05m Or 5cm	.0005m Or .5mm	100 meter	27 minutes 30 seconds	1.8
Highest	.02m Or 2cm	.0002m Or .2mm	100 meter	170 minutes	.35

ScanStation C10 Components

Target Assemblies

Twin Target Pole

Ext. Twin Target Pole

Single 6" HDS

Single 6" B & W

6" HDS Shere

ScanStation C10 Display Window Definitions

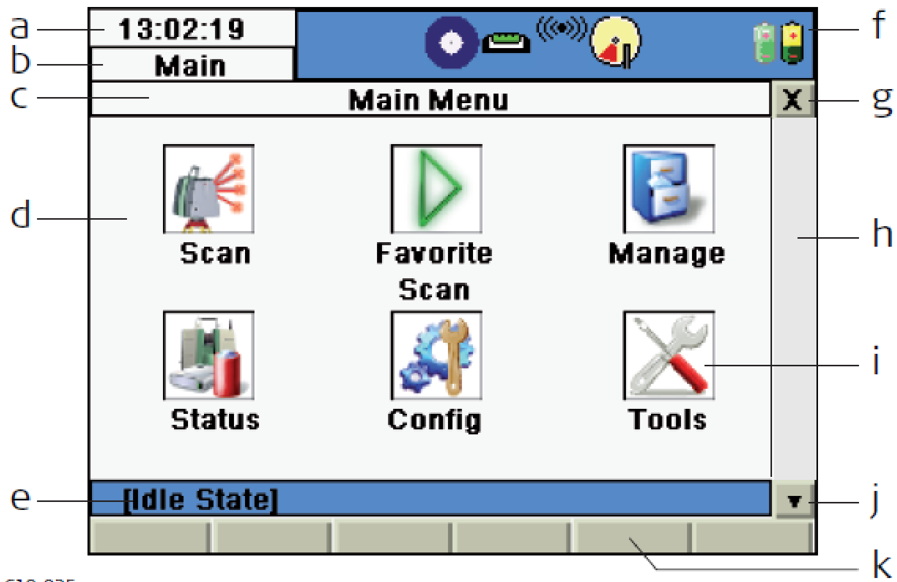

C10_035

a) Time
b) Caption
c) Title bar
d) Screen area
e) Message bar
f) Status bar
g) Escape button
h) Scroll bar
i) Menu icon
j) SHIFT button
k) Softkeys

The icons in the status bar display the current status information of the instrument. Clicking a status icon gives direct access to a detailed status description.

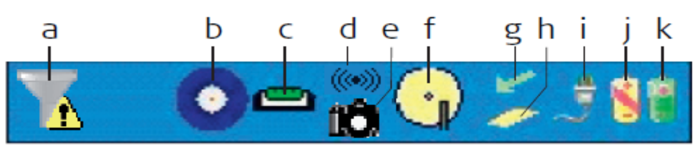

C10_036

a) Range Filter
b) Active target type
c) Dual-axis compensator*
d) WiFi
e) External camera
f) Internal hard disc
g) Status of external memory
h) External memory
i) External battery / AC power supply
j) Internal battery A
k) Internal battery B

* Optional for C5

Battery installation A and B

Hot Swap procedure

Target Heights and Dimensions

Leveling targets

	**Determining the Instrument Height** Supplied tape measure to obtain instrument height in meters
	This clips to one on the tribrach knob poles and the end of the tape clip in to it. Flip out the black tab on the bottom of tape case and touch it to the ground or nail below the C10. See the next picture

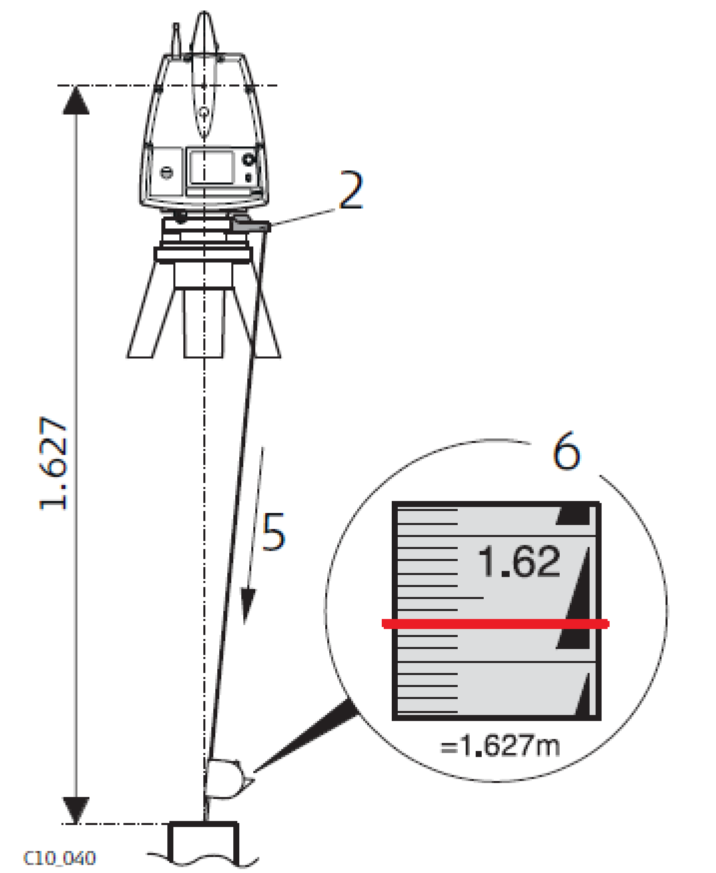

1. Place tripod centrally over the ground point, level instrument.
2. Click GHT196 distance holder to tribrach. It must "snap" onto the cover over an adjusting screw.
3. Unfold measuring tongue, pull out tape measure a little.
4. Insert GHM008 instrument height meter in the distance holder and attach.
5. Swivel measure in the direction of the ground point, pull out until the tip of the measuring tongue touches the point on the ground, keep under tension and do not allow to sag, clamp if necessary.
6. Read height of the instrument (ground - tilt axis) in the reading window at the red marking (in the example 1.627 m).

GENERAL PROCEDURES OVER VIEW

SETUP

Began by mounting the C10 on the tripod and leveling the scanner using exterior circle level.

Turn on C10 by pressing the silver power button.

Select Status icon

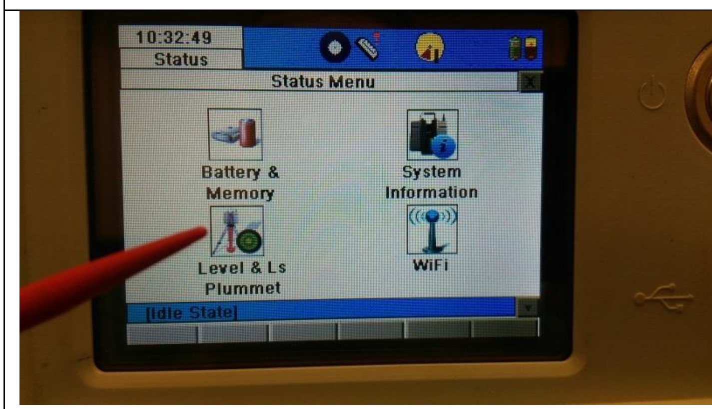

SETUP

Select Level & Ls Plummet icon

Internal Level Bubble

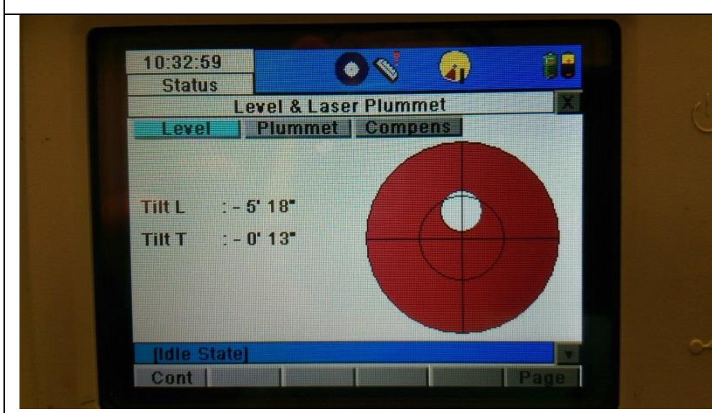

SETUP

Level is out of range when red

<table>
<tr>
<td>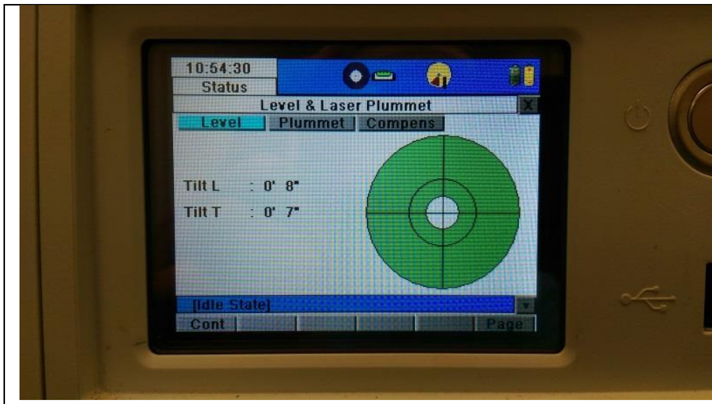
</td>
<td>SETUP

Level is within range when green
The Dual Axis Compensator (DAC) is active when green.</td>
</tr>
</table>

<table>
<tr>
<td>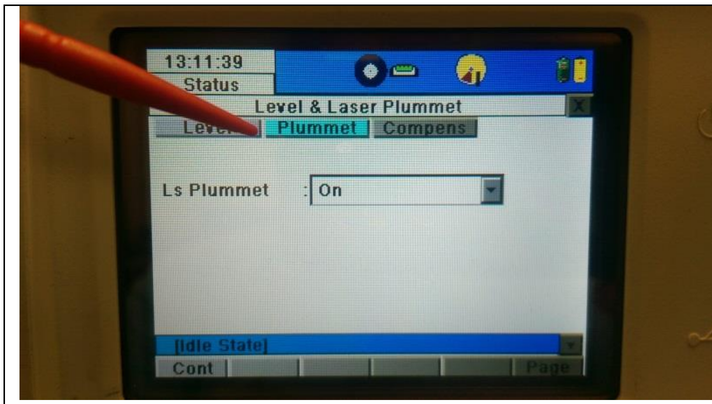
</td>
<td>SETUP

Select Plummet

To use the Laser Plummet to mark ground location</td>
</tr>
<tr>
<td>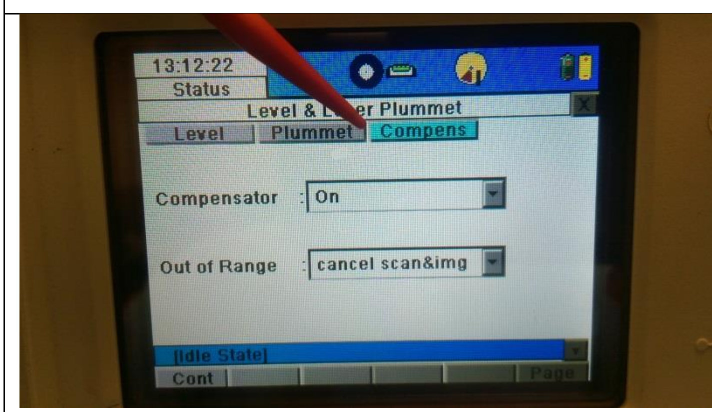
</td>
<td>SETUP

Compens

Turns the compensator on/off

And

Out of Range options</td>
</tr>
</table>

SETUP

Select Cont to proceed

SETUP

Status bar will display current information when pressed and held using the stylus

Creating Project

Create a new project to store scan data

Manage

<table>
<tr>
<td>
</td>
<td>Creating Project

Projects</td>
</tr>
<tr>
<td>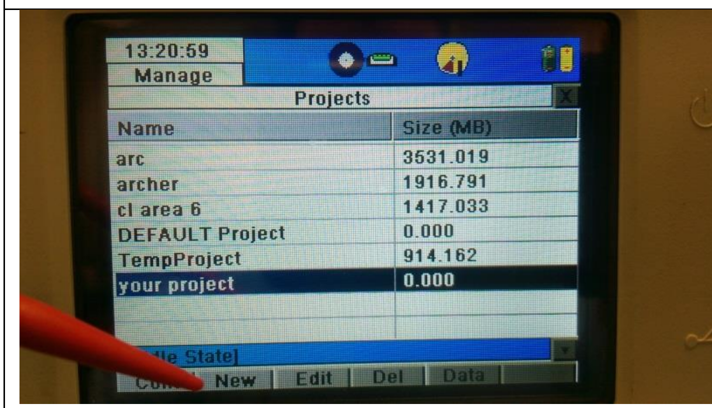
</td>
<td>Creating Project

New to create new project

Or

Select an existing project

Then

Cont</td>
</tr>
<tr>
<td>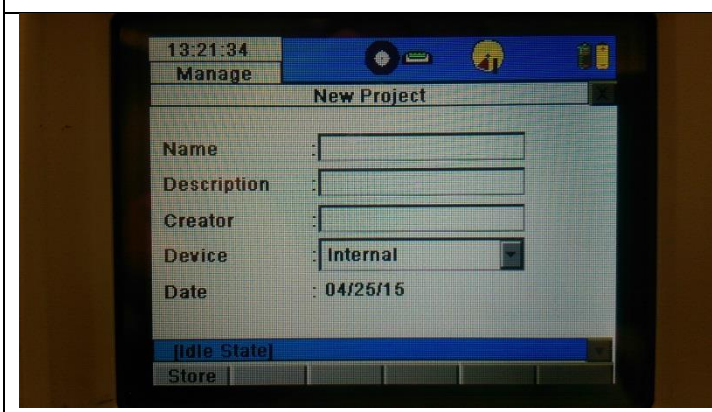
</td>
<td>Creating Project

To name the project touch name box with stylus</td>
</tr>
</table>

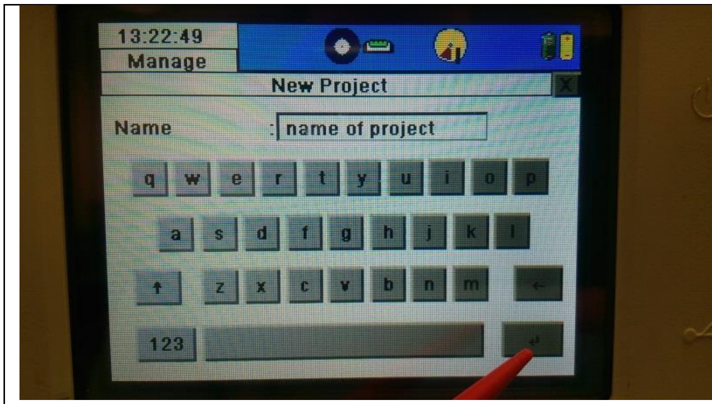

Creating Project

Use the keyboard that appears to type name

Creating Project

Enter a description if desired

Creating Project

Added creators name and locate to store the data

Store button to save the project

Creating Project

Cont

To proceed with the highlighted job

Or

Touch the preferred job to highlight then **cont**

Scan Setup

To start the scan process select the

Scan icon

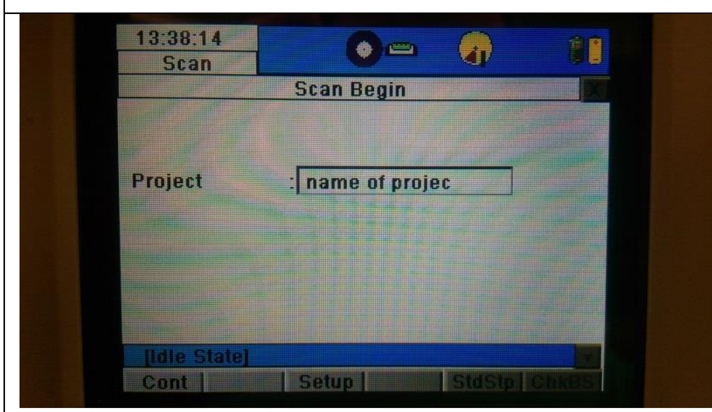

Scan Setup

The current project name appears in box
If this is the correct project select **cont**

If not, touch name box and the project list will appear.
Highlight the correct project and

Cont

Select **StdStp**

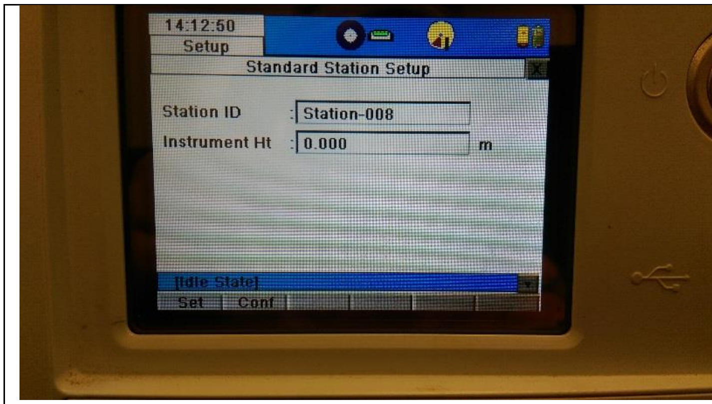	**Scan Setup** Standard Setup uses preset settings Enter Instrument Height for this station Select **enter** button
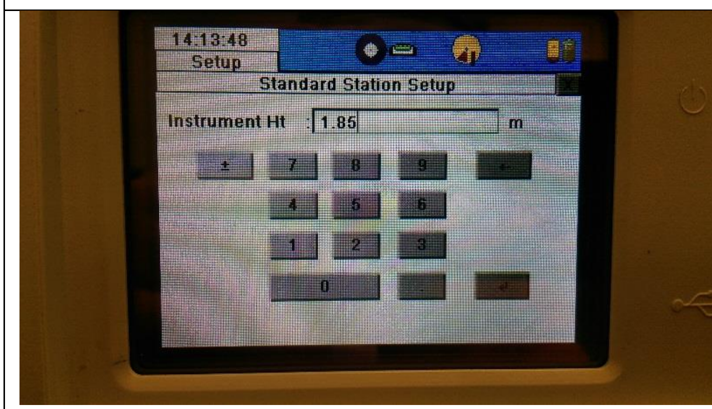	**Scan Setup** Select **Set** to store station Information This store the station ID and HI Scan Parameter screen appears

	**Scan Setup** Field of View definition selection screen **Target All** is most common setting

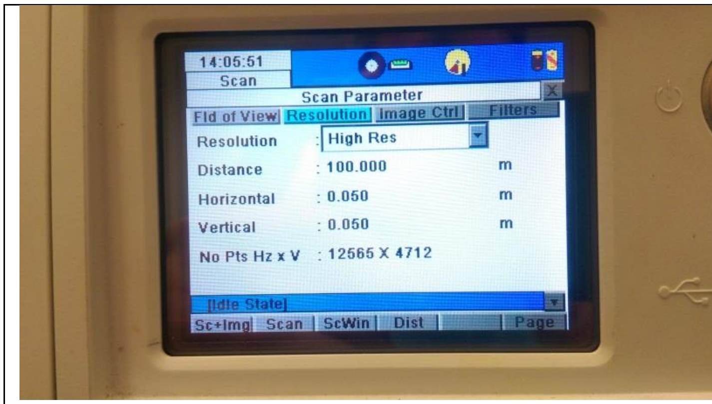	**Scan Setup** Resolution Selection Screen <u>Options:</u> Custom High Med Low (see page two for table x.xx)
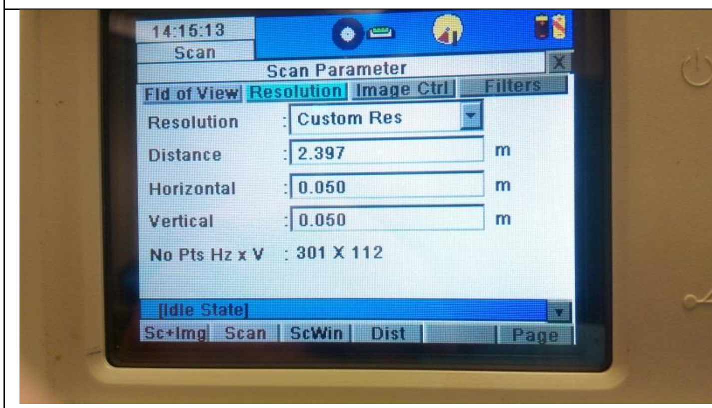	**Scan Setup** **Distance -** OPTIONAL Distance measurement to help determine the resolution at the measured distance from the C10 Example from picture on the left Distance = 2.397m with a 0.05m x 0.05m point spread No Pts Hz x V = 301 x 112 Total Pts = 301*112 = 33712 pts in this scan
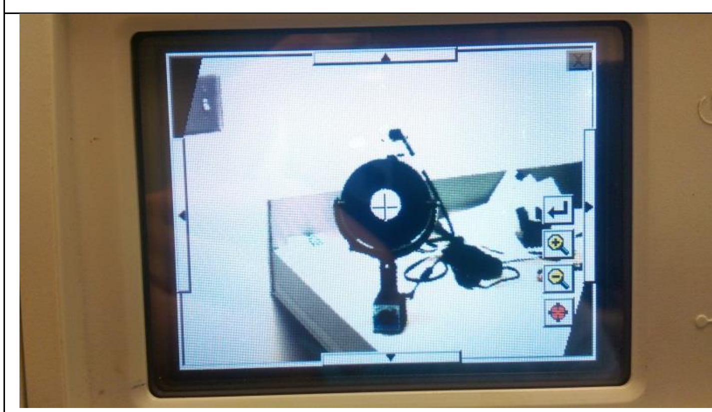	**Scan Setup** **Distance -** OPTIONAL Select **Dist** and pick from video image on screen Select item to measure distance from scanner using the **seek** button (red) Then **Enter** button Back to Scan Parameter screen

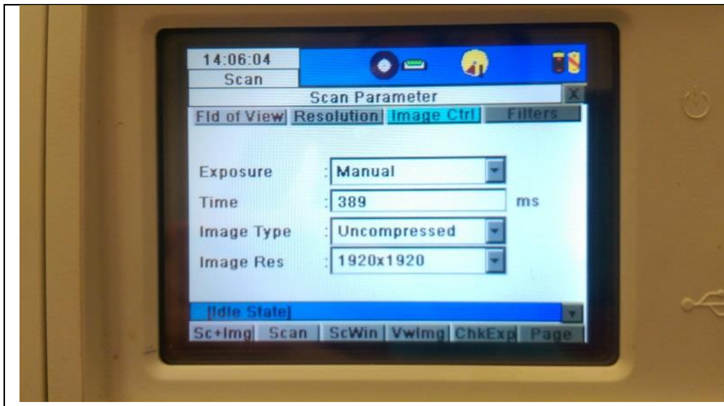	**Scan Setup** **Image Control to adjust the camera's contrast** **Chkexp**
	**Scan Setup** Use the Slide bar to control exposure Then select the **enter** button Use the **Seek** button focus camera to interest area.
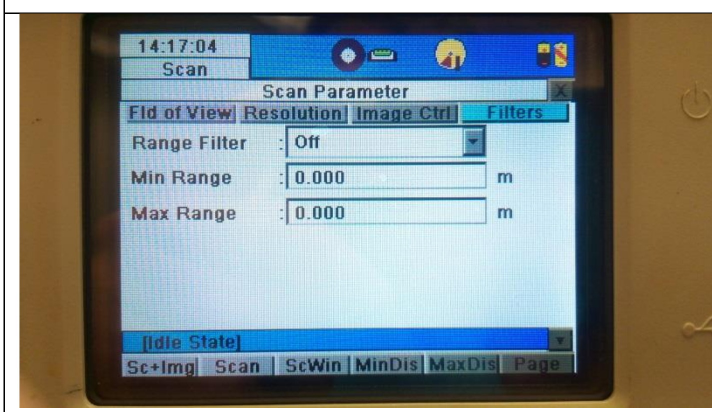	**Scan Setup** Filters This limits the minimum and maximum distances that the sensor will record data when turned on.

Scan Setup

Button to right of idle state bar show more options

It is a triangle that points down for one menu and when touch by the stylus will point up.

When the triangle points up the Target menu is displayed.

Select **Target** to add targets to the scan

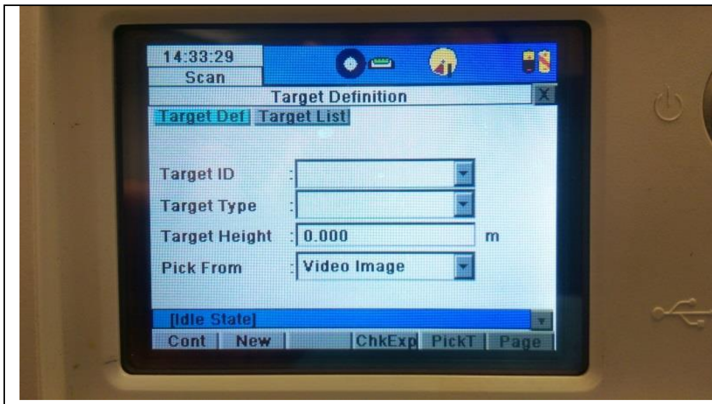

Scan Setup for Targets

Targets are preferred to be scanned before study area. If there are problems with targets it is better to discover before scanning the study.

Select the **Target** button below or **Target Icon** on top to open the Target Definition screen

Define the targets

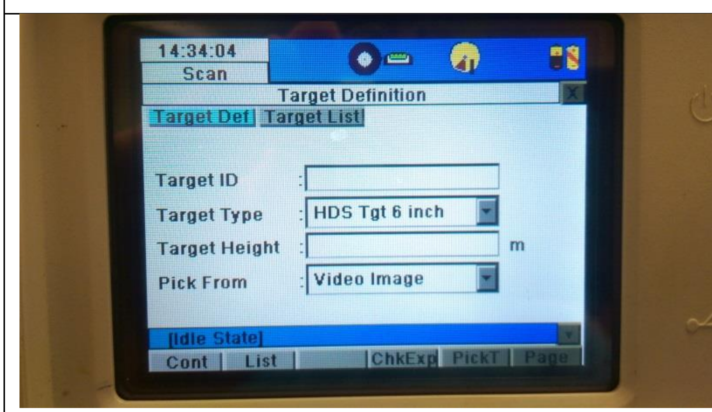

Scan Setup for Targets

Select the type of target being used from pull-down menu

Enter the Target ID and Target Height

Twin Targets poles have predefined heights and will automatically fill in the heights for the selected choice.

See target configurations on page 3.X

All other targets will need a height entered

Scan Setup for Targets

<u>Pick from video image</u> allows the user to turn the C10 towards the target and pick it the stylus.

The camera of the C10 points to the right when the user is looking at the display screen.

Touch **PickT** and camera turns on and displays in window

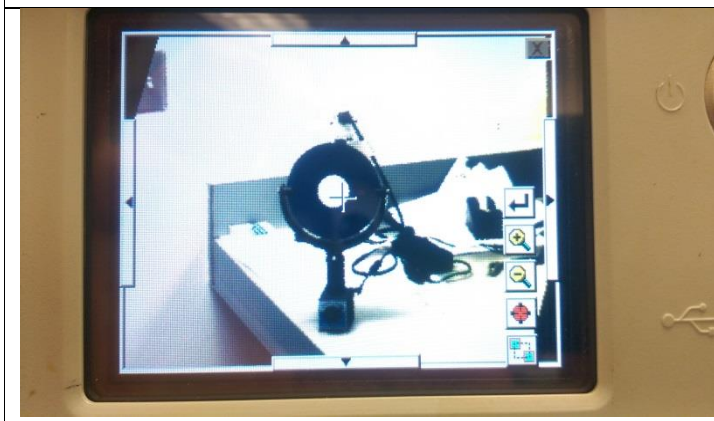

Scan Setup for Targets

In the image display window, use the stylus to located the target by selecting the **seek** button which is
blue when not active
red when it is active

Touch the screen and the camera will focus to that point
Zoom + - as needed

pick the target close to center of white circle and select enter **button**

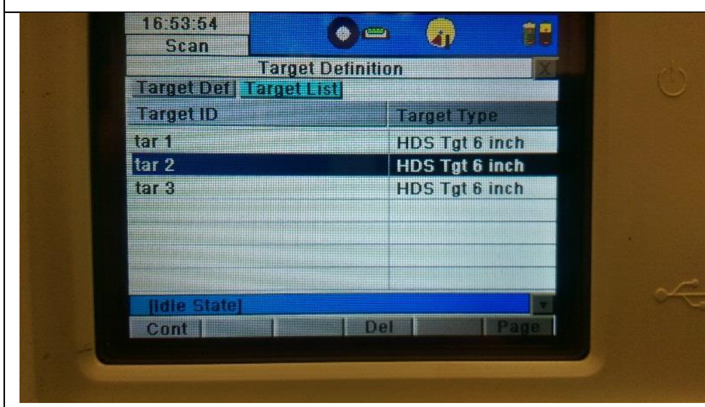

Scan Setup for Targets
<u>Repeat</u> this process until <u>all</u> targets have entered.
Target List displays the target to be scanned.

From this screen to left
Select **Cont** to begin the target scanning process.

Targets are scanned in the order that they were selected.

Select **Cont** to start acquiring the targets

Scan Setup for Targets
Target Scan Progress Screen while scanning targets

The C10 will scan the targets and display them in a list with a status of bad or ok.

When completed the following Target Results screen will display the status of the scanned targets.

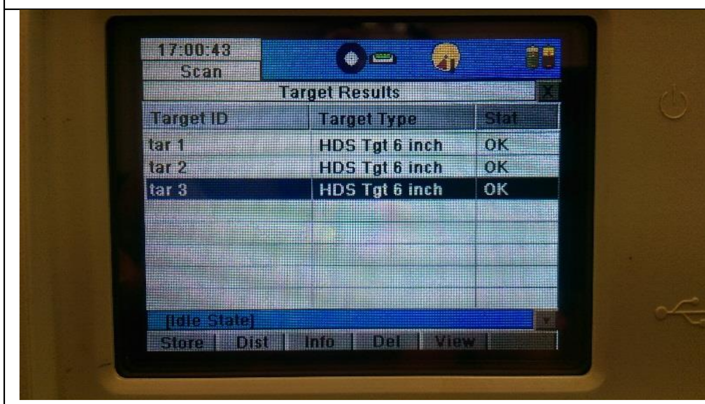

Scan Setup for Targets

<u>Before selecting **Store** to save the targets</u>

Highlight the target row to review the target information by selecting the **Info** button

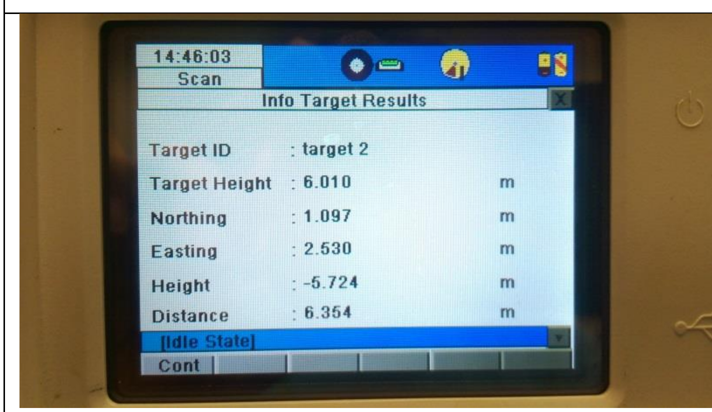

Scan Setup for Targets

Target Information Results Display for Target 2

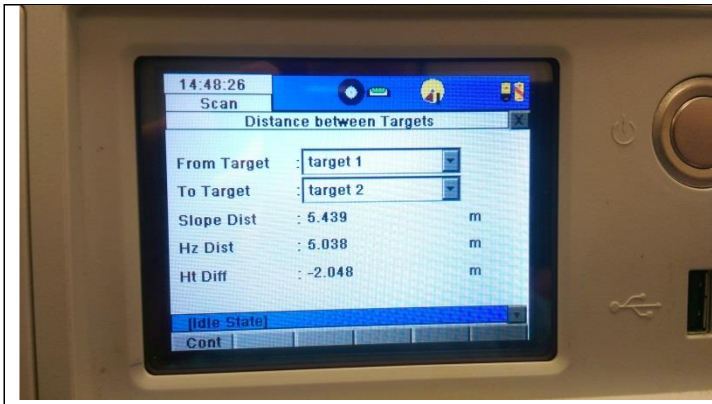

Scan Setup for Targets

Dist button will display

Geographical information between the selected Targets

Cont to go back to Target Result screen to review remaining targets.

Targets can be Deleted if necessary

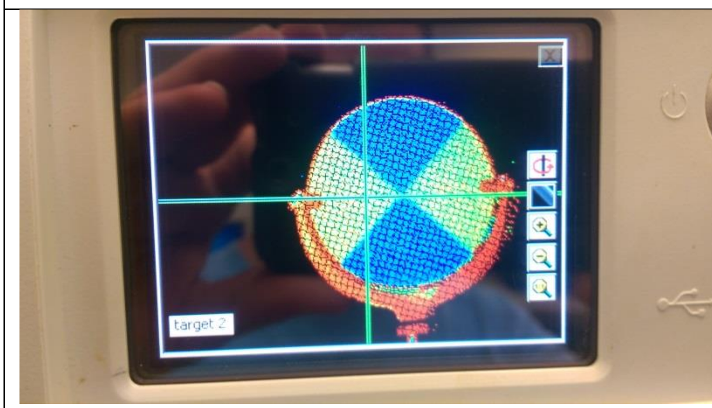

Scan Setup for Targets

From the Target Result screen select
View

Allows the user to view the scan of the target

Top button rotates the screen

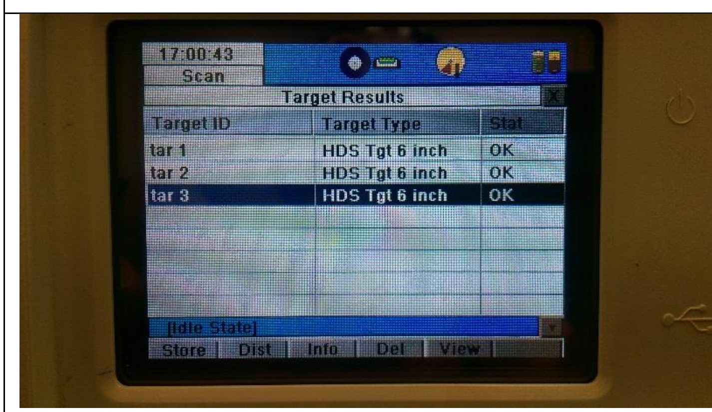

Scan Setup for Targets

DO NOT FORGET TO STORE THE TARGETS

Select **Store**

Next Step is to scan the subject area!

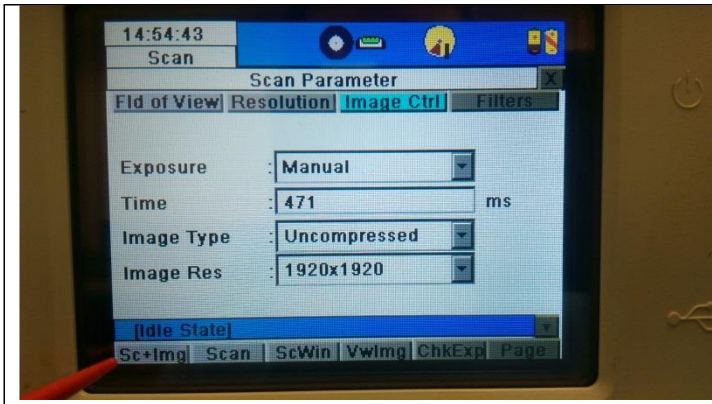

Scan Procedure

To start the scanning the study area

Press the

Sc+Img – Scans then images
or
Scan - to scan only

The C10 will calibrate then start scanning

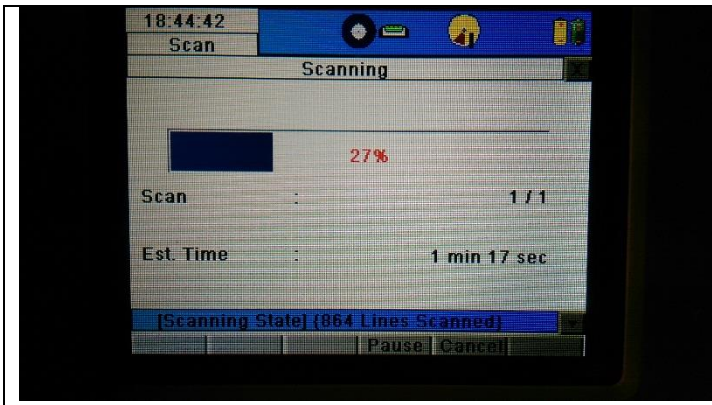

Scan Procedure in progress

Progress display of the main scan

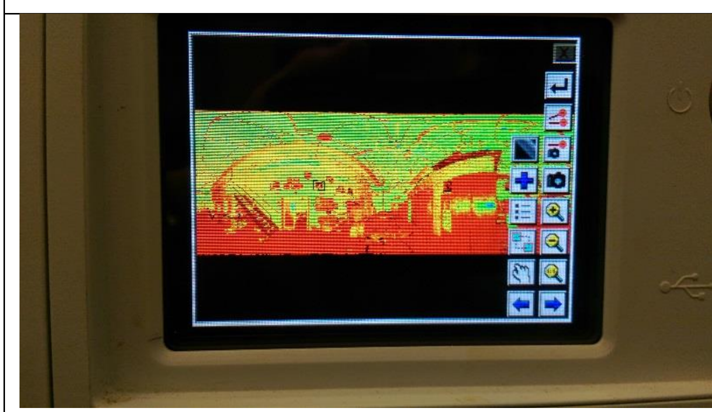

Scan Completed

When scanning has completed the data will display in window.

The data can be inspected and visualized here.

Now that you are finished with the present scan station,

Select **X**, the escape button, (top right) to go to previous window screen.

Select **X** at Main Menu screen to power down C10

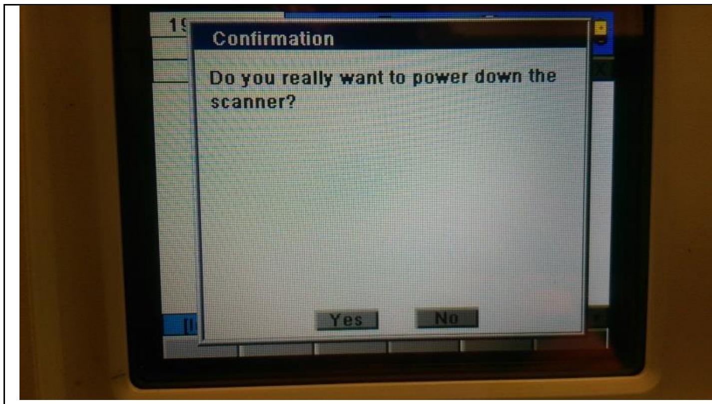	A pop-up screen will appear asking if you want to power down the C10. Select **Yes** Now you can move the C10 and tripod to the next station that will be scanned. Remember that at least three (3) common targets must be in each scan for registration purposes.
	**Shut Down and Move** After setting up on next station and leveling C10 with circular level. Power up the C10 using silver button. Now there is slightly different method after the first setup which is complicated Targets that were saved are stored in memory and will be selectable in the pull-down menu in defining targets.

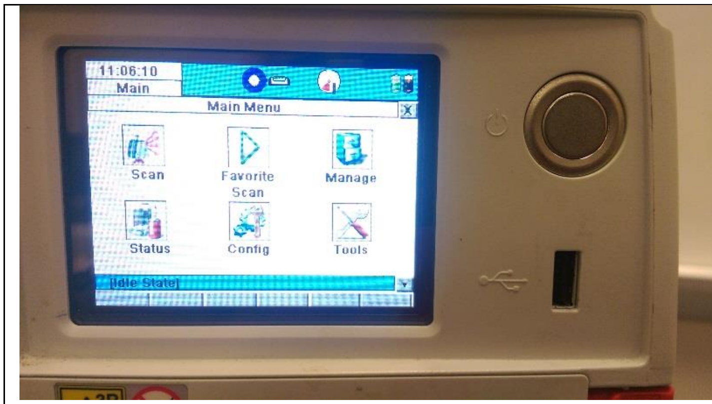	**Setting up Next Station** Starting the next scanning station. Boot and leveling the C10 as before Set up any new targets that are needed and record in their name/ID in the scan plan.
	**Setting up Next Station** Check the current station information by touching the **Idle State bar**. Project: test Station ID: Stat-001 Scan World: SW-001 This is the previous station.
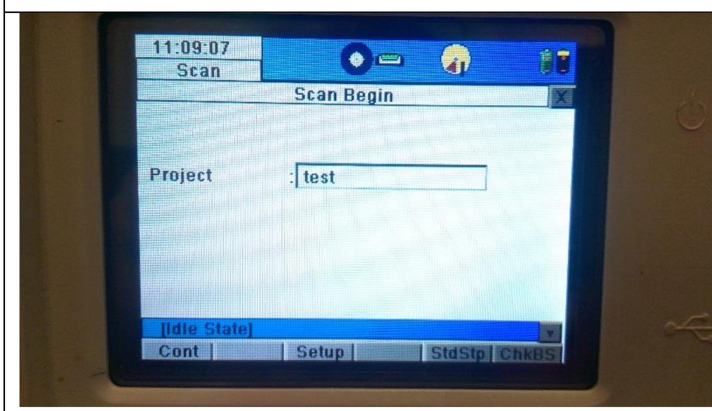	**Setting up Next Station** Select the **Scan** icon To move the C10 to the next station 002, Select **StdStp** (standard setup) button If you were adding more data to Station – 001 you select **Cont** Then select yes in next picture on next page(top). Selecting **StdStp** advances the C10 to station - 002

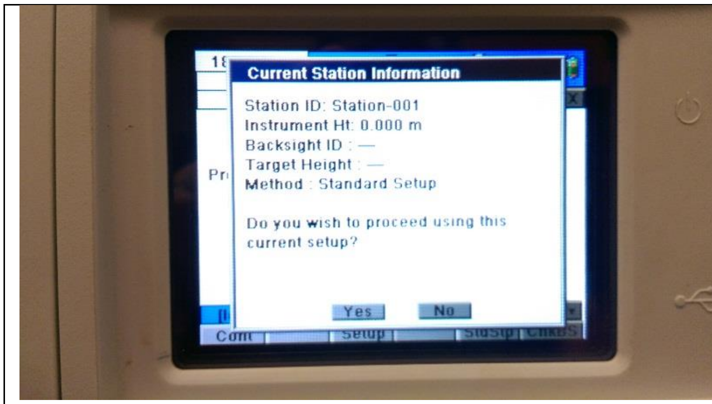

Setting up Next Station

If **Yes** is selected then data is saved in Station – 001

Select **No** to add data to next station – 002
then
Select **StdStp**

Setting up Next Station

Verify that the station ID is correct.

Enter the Instrument Height

Select **Set**

Setting up Next Station

Verify that the scan parameters are the same as before
Check:

Field of View
Resolution
Image Control
Filters

Setting up Targets Next Station

Add any new targets by selecting **New** and define.

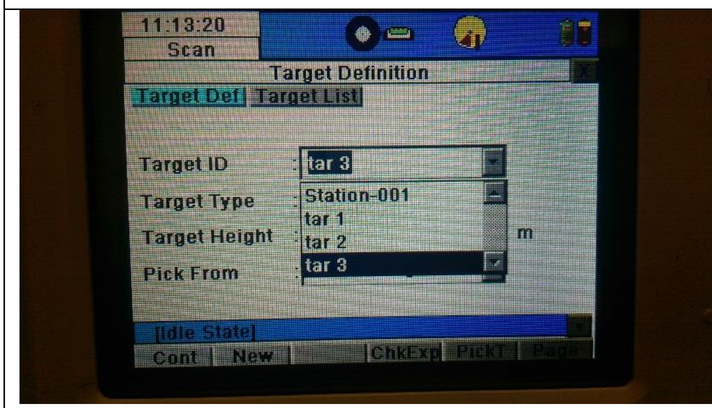

Setting up Targets Next Station

Any targets that were already saved in previous station will appear in the drop-down menu.

Select New and use the drop-down menu to select any of the previous targets. The height info is already defined. Select New add the next target until all targets are input.

Then select **Cont** to acquire the targets

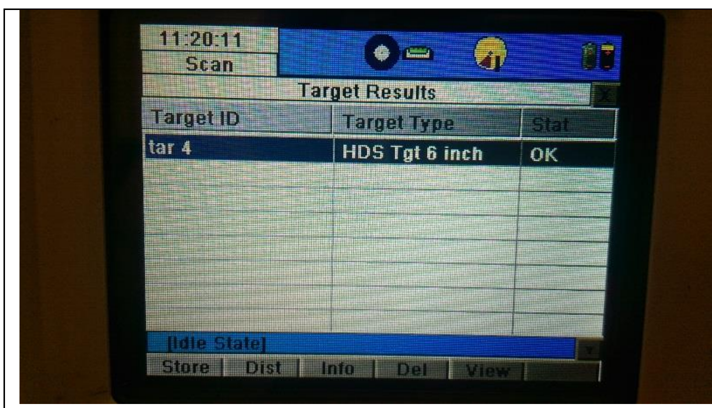

Setting up Targets on Next Station

After the C10 scans and acquires the targets
Check status of targets in the list

Select **Store** to save the targets

Starting the Scan

To scan the study area

Select **Sc + Img** – scan then image
OR
Select **Scan** – scan only

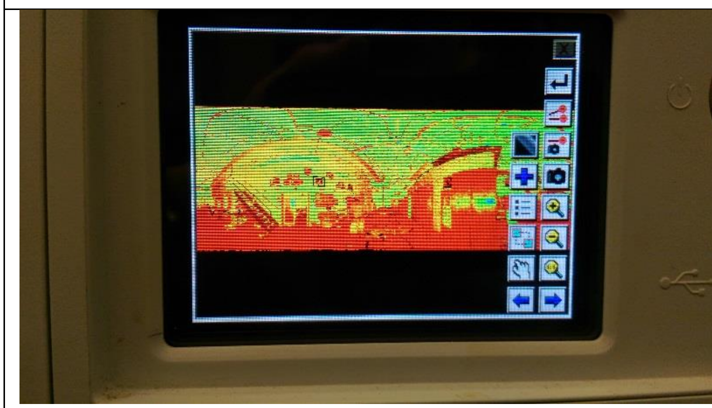

Scan Complete

After the C10 has completed the scan, then the data will display in the window.

Visualize the data if needed then shut down the C10
By selecting the **X** escape button twice or until confirmation window pops up.

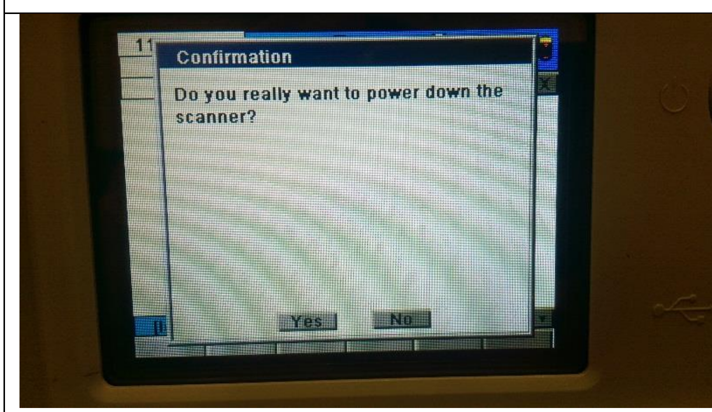

Shut down and move

Select Yes to power off C10.

Move to the next scan station and repeat the following process.

When finished, pack equipment back into their cases.

APPENDIX C

LEICA CYCLONE POINT-CLOUD MODELING PROTOCOL

Cyclone 9.0 Protocol

“Registering Scans, Creating a 3D ModelSpace and Cleaning Traffic Noise”

Updated for Fall 2017 Laser Scanning Sr. Project

Written by: Mariah Peart

Software Configuration Setup

1. Open Cyclone 9.0
2. For first-time users, a window will ask to run the configuration setup
    a. Select OK and the License Server Configuration will appear
    b. Set the license server to **@GSP1V-LICAPP001**

Data Import

1. In the main Cyclone screen, click on the plus sign **[+]** next to SERVERS

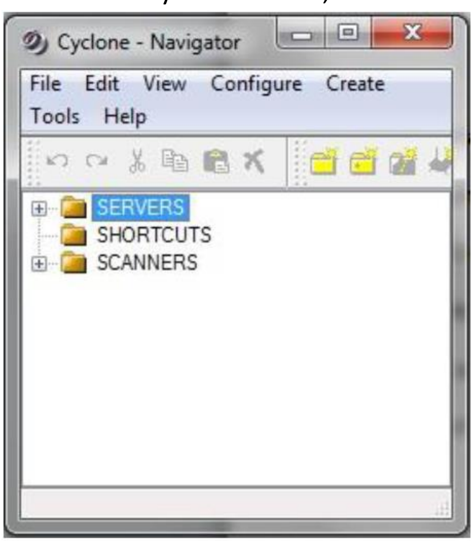

2. Right-click on the unshared server, **CMCE2321118XR02 (unshared)**
3. Select “Databases”
4. Select “Add”

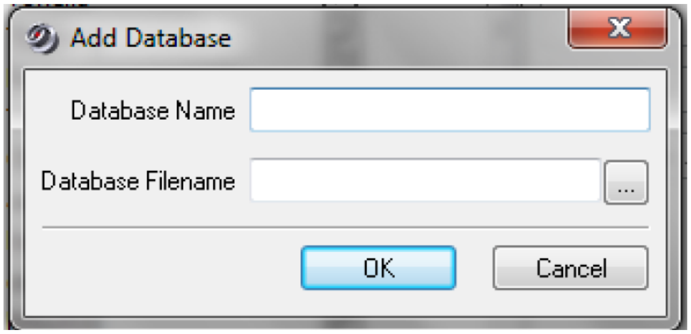

a. To add a new database, enter a desired name in the "Database Name" section, then select OK
b. To import a database, select the **[…]** button next to the "Database Filename" section. Select the database, "**Fall2017**".imp file, and click Open

5. Click on the plus sign **[+]** next to CMCE2321118XR02 (unshared) and right-click on the newly created database
6. Go to "**Import ScanStation C5/C10 Data**", then select "**Import ScanStation C5/C10 Data Project**"
7. Select the main project folder (**Gnat**), that contains the RAW scanner data, to import all scans.
8. In the window that appears, make sure that ONLY "Generate Scan Thumbnails," "Map Colors" and "Estimate Normals" are checked, then select OK
9. Cyclone will import the raw data

Creating Registration

1. Open your database
2. Right-click on the main file folder (**Gnat**)
   a. Go to "**Create**," then select "**Registration**"
3. Double-click on the new registration (should appear as **Registration 1**)
4. Add scanworlds to the registration
   a. Click on the "**Scanworld**" tab at the top of screen, then select "**Add ScanWorld**"

  b. Select all scanworlds (Stations) that you want to register.
    i. For this project you will add Stations **001-009**, **012-031**, **033-036** and **038-044**
  c. Then, click on the **[>>]** button to add each scanworld/station
  d. Select OK, when finished
5. Open the "**Constraint**" tab at the top of screen, then select "**Auto-Add Constraints (Target ID only)**"
6. Open the "**Constraint List**" tab
7. Open the "**Registration**" tab at the top of screen, then select "**Auto-Update**" (Auto-Update should be checked after any changes in the registration)

Constraint ID	ScanWorld	ScanWorld	Type	Status	Weight	Error	Error Vector
GL8	Station-022: S...	Station-032: S...	Coincident: Sphere - Sphere	On	1.0000	68.238 m	(-15.872, 66.365, 0.39...
GL8	Station-023: S...	Station-032: S...	Coincident: Sphere - Sphere	On	1.0000	68.237 m	(-15.873, 66.364, 0.39...
GL8	Station-013: S...	Station-032: S...	Coincident: Sphere - Sphere	On	1.0000	67.998 m	(-15.985, 66.091, 0.40...
GL8	Station-016: S...	Station-032: S...	Coincident: Sphere - Sphere	On	1.0000	67.785 m	(-16.695, 65.696, 0.39...
GL8	Station-026: S...	Station-032: S...	Coincident: Sphere - Sphere	On	1.0000	67.762 m	(-16.530, 65.714, 0.39...
GL8	Station-015: S...	Station-032: S...	Coincident: Sphere - Sphere	On	1.0000	66.211 m	(-16.874, 64.024, 0.39...
GL8	Station-020: S...	Station-032: S...	Coincident: Sphere - Sphere	On	1.0000	64.805 m	(-17.592, 62.370, 0.39...
GL8	Station-014: S...	Station-032: S...	Coincident: Sphere - Sphere	On	1.0000	63.879 m	(-18.863, 61.029, 0.39...
GL8	Station-021: S...	Station-032: S...	Coincident: Sphere - Sphere	On	1.0000	63.255 m	(-18.680, 60.433, 0.39...

8. In the Constraints List tab, click on "**Error**" until the constraint list is sorted from highest error to lowest error.
9. Disable targets, containing high errors, until you have reached a desired error limit (usually 0.010 meters)
  a. In the Diagnostics window, right-click on the target of choice, then select "**Disable**"
  b. The program will update automatically and generate new errors for all targets.

Creating a ModelSpace

1. When the registration is complete, at the top of screen, select "Registration" and click on "**Create Scanworld/Freeze Registration**"
2. Close the registration
3. In the main screen, double-click on the registration (in this case, **Registration 1**), right-click on "ModelSpaces," click on "Create," then select "ModelSpace"
4. Double-click on the newly created modelspace (in this case, **ModelSpace 1**), then select "Create and Open ModelSpace View"

How to Clean Traffic Noise and Sunbeam Rays

1. For traffic noise, including vehicles and pedestrians:
    a. Create a fence around the area of interest by selecting the “**Polygonal Fence Mode**” icon and drawing the fence around the traffic noise. 
    b. Right-click in the fenced area, select “**Point Cloud Sub-selection**” and “**Add Inside Fence**”
    c. Next, define the surface (i.e. road or sidewalk) by selecting the Multi-Pick Mode icon and CAREFULLY place points only on the surface, in the fenced area. Place as many points as you desire. 
    d. Right-click on the fenced area, select “**Region Grow**” and “**Smooth Surface**”
    e. A window will appear and it will not be necessary to change any parameters, unless specified.
    f. Once the surface has been defined, press OK.
    g. Make sure the traffic noise is highlighted, only! Use the View Mode icon to check. Then, press the “delete” button. 
    h. If the traffic noise and surface were highlighted after the previous step, click on the “**Selection**” tab at the top of screen and press “**Deselect**.” Then, repeat the previous steps from the beginning.
2. For Sunbeam Rays:
    a. Use the Pick Mode icon to select a point from the sun ray. This will highlight the entire sunbeam from the other points in the model. 
    b. Use the Seek Mode icon to locate the scan station. 
    c. Zoom in to the scan station until you are viewing the first point of the sun ray.
    d. Use the View Mode icon to rotate upwards until the entire sunray is in a clear view. 
    e. Use the Polygonal Fence Mode icon to draw a fence around the sunray points. 
    f. Right-click, select “**Fence**,” then press “**Delete Inside**”

Note: In this process, please be careful of points from powerlines, trees, buildings, etc.

Reference for Scanworld Icons

Polygonal Fence Mode	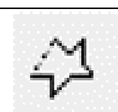
View Mode	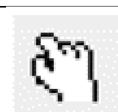

Seek Mode	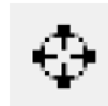
Pick Mode	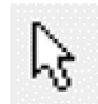
Multi-Pick Mode	

APPENDIX D

GEO-REFERENCING A 3-D POINT-CLOUD MODEL

Cyclone 9.0 Protocol

"Georeferencing a 3-D Point Cloud Model"

Updated for Fall 2017 Laser Scanning Sr. Project

Written by: Mariah Peart

Creating a GPS Coordinate Text Document

1. Open the Notepad application
2. Create a new text document
3. Enter the GPS coordinates, as shown in the following figure
    c. Separate the columns, equally, by using the tab button
    d. The headers are NOT necessary

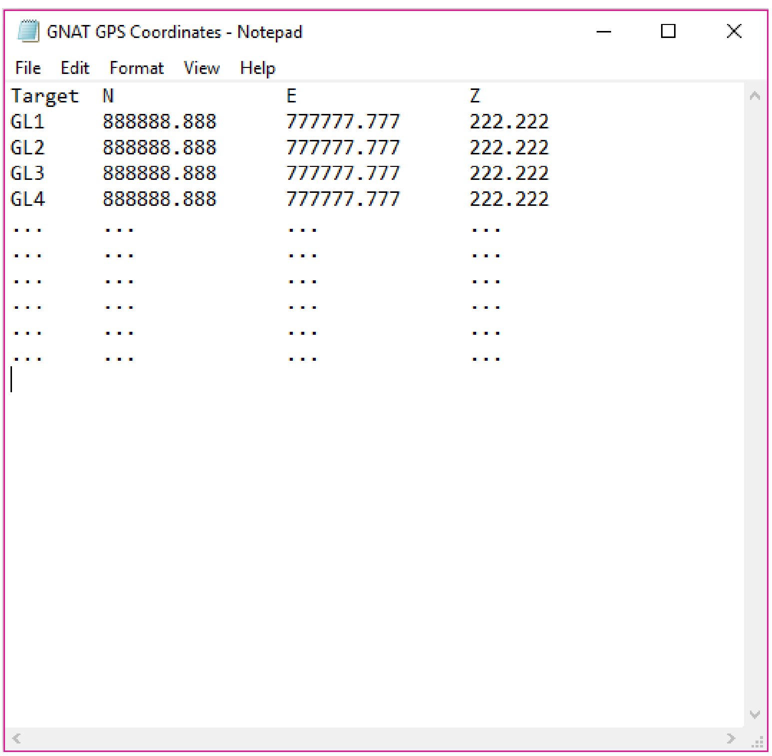
GNAT GPS Coordinates - Notepad

File Edit Format View Help

Target	N	E	Z
GL1	888888.888	777777.777	222.222
GL2	888888.888	777777.777	222.222
GL3	888888.888	777777.777	222.222
GL4	888888.888	777777.777	222.222
...	...	...	...
...	...	...	...
...	...	...	...
...	...	...	...
...	...	...	...
...	...	...	...

Importing Control Points for Georeferencing

1. Open Cyclone 9.0
2. Double-click on your database
3. Right-click on the main project folder, then go to "**Create**" and select "**ScanWorld**"
    a. Rename the scanworld as "**Control Points**"

4. Right-click on the “Control Points” scanworld and select “**Import**”
5. Locate the created text document, containing the GPS coordinates and click on “**Open**”
6. The “**Import: ASCII File Format**” window will open, as shown in the following figure

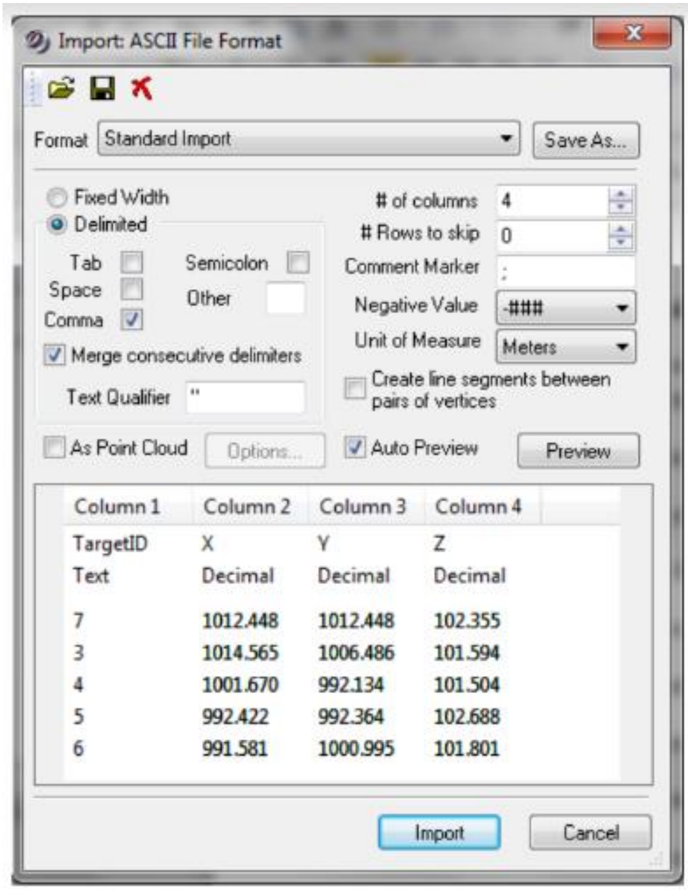

7. Under the “**Delimited**” section, select “**Tab**”
8. Adjust the “**Unit of Measure**” to **US Survey Feet**
9. Select the first row under the Column number
10. Adjust the “**Point Number**” to “**TargetID**”
    a. Also, check to make sure the Northing, Easting, and Elevation are set correctly
11. If you have a header row, from the text document, set the “**# Rows to skip**” to “**1**”
12. Select “**Import**,” when finished

Creating Registration

1. Open your database
2. Right-click on the main file folder (**Gnat- 45**)
    a. Go to “**Create**,” then select “**Registration**”
3. Double-click on the new registration (should appear as **Registration #**)
4. Add scanworlds to the registration
    a. Click on the “**Scanworld**” tab at the top of screen, then select “**Add ScanWorld**”

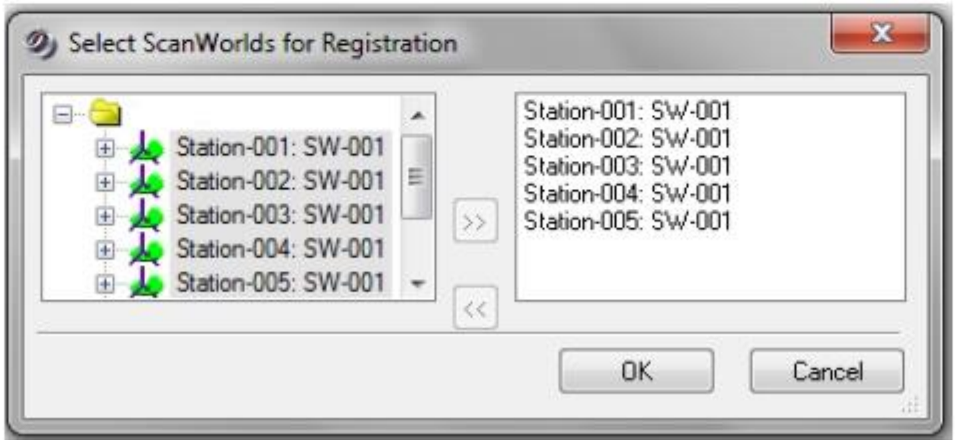

   b. Select the previously registered scanworld and the "Control Points" scanworld for the new registration
      i. For this project you will add the registration that contains Stations **001-009**, **012-031**, **033-036** and **038-044**
   c. Then, click on the **[>>]** button to add each scanworld
   d. Select OK, when finished
5. Open the "**Constraint**" tab at the top of screen, then select "**Auto-Add Constraints (Target ID only)**"
6. Open the "**Constraint List**" tab
7. Open the "**Registration**" tab at the top of screen, then select "**Auto-Update**" (Auto-Update should be checked after any changes in the registration)

Constraint ID	ScanWorld	ScanWorld	Type	Status	Weight	Error	Error Vector
GL8	Station-022: S...	Station-032: S...	Coincident: Sphere - Sphere	On	1.0000	68.238 m	(-15.872, 66.365, 0.39...
GL8	Station-023: S...	Station-032: S...	Coincident: Sphere - Sphere	On	1.0000	68.237 m	(-15.873, 66.364, 0.39...
GL8	Station-013: S...	Station-032: S...	Coincident: Sphere - Sphere	On	1.0000	67.998 m	(-15.985, 66.091, 0.40...
GL8	Station-016: S...	Station-032: S...	Coincident: Sphere - Sphere	On	1.0000	67.785 m	(-16.695, 65.696, 0.39...
GL8	Station-026: S...	Station-032: S...	Coincident: Sphere - Sphere	On	1.0000	67.762 m	(-16.530, 65.714, 0.39...
GL8	Station-015: S...	Station-032: S...	Coincident: Sphere - Sphere	On	1.0000	66.211 m	(-16.874, 64.024, 0.39...
GL8	Station-020: S...	Station-032: S...	Coincident: Sphere - Sphere	On	1.0000	64.805 m	(-17.592, 62.370, 0.39...
GL8	Station-014: S...	Station-032: S...	Coincident: Sphere - Sphere	On	1.0000	63.879 m	(-18.863, 61.029, 0.39...
GL8	Station-021: S...	Station-032: S...	Coincident: Sphere - Sphere	On	1.0000	63.255 m	(-18.680, 60.433, 0.39...

8. In the Constraints List tab, click on "**Error**" until the constraint list is sorted from highest error to lowest error.
9. To view the constraint (target) from a selected scan-station, right-click on the target, then select "**Show Constraint**"
10. Disable targets, containing high errors, until you have reached a desired error limit (usually 0.010 meters)
   a. In the Diagnostics window, right-click on the target of choice, then select "**Disable**"

b. The program will update automatically and generate new errors for all targets.

Creating a ModelSpace

1. When the registration is complete, at the top of screen, select “Registration” and click on “**Create Scanworld/Freeze Registration**”
2. Close the registration
3. In the main screen, double-click on the registration (in this case, **Registration #**), right-click on “ModelSpaces,” click on “Create,” then select “ModelSpace”
4. Double-click on the newly created modelspace (in this case, **ModelSpace #**), then select “Create and Open ModelSpace View”

APPENDIX E

POINT ACQUISITION WITH ROBOTIC TOTAL STATION PROTOCOL

Point Acquisition Protocol

Leica TCRP 1201+ Robotic Total Station and Data Collector

Built Environment and Modeling Lab
Georgia Southern University
Department of Civil Engineering and Construction
Written by: Mariah Peart
Fall 2018

Level & Laser Plummet

- Turn on the Robotic Total Station Instrument.
- Level the instrument with the tripod stand, then complete the procedure with the leveling screws.
- Be sure to place laser plummet at the center location of the station (center of the nail).

Please note the following procedures are performed with a stylus. Procedures can vary without this tool.

Data Collector

- Turn on the Data Collector as a remote to the instrument.
- The **Instrument Mode Selection** screen will appear, as shown in Figure 1.
- Set **Choose Sensor** to "**TPS"**
- Set **Show at Startup** to "**Yes"**
- Then, press **CONT**

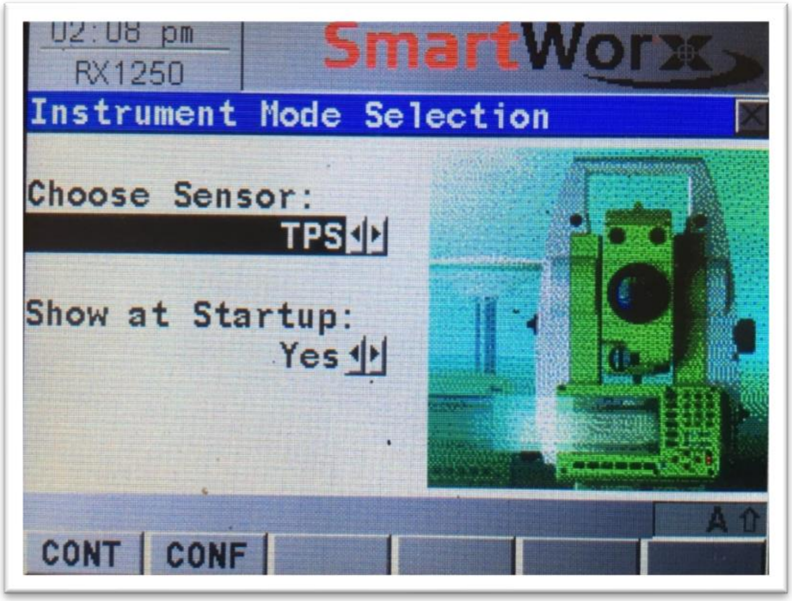

Figure 1: Instrument Mode Selection

Figure 2: Main Menu

Define Job Name

- From the main menu, select **Manage**, as shown in Figure 2.
- From the Management window, select **Jobs**, as shown in Figure 3 (a).
- From the Jobs window, select **NEW**, as shown in Figure 3 (b).
- Name your New Job, then press **STORE**, as shown in Figure 3 (c).

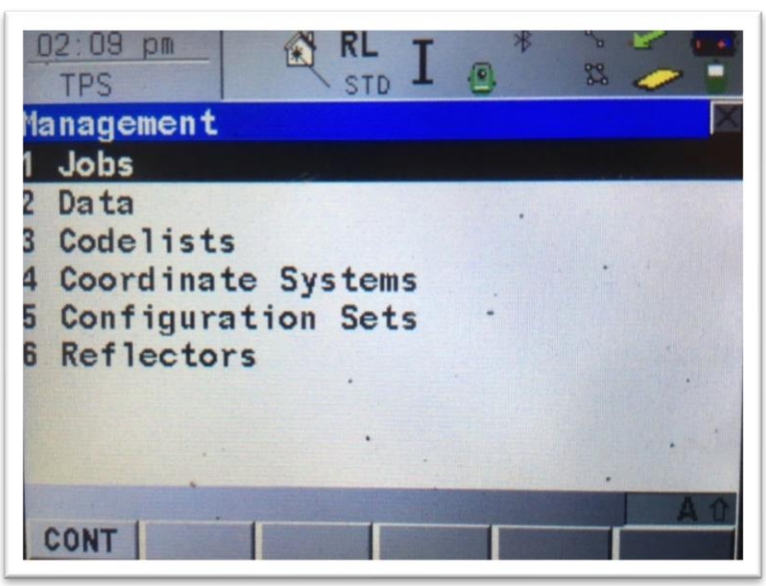

Figure 3 (a): Management Window

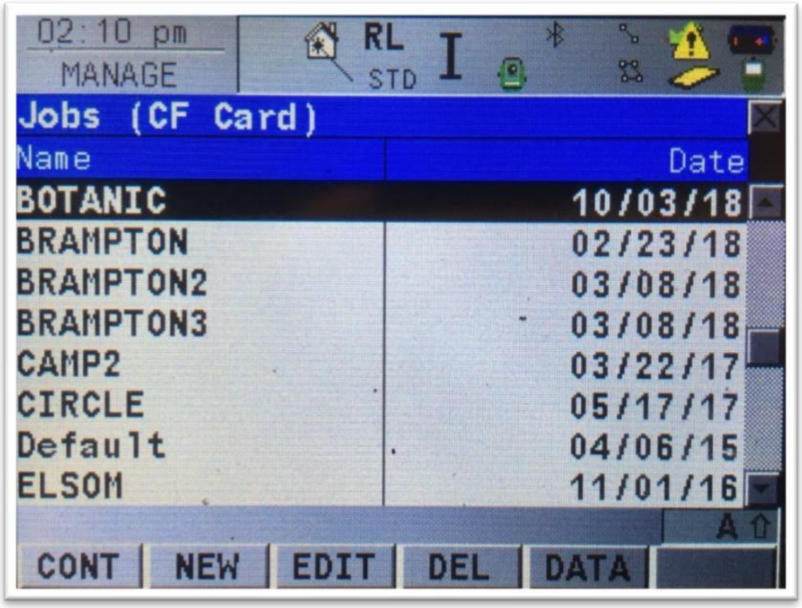

Figure 3 (b): Job List

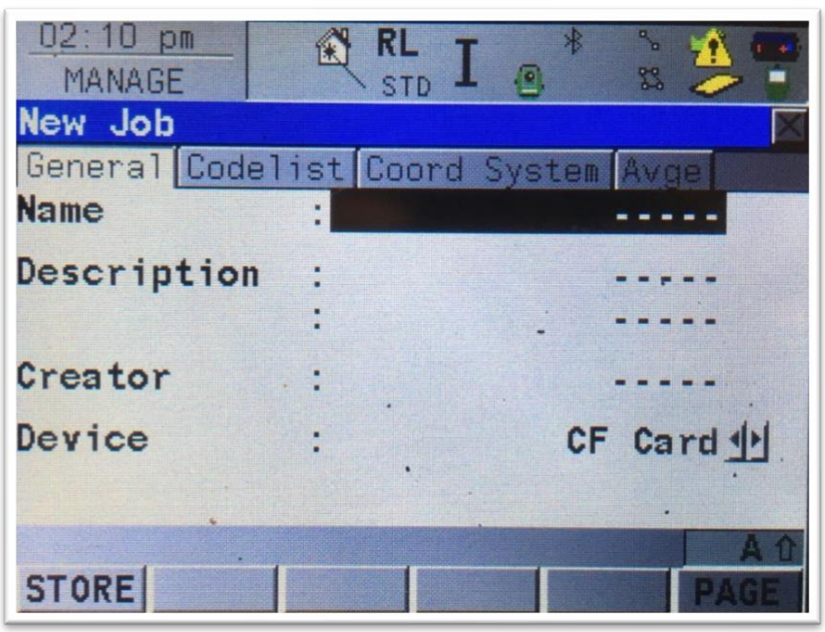

Figure 3 (c): Creating a New Job

Setting Instrument to Reflectorless

- From the main menu, select **Manage**.
- From the Management menu, select **Reflectors**, choose **Reflectorless,** then press **CONT**, as shown in Figure 4 (a - b).

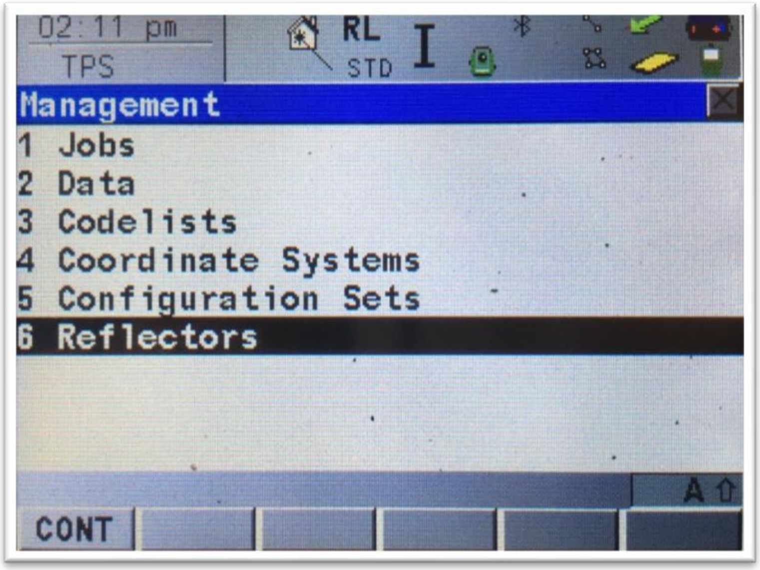

Figure 4 (a): Management Menu (Reflectors)

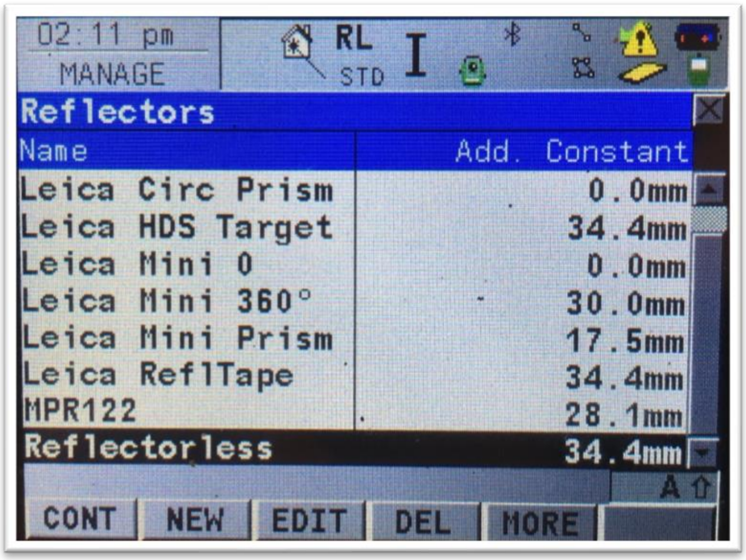

Figure 4 (b): Reflector List

Station Setup

- From the main menu, select **Survey.**
- The **Survey Begin** window will appear, as shown in Figure 5.
- Check all parameters (Mainly, consider the “Job” and “Reflector” settings).
- Then, select **SETUP**.

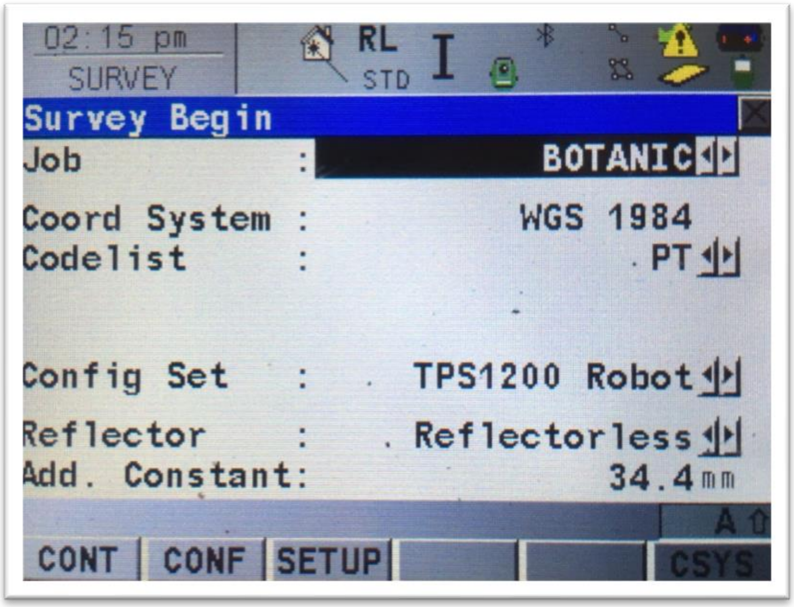

Figure 5: Survey Begin Window

The Station Setup Window will appear, as shown in Figure 6 (a).

- Set **Method** to **“Known BS Point”**
- Set **Station Coord** to **“Frm Control Job”**
- Set a new **Station ID** (this will be the I.D. for the current station)
    - Select the current (highlighted) Station ID name.
    - The Data window will appear, as shown in Figure 6 (b).
    - Then, select **NEW**
    - The **New Point** screen will appear, as shown in Figure 6 (c).
    - Input a new name for the **Point ID**
    - Input the known Northing, Easting and Height (Elevation) coordinates of the current station.
    - Press **STORE**.
    - Be sure the new Point ID (Station ID) is highlighted, then select **CONT**.

- Measure and Input the **Instrument Height**.
- Check **Control Job** name (same as the Job name that is created).
- Then, select **CONT**.

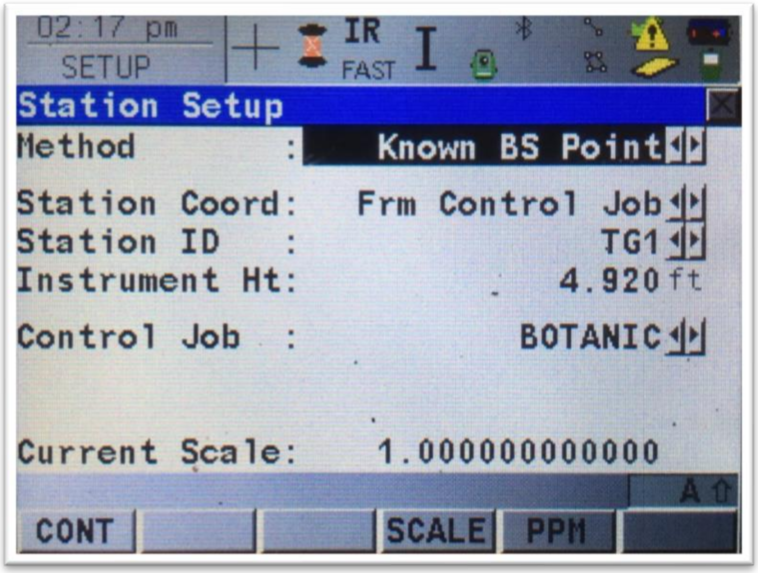

Figure 6 (a): Station Setup

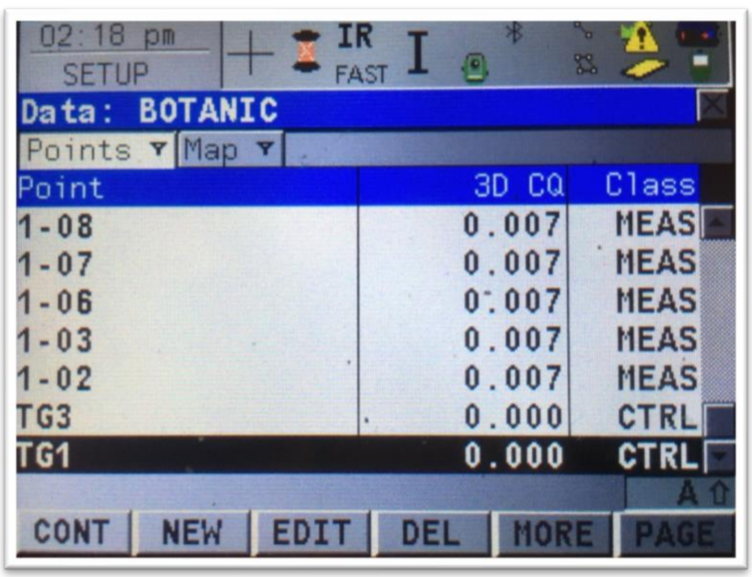

Figure 6 (b): Data Window

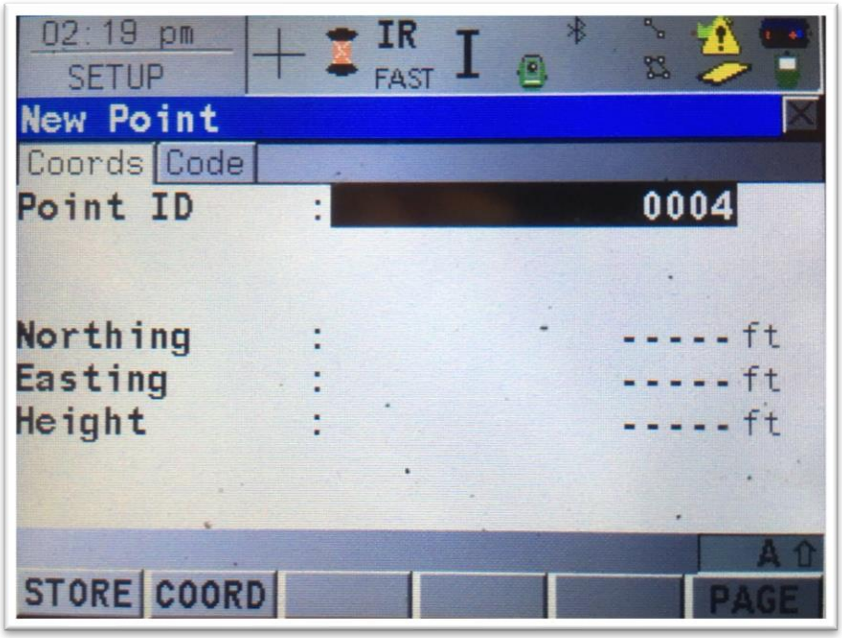

Figure 6 (c): New Point Window

Set Station & Orientation - Known BS Point

The “Set Stn & Ori – Known BS Point” window will appear, as shown in Figure 7.

- Select a new **Backsight ID** (This will be the name of the station where the reflector is located).
- Press on the current (highlighted) Backsight ID name.
- The Data window will appear, as shown in Figure 6 (b).
  - Select **NEW**
  - The New Point window will appear, as shown in Figure 6 (c).
  - Input a new name for the **Point ID** (Backsight ID).
  - Input the known Northing, Easting and Height (Elevation) coordinates of the Backsight ID.
  - Press **STORE**
  - Be sure the new Point ID (Backsight ID) is highlighted, then select **CONT.**

- Measure and Input the **Reflector Height**
- Aim the instrument towards the reflector’s center point.
- When the instrument is set, select **DIST.**
- Then, choose **SET.**
- The following message will appear, ***“Station and Orientation has been set.”***
- Then, press **OK**

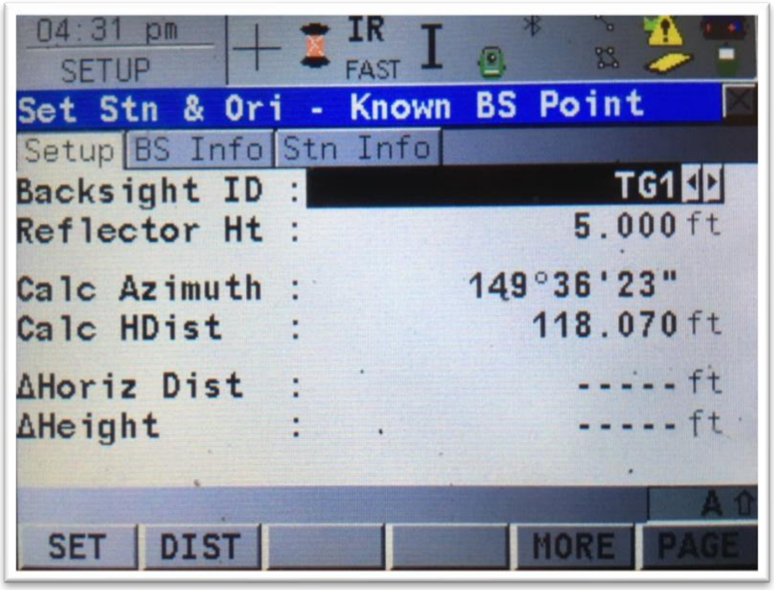

Figure 7: “Set Stn & Ori – Known BS Point” Window

Note: If the Station Setup screen appears, as shown in Figure 6 (a), after the last step in the “Set Station & Orientation –Known BS Point” procedures, then press **CONT**.

Survey (Point Acquisition)

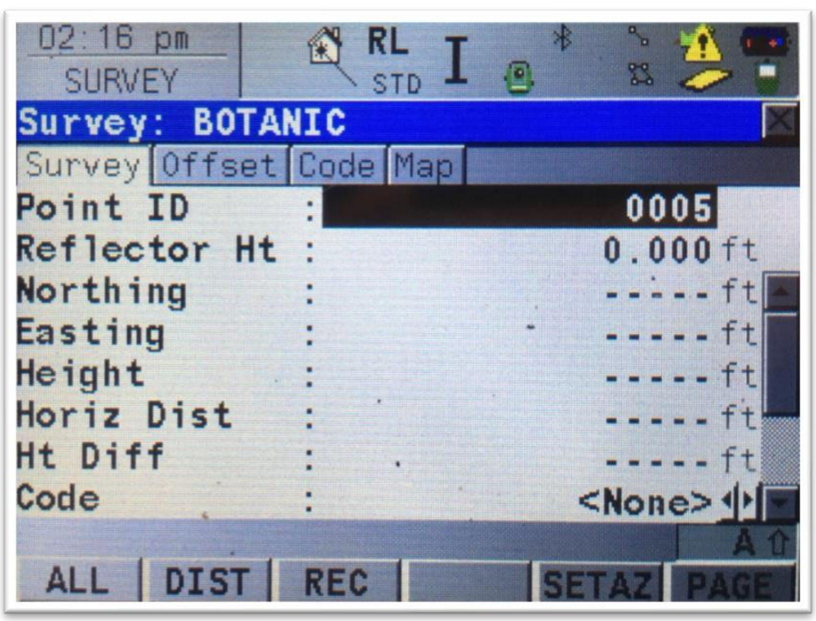

Figure 8: Survey: (Job Name)

The Survey window will appear, as shown in Figure 8.

- Choose a Point ID name, by selecting the current (highlighted) name and input a new ID (optional).
- Since the Reflectorless mode was selected, previously, the Reflector Height will remain at zero (in the either unit).
- Aim the instrument towards the center of desired point.
- Select **DIST** (to obtain the coordinates of the point).
- Select **REC** (to store the data). Be sure to not move the instrument before the data has been stored.
- Then, the next point is ready to be obtained.
- Repeat the **Survey** steps until all points are acquired.

New Station Setup

- Move to the next station.
- Repeat the Leveling procedures.
- Repeat the procedures to set up a **new Station ID** (Be sure to measure and insert a new Instrument Height)
- Also, repeat the procedures to set up a **new Backsight ID** (The Reflector Height should remain the same).
- Note: Any previous Station ID or Backsight ID that may be used for the new station can be simply selected from the Data window to avoid repeating the coordinate input process.
- Then, repeat the **Survey** steps to acquire the next set of points.

APPENDIX F

AGISOFT PHOTOSCAN TUTORIAL FOR TOPOGRAPHICAL FEATURES WITH GROUND CONTROL POINTS

(Adapted from Agisoft PhotoScan, 2017)

Tutorial (Beginner level): Orthomosaic and DEM Generation with Agisoft PhotoScan Pro 1.3 (with Ground Control Points)

Overview

Agisoft PhotoScan Professional allows to generate georeferenced dense point clouds, textured polygonal models, digital elevation models and orthomosaics from a set of overlapping images with the corresponding referencing information. This tutorial describes the main processing steps of DEM/Orthomosaic generation workflow for a set of images with the ground control points.

PhotoScan Preferences

Open *PhotoScan Preferences* dialog using corresponding command from the *Tools* menu:

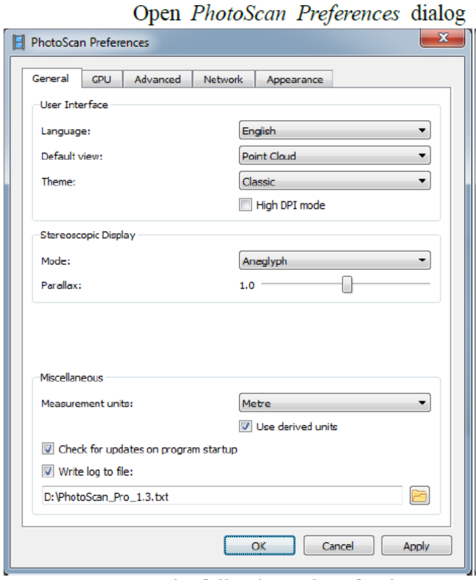

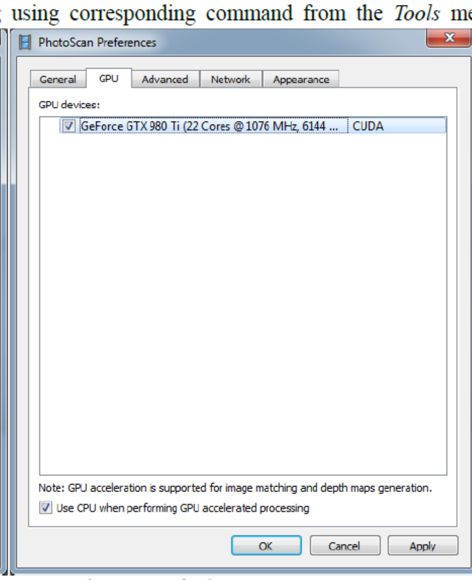

Set the following values for the parameters on the *General* tab:

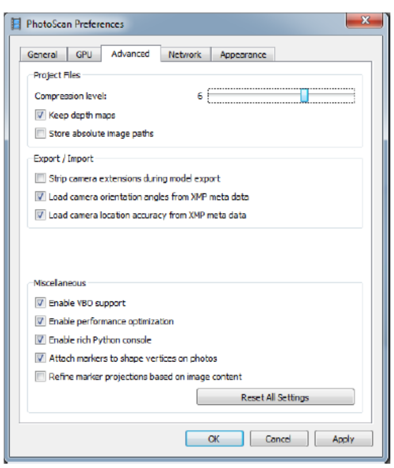

<u>Stereo Mode:</u> *Anaglyph* (use *Hardware* if your graphic card supports Quad Buffered Stereo)

<u>Stereo Parallax:</u> *1.0*

<u>Write log to file:</u> *specify directory where Agisoft PhotoScan log will be stored*

(in case of contacting the software support team it could be required)

Set the parameters in the *GPU* tab as following: *Check on any GPU devices detected by PhotoScan in the dialog. Check on "Use CPU" option when less than two GPU are used.*

Set the following values for the parameters on the *Advanced* tab:

<u>Project compression level:</u> *6*

<u>Keep depth maps:</u> *enabled*

<u>Store absolute image paths:</u> *disabled*

<u>Check for updates on program startup:</u> *enabled*

<u>Enable VBO support:</u> *enabled*

Add Photos

To add photos select *Add Photos...* command from the *Workflow* menu or click *Add Photos* button located on *Workspace* toolbar.

In the *Add Photos* dialog browse the source folder and select files to be processed. Click *Open* button.

Load Camera Positions

At this step coordinate system for the future model is set using camera positions.

Note: If camera positions are unknown this step could be skipped. The align photos procedure, however, will take more time in this case.

Open *Reference* pane using the corresponding command from the *View* menu.

Click *Import* button on the *Reference* pane toolbar and select the file containing camera positions information in the *Open* dialog.

The easiest way is to load simple character-separated file (*.txt, *.csv) that contains x- and y-coordinates and height for each camera position (camera orientation data, i.e. pitch, roll and yaw values, could also be imported, but the data is not obligatory to reference the model).

In the *Import CSV* dialog indicate the delimiter according to the structure of the file and select the row to start loading from. Note that # character indicates a commented line that is not counted while numbering the rows. Indicate for the program what parameter is specified in each column through setting correct column numbers in the *Columns* section of the dialog. Also it is recommended to specify valid coordinate system in the corresponding field for the values used for camera centers data.

Check your settings in the sample data field in *Import CSV* dialog.

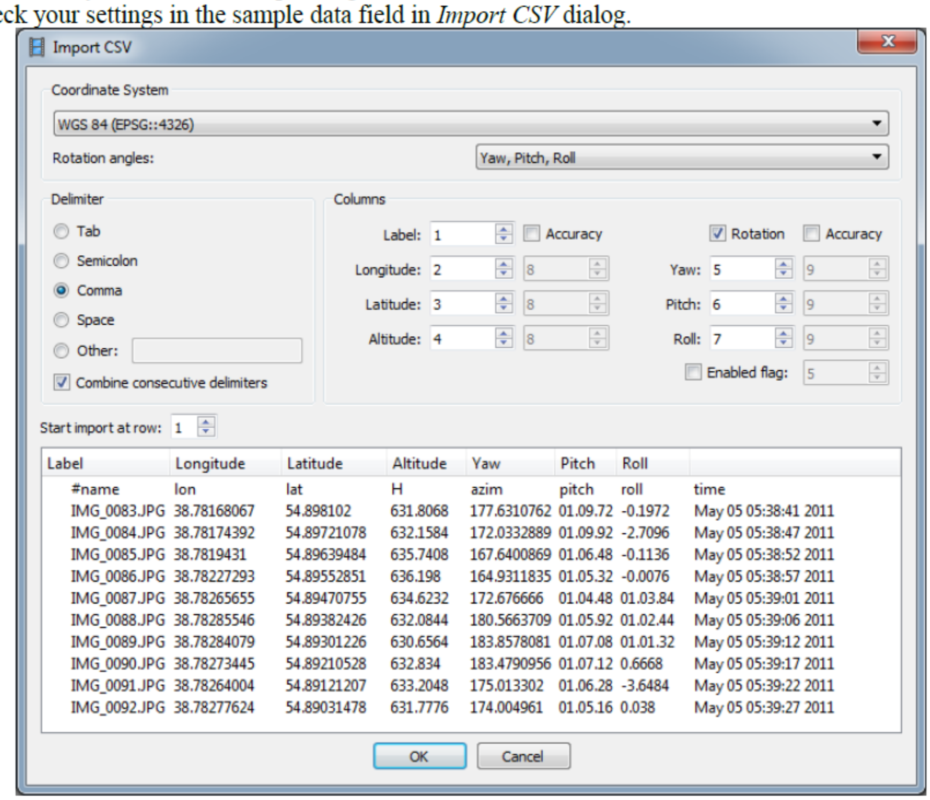

Click *OK* button. The data will be loaded into the *Reference* pane.

Import EXIF button located on the *Reference* pane can also be used to load camera positions information if EXIF meta-data is available.

Then click on the *Settings* button in the *Reference* pane and in the *Reference Settings* dialog select corresponding coordinate system from the list, if you have not selected it in the *Import CSV* dialog yet. Set up *Camera Accuracy* in meters and degrees according to the measurement accuracy:

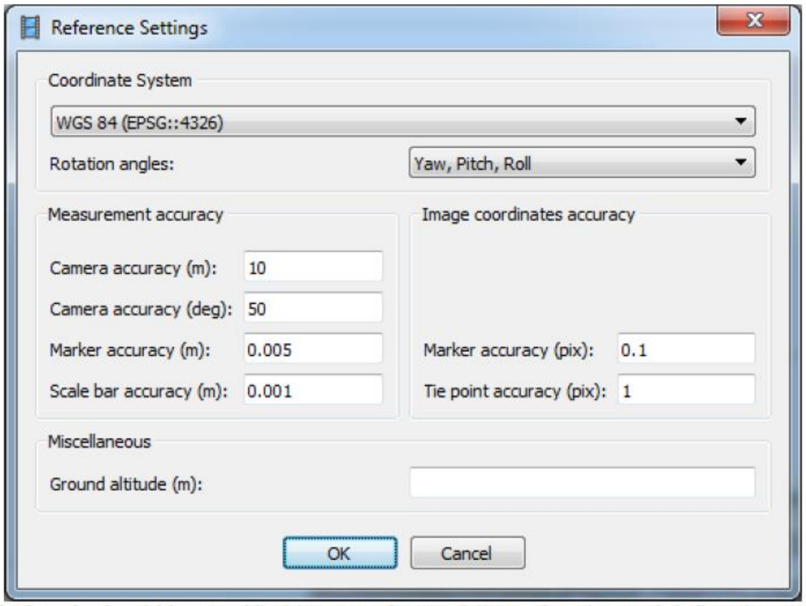

Ground Altitude should be specified in case of very oblique shooting and define the average ground altitude level above the ellipsoid in the selected coordinate system.

Click OK and camera positions will be marked in *Model View* using their geographic coordinates:

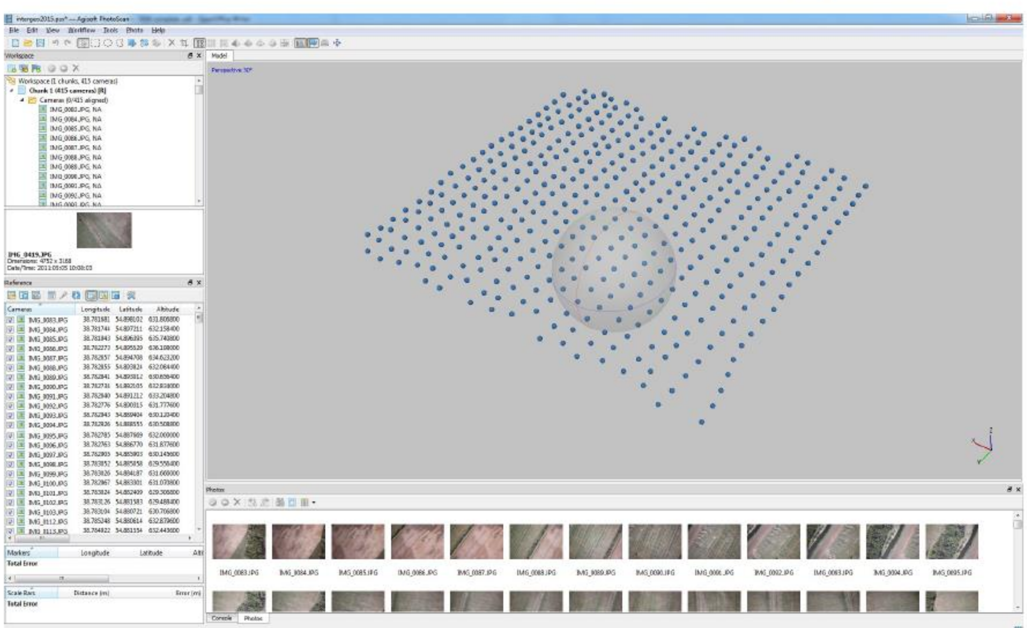

If you do not see anything in the Model view, even though valid camera coordinates have been imported, please check that Show Cameras button is pressed on the Toolbar. Then click Reset View button also located on the Toolbar.

Check Camera Calibration

Open Tools Menu → Camera Calibration window.

By default PhotoScan estimates intrinsic camera parameters during the camera alignment and optimization steps based on the Initial values derived from EXIF. In case *pixel size* and *focal length* (both in mm) are missing in the image EXIF and therefore in the camera calibration window, they can be input manually prior to the processing according to the data derived from the camera and lens specifications.

If precalibrated camera is used, it is possible to load calibration data in one of the supported formats using Load button in the window. To prevent the precalibrated values from being adjusted by PhotoScan during processing, it is necessary to check on *Fix Calibration* flag.

PhotoScan can process the images taken by different cameras in the same project. In this case in the left frame of the *Camera Calibration* window multiple camera groups will appear, split by default according to the image resolution, focal length and pixel size. Calibration groups may also be split manually if it is necessary.

In case ultra-wide or fisheye angle lens is used, it is recommended to switch camera type from *Frame* (default) to *Fisheye* value prior to processing.

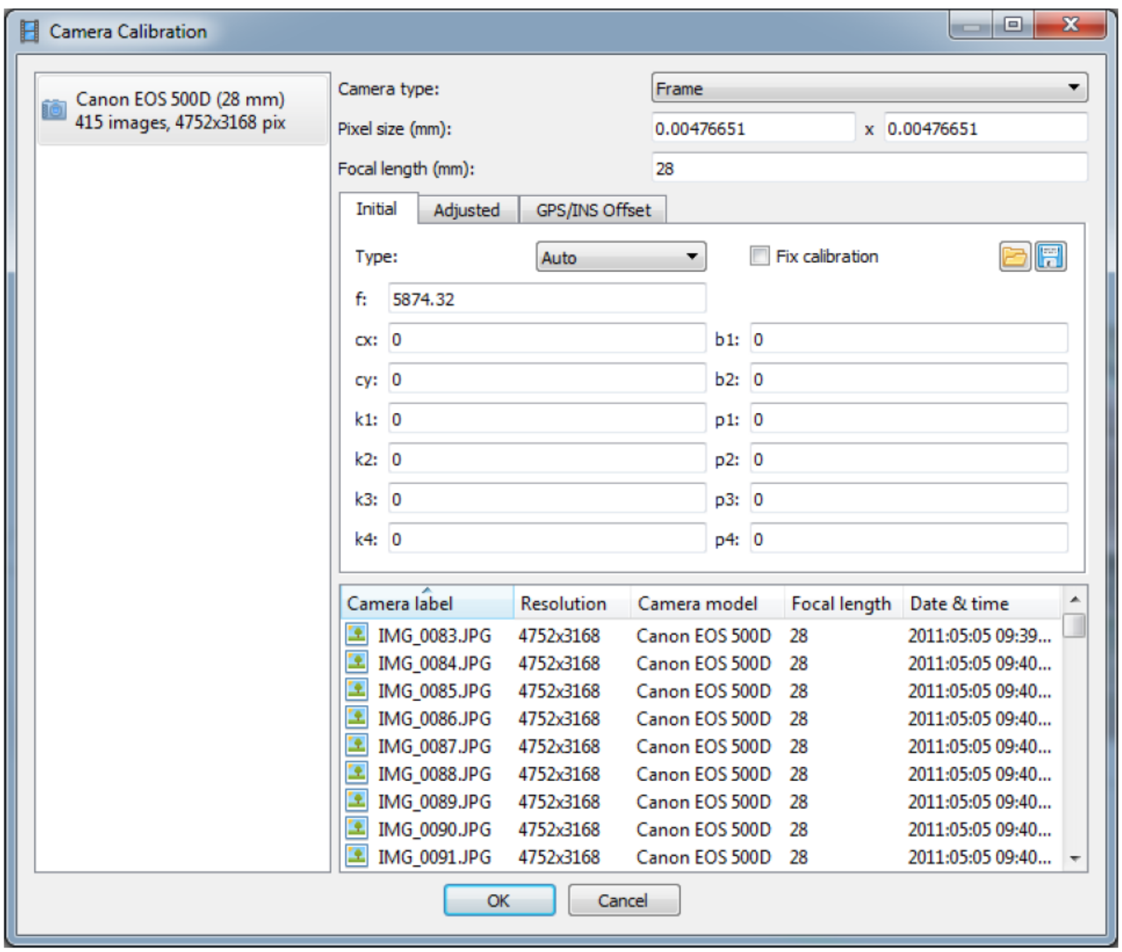

Align Photos

At this stage PhotoScan finds matching points between overlapping images, estimates camera position for each photo and builds sparse point cloud model.

Select *Align Photos* command from the *Workflow* menu.

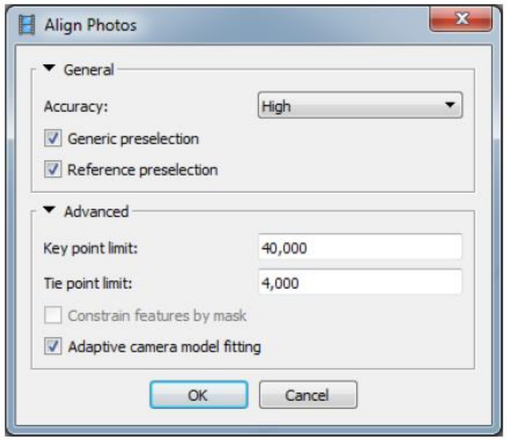

Set the following recommended values for the parameters in the *Align Photos* dialog:

Accuracy: *High* (lower accuracy setting can be used to get rough camera positions in a shorter time)

Pair preselection: *Reference* + *Generic* (in case camera positions are unknown – only *Generic* preselection mode should be used)

Constrain features by mask: *Disabled* (*Enabled* in case any areas have been masked)

Key point limit: *40,000*

Tie point limit: *4,000*

Adaptive camera model fitting: *Enabled* (to let PhotoScan distortion parameters estimation).

Click *OK* button to start photo alignment. In a short period of time (depends on the number of images in the project and their resolution) you will get sparse point cloud model shown in the Model view. Camera positions and orientations are indicated by blue rectangles in the view window:

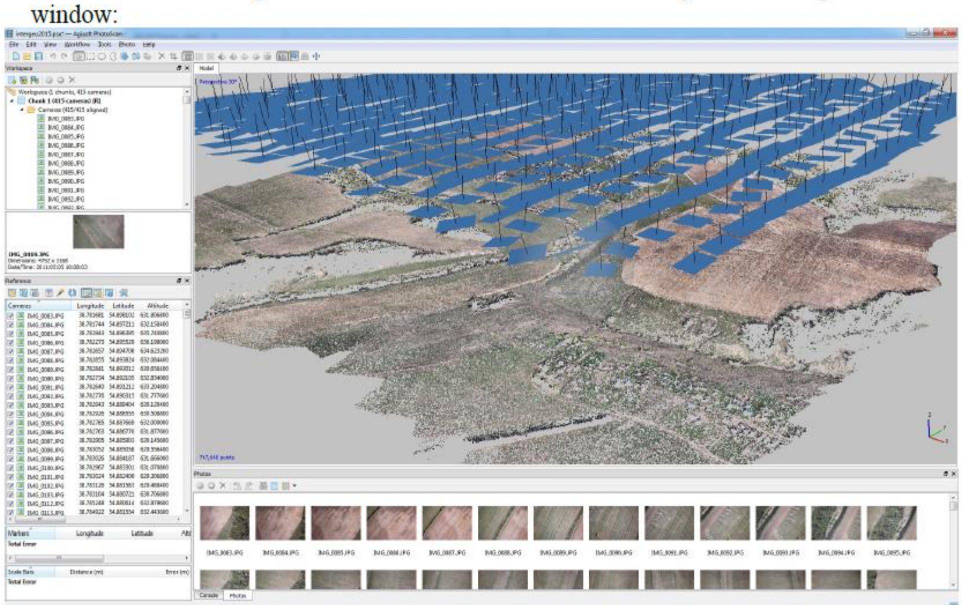

Place Markers

Markers are used to optimize camera positions and orientation data, which allows for better model referencing results.

To generate accurately georeferenced orthomosaic at least 10 – 15 ground control points (GCPs) should be distributed evenly within the area of interest.

To be able to follow guided marker placement approach (which would be faster and easier), you need to reconstruct geometry first.

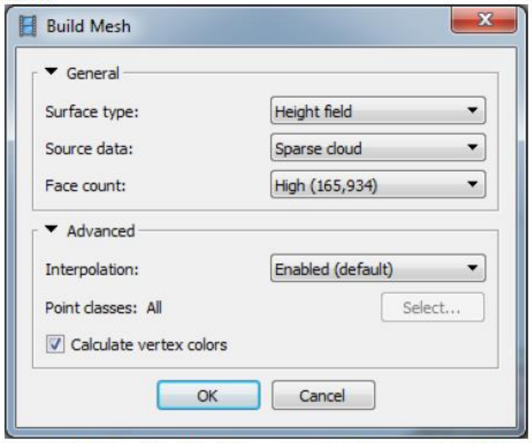

Select *Build Mesh* command from the *Workflow* menu and specify following parameters in the *Build Mesh* dialog:

Click OK button.

Then, when geometry is built (it usually takes a few seconds to reconstruct mesh based on the sparse point cloud), open a photo where a GCP is visible in Photo View by double-clicking on its icon on the *Photos* pane. Zoom in to locate the GCP on the photo and place a marker in the corresponding point of the image using *Create Marker* command from the photo context menu available on right-click on the opened photo in the corresponding position:

Input Marker Coordinates

Finally, import marker coordinates from a file. Click *Import* button on the *Reference* pane toolbar and select file containing GCP coordinates data in the *Open* dialog. The easiest way is to load simple character-separated file (*.txt) that contain markers name, x-, y- coordinates and height.

In *Import CSV* dialog indicate the delimiter according to the structure of the file and select the row to start loading from. Note that # character indicates a commented line that is not counted while numbering the rows. Indicate for the program what parameter is specified in each column through setting correct column numbers in the *Columns* section of the dialog.

Also it is recommended to specify valid coordinate system in the corresponding field for the values used for camera center data.

Check your settings in the sample data field in *Import CSV* dialog:

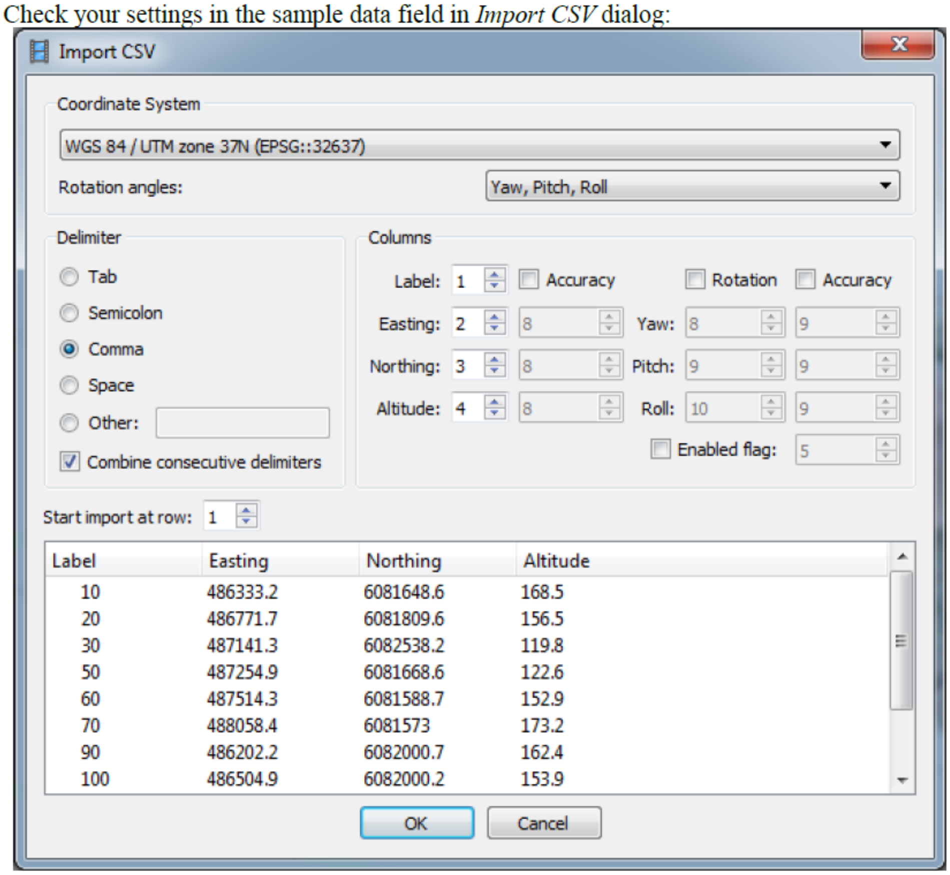

Click *OK* button. The data will be loaded into the *Reference* pane.

Optimize Camera Alignment

To achieve higher accuracy in calculating camera external and internal parameters and to correct possible distortion (e.g. "bowl effect" and etc.), optimization procedure should be run. This step is especially recommended if the ground control point coordinates are known almost precisely – within several centimeters accuracy (marker based optimization procedure).

Click the *Settings* button in the *Reference* pane and in the *Reference Settings* dialog select corresponding coordinate system from the list according to the GCP coordinates data.

Prior to optimization it is also possible to remove the points with the highest reprojection error values using corresponding criterion in Edit Menu → Gradual Selection dialog.

Set the following values for the parameters in *Measurement accuracy* section and check that valid coordinate system is selected that corresponds to the system that was used to survey GCPs:

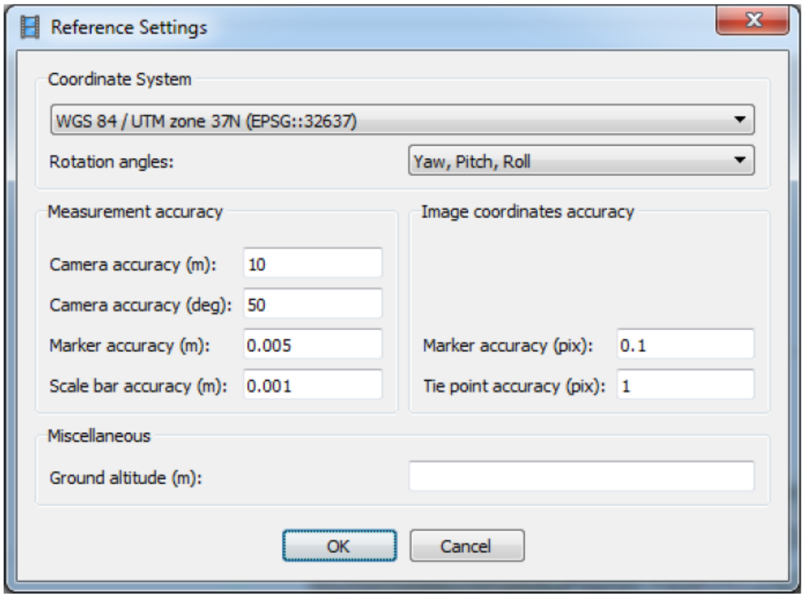

Marker accuracy: *0.005* (specify value according to the measurement accuracy).
Scale bar accuracy: *0.001*
Projection accuracy: *0.1*
Tie point accuracy: *1*

Click OK button.

On the *Reference* pane **uncheck all photos** and check on the markers to be used in optimization procedure. The rest of the markers that are not taken into account can serve as validation points to evaluate the optimization results. It is recommended since camera coordinates are usually measured with considerably lower accuracy than GCPs, also it allows to exclude any possible outliers for camera positions caused by the onboard GPS device failures.

Click *Optimize* button on the *Reference* pane toolbar.

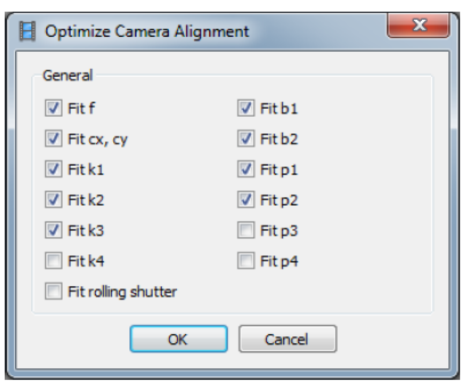

Select camera parameters you would like to optimize. Click *OK* button to start optimization process. (For DJI drone cameras it is usually suggested to optimize the rolling shutter).

Set Bounding Box

Bounding Box is used to define the reconstruction area.

Bounding box is resizable and rotatable with the help of Resize Region and Rotate Region tools from the Toolbar.

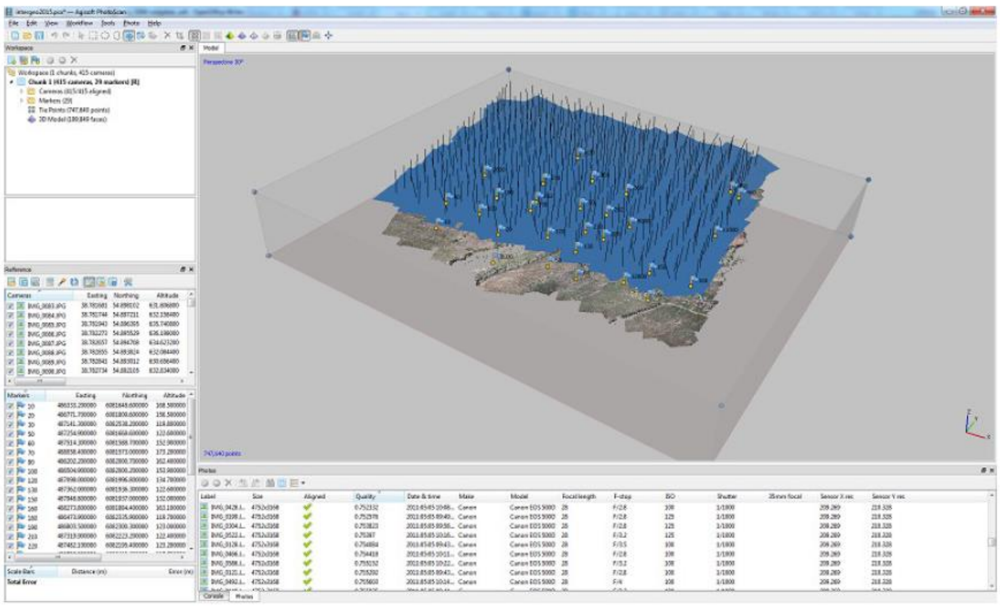

<u>**Important:** The colored side of the bounding box indicates the plane that would be treated as ground plane and has to be set **under** the model and **parallel** to the XY plane. This is important if mesh is to be built in Height Field mode, which is reasonable for aerial data processing workflow.</u>

Build Dense Point Cloud

Based on the estimated camera positions the program calculates depth information for each camera to be combined into a single dense point cloud.

Select *Build Dense Cloud* command from the *Workflow* menu.

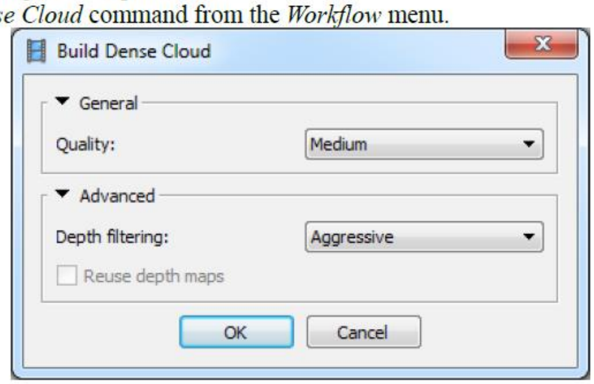

Set the following recommended values for the parameters in the *Build Dense Cloud* dialog:

<u>Quality</u>: *Medium* (higher quality takes quite a long time and demands more computational resources, lower quality can be used for fast processing)

<u>Depth filtering</u>: *Aggressive* (if the geometry of the scene to be reconstructed is complex with numerous small details or untextured surfaces, like roofs, it is recommended to set *Mild* depth filtering mode, for important features not to be sorted out)

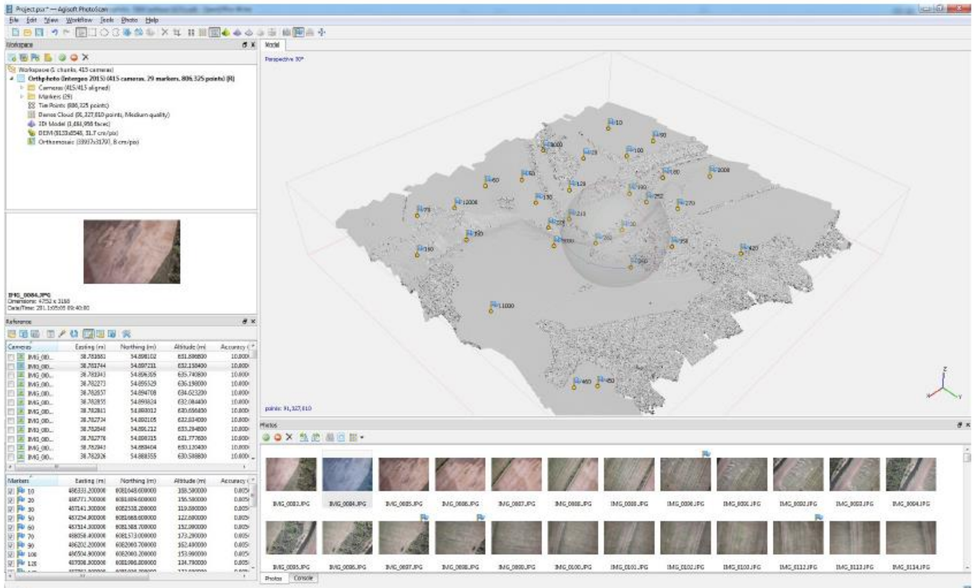

Points from the dense cloud can be removed with the help of selection tools and *Delete/Crop* instruments located on the Toolbar.

Build Mesh (optional: can be skipped if polygonal model is not required as a final result)

After dense point cloud has been reconstructed it is possible to generate polygonal mesh model based on the dense cloud data.

Select Build Mesh command from the Workflow menu.

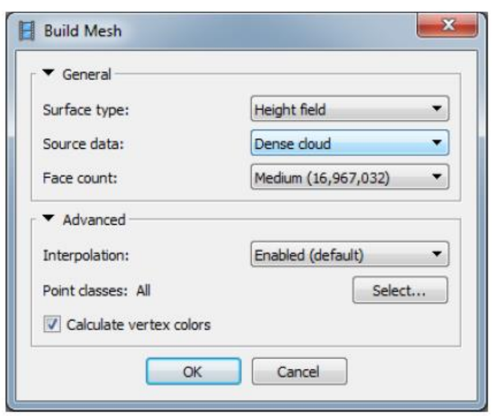

Set the following recommended values for the parameters in the *Build Mesh* dialog:

<u>Surface type:</u> *Height Field*

<u>Source data</u>: *Dense cloud*

<u>Polygon count</u>: *Medium* (maximum number of faces in the resulting model. The values indicated next to *High/Medium/Low* preset labels are based on the number of points in the dense cloud. Custom values could be used for more detailed surface reconstruction).

<u>Interpolation</u>: *Enabled*

Click *OK* button to start mesh reconstruction.

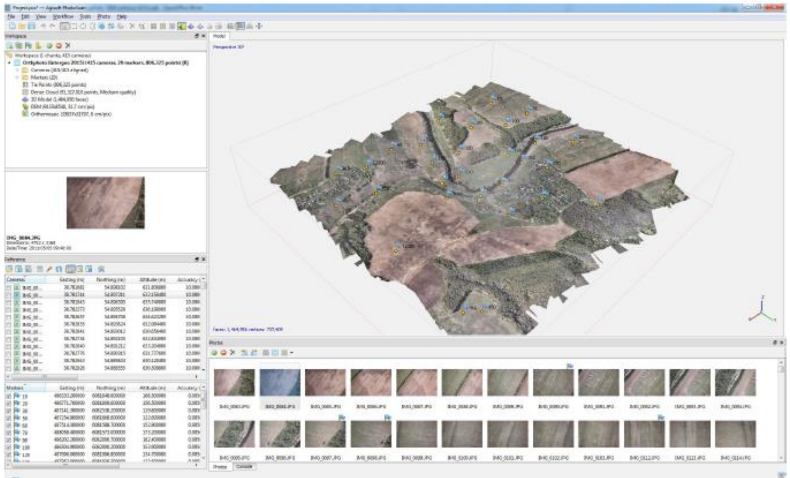

Edit Geometry

Sometimes it is necessary to edit geometry before building texture atlas and exporting the model.

Unwanted faces could be removed from the model. Firstly, you need to indicate the faces to be deleted using selection tools from the toolbar. Selected areas are highlighted with red color in the Model View. Then, to remove the selection use Delete Selection button on the Toolbar (or Del key) or use Crop Selection button on the Toolbar to remove all but selected faces.

If the overlap of the original images was not sufficient, it may be required to use *Close Holes* command from the *Tools* menu at geometry editing stage to produced holeless model. In *Close Holes* dialog select the size of the largest hole to be closed (in percentage of the total model size).

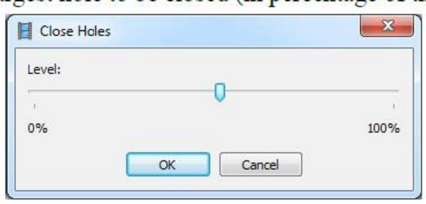

PhotoScan tends to produce 3D models with excessive geometry resolution. That's why it is recommended to decimate mesh before exporting it to a different editing tool to avoid performance

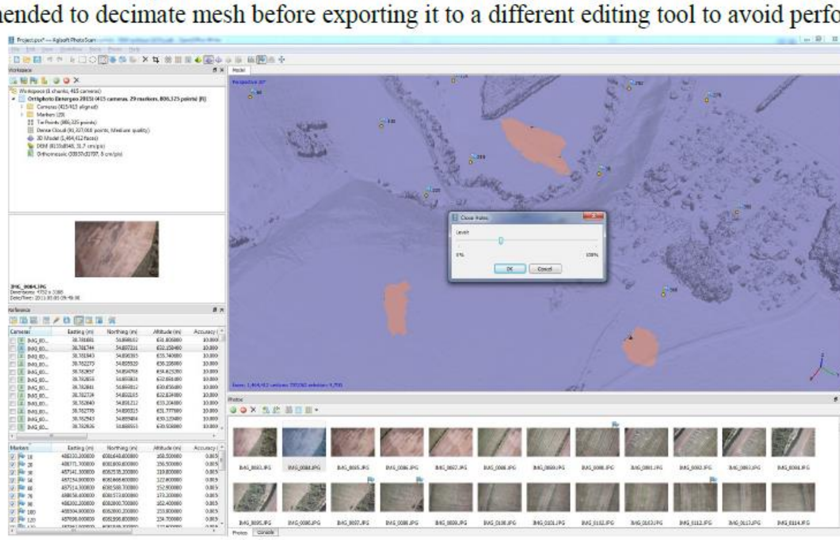

decrease of the external program.

To decimate 3D model select *Decimate Mesh...* command from the Tools menu. In the *Decimate Mesh* dialog specify the target number of faces that should remain in the final model. For PDF export task or web-viewer upload it is recommended to downsize the number of faces to 100,000 - 200,000.

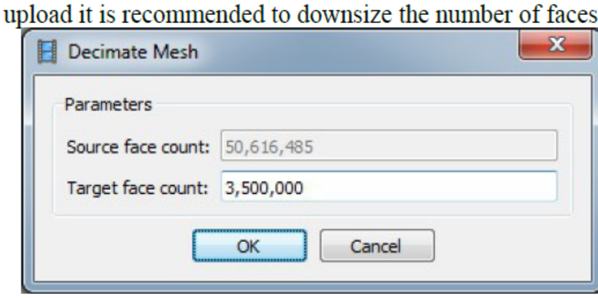

Click *OK* button to start mesh decimation procedure.

Build Texture (optional; applicable only to polygonal models)

This step is not really needed in the orthomosaic export workflow, but it might be necessary to inspect a textured model before exporting it or it might be helpful for precise marker placement.

Select *Build Texture* command from the *Workflow* menu.

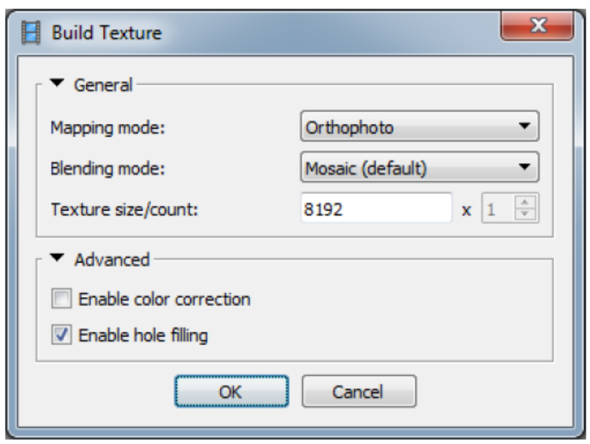

Set the following recommended values for the parameters in the *Build Texture* dialog:

Mapping mode: Orthophoto
Blending mode: *Mosaic*
Texture size/count: 8192 (width & height of the texture atlas in pixels)
Enable color correction: *disabled* (the feature is useful for processing of data sets with extreme brightness variation, but for general case it could be left unchecked to save the processing time)

Click *OK* button to start texture generation.

APPENDIX G

CASE STUDY 3: CLOSE-RANGE AERIAL PHOTOGRAMMETRY RESULTS ON CITY STREET INTERSECTION 2

Aerial Close-Range Photogrammetry versus Robotic Total Station

After aligning 1200+ DJI images, the photo-based model was geo-referenced with GPS coordinates from the Georgia-East State Plane Coordinate System. The PhotoScan software displayed a reference setting panel for the operator to set any parameters that may be appropriate for a specific output from the photo-based model. Since this case study focuses on the accuracy of distance measurements, marker accuracy and scale bar accuracy must be taken into consideration. Initially, the marker and scale bar accuracies were set to 0.001 meters (1 millimeter) and 0.01 pixels, along with 1 pixel per tie point. Camera accuracy was set to the default setting of 10 m and 2° in angular accuracy (Figure 25). With these parameter settings, the software estimated an inherent error of 11 mm for the point coordinates (Figure G.1) and an inherent error of 2 mm for the scale bar measurements (Figure G.2).

Each geo-referenced control point was acquired via a rapid RTK approach, stationing the GPS instrument for only about 15 seconds on each of them. This resulted in errors in their position coordinates, as seen in Table G.1. Consequently, after geo-referencing, the inherent or minimum relative position error in this study is 0.034 ft (i.e., 0.42 inches) or 11 mm. Including the geo-referenced control points, a total of 40 sample points was acquired in the photo-based model. Due to points unable to be attained in the field with the benchmark instrument, the remaining 30 points were employed for this comparison analysis. Due to three inconsistent outliers (S6, S7 and S8) were present in each measurement. They have component discrepancies between 0.52 ft and 51.87 ft, respectively shown in Table G.1. It was realized that those three points represented data erroneously collected in the field and, consequently, they were removed from the present study which was completed with the remaining 27 surrounding points.

Markers	X est (ft)	Y est (ft)	Z est (ft)	Accuracy (m)	Error (m)	Projections	Error (pix)
E1	884877.834691	773971.417715	208.995836			15	0.083
E4	884873.911947	773953.861366	183.909127			8	0.049
E5	884929.621113	774026.765320	210.956769			11	0.019
E9	884975.774105	773972.168101	213.931989			26	0.328
E10	884898.043781	773945.005990	212.367442			24	0.148
E11	885027.802711	774013.475729	214.557524			27	3.760
E12	884936.921125	774023.267997	213.945667			19	1.444
GL1	884591.216378	773877.587980	211.876817	0.001000	0.005410	12	0.098
GL2	884792.014921	773822.787151	210.165035	0.001000	0.017372	45	0.062
GL3	884908.352003	773908.401224	210.703829	0.001000	0.013427	28	0.520
GL5	885240.765188	773872.216959	210.229941	0.001000	0.005407	26	0.017
GL8	885203.200590	774289.124523	207.521531	0.001000	0.004201	17	0.024
N1	884991.797180	773942.102451	207.048766			33	1.215
N11	884989.281793	773952.503896	207.205269			26	1.559
N12	884935.275119	773896.530363	210.711719			53	0.508
N19	884964.744479	773894.216305	210.816783			65	0.280
N20	884998.395348	773966.623197	207.900583			21	0.887
N21	885085.553549	773954.051398	198.136307			22	0.006
N22	885030.831245	773957.021146	202.887657			26	0.239
N23	885347.964915	773973.177970	201.509561			10	0.071
N24	885361.713303	773955.575113	192.722747			9	0.046
N25	885246.144342	774030.947698	193.611056			4	2.916
N26	885135.909642	773968.538659	198.273802			17	2.708
N28	885360.444069	773965.516122	193.012947			9	1.070
S2	884670.861760	773808.957666	207.930082			24	0.068
S3	884685.464422	773813.840798	181.496084			10	0.017
S6	884437.147355	773843.417840	185.048491			7	0.026
S7	884454.955672	773774.819573	183.368218			9	0.001
S8	884436.237362	773853.840184	198.069021			9	0.047
S10	884759.886465	773828.281499	209.322605			14	0.026
S11	884753.164400	773859.989092	211.415212			20	0.447
S12	884721.901549	773891.633064	212.001782			9	0.605
S12b	884623.342101	773876.010365	212.342424			14	0.179
S13	884725.612951	773860.398364	211.804106			11	1.412
S13b	884627.318329	773844.477995	212.222283			27	0.112
W1	884885.948828	773851.543710	203.751080			41	0.041
W3	884920.549438	773863.977559	198.209056			32	0.268
W6	884942.874079	773760.951469	189.599556			6	0.018
W11	884800.483933	773764.602461	206.839547			33	0.017
W12	884835.698767	773803.704016	209.763747			47	0.206
W13	884852.601009	773809.893188	209.751649			55	0.146
W14	884906.197569	773757.906556	189.979483			18	0.012
Total Error							
Control points					0.010566		0.248
Check points							0.980

Figure G.1: Estimated Point Coordinates and Error Measurement via PhotoScan Software

GL8_S6	270.225474	
GL8_S7	276.842764	
GL8_S8	268.811743	
GL8_S10	194.907287	
GL8_S11	189.542104	
GL8_S12	190.266956	
GL8_S13	195.622735	
GL8_W1	164.744621	
GL8_W3	155.635960	
GL8_W6	179.562969	
GL8_W11	201.561618	
GL8_W12	185.577191	
GL8_W13	180.987849	
GL8_W14	185.581036	
Total Error		
Control scale ...		0.001871
Check scale b...		

Figure G.2: Sample of Estimated Distances and Total Error via PhotoScan Software

The ranges of these discrepancies (max and min values), their mean values, root mean square (RMS) values and standard deviations are summarized in Table G.2. It can be observed that all three RMS values and their associated standard deviations range in magnitude from 0.15 ft to 16.75 ft (or from 1.8 inches to 201 inches). That is, about 46 mm to 5105 mm each of them. This error is statistically more than one-sigma and it is not consistent with the inherent error in this study. From this observation, the sample size still contains one more outliers that may need to be removed for an improved analysis.

The measured coordinates of the selected center points (GL1, GL2, GL3, GL5, GL8 and N12) are listed in Table G.3. The control points were chosen as center points for 179 distances, due to the minimum amount of discrepancy compared to the known GPS coordinates. Aside from the control points, sample point N12 was chosen as a center point because it consisted the lowest discrepancy at the center, compared to other sample points. So, an assumption was made that sample point N12 would be an appropriate center point for this analysis. All coordinates of each point location were displayed in metric units within the PhotoScan software. A conversion factor of 1 ft = 0.3048 m was applied to the photogrammetric distance estimations from meters to feet, so the analysis is in the same unit of measurement as the robotic total station.

Table G.1: Discrepancy in 30 Coordinates (Photogrammetry versus Robotic Total Station)

Discrepancy in Coordinates (UAV vs. Total Station)									
Sample Size	**Point Labels**	**Diff. in Northing (ft)**	**Diff. in Easting (ft)**	**Diff. in Elevation (ft)**	**Sample Size**	**Point Labels**	**Diff. in Northing (ft)**	**Diff. in Easting (ft)**	**Diff. in Elevation (ft)**
1	**E1**	-0.369	-0.425	-4.115	16	**N28**	0.182	0.352	-32.702
2	**E4**	0.029	-0.141	-52.415	17	**S2**	-0.018	0.070	-5.538
3	**E5**	-0.561	0.172	-1.263	18	**S3**	-0.287	0.545	-56.505
4	**E9**	-0.369	0.325	4.618	~~19~~	~~**S6**~~	~~0.959~~	~~0.926~~	~~-50.207~~
5	**E10**	-0.272	-0.214	2.369	~~20~~	~~**S7**~~	~~0.895~~	~~1.234~~	~~-51.870~~
6	**E11**	-0.078	0.634	5.249	~~21~~	~~**S8**~~	~~0.831~~	~~0.522~~	~~-25.360~~
7	**E12**	-0.505	0.330	4.413	22	**S10**	0.247	-0.051	-2.059
8	**N1**	-0.347	0.430	-8.313	23	**S11**	0.025	-0.272	1.150
9	**N11**	-0.343	0.465	-8.046	24	**S12**	-0.099	-0.458	1.354
10	**N12**	-0.079	0.204	0.099	25	**S13**	0.224	-0.280	1.375
11	**N19**	-0.306	0.391	0.099	26	**W1**	-0.043	0.477	-12.620
12	**N21**	-0.320	0.444	-25.358	27	**W3**	0.025	0.685	-23.599
13	**N24**	0.098	0.325	-33.025	28	**W6**	-0.036	0.620	-37.447
14	**N25**	-0.345	0.182	-32.433	29	**W11**	0.133	0.094	-4.950
15	**N26**	-0.145	0.465	-25.295	30	**W14**	0.128	0.579	-37.057

Table G.2: Statistical Analysis of 27 Coordinate Discrepancies

	|Diff.| in Northing (ft)	|Diff.| in Easting (ft)	|Diff.| in Elevation (ft)
Min =	0.018	0.051	0.099
Max =	0.561	0.685	56.505
Mean =	0.208	0.357	15.684
Std Dev. =	0.152	0.174	16.751
RMS =	0.374	0.480	25.866

161 Distances measured with the robotic total station ranged from approximately 30 ft to 774 ft. The ranges of these discrepancies (max and min values), their mean values, root mean square (RMS) values and standard deviations are summarized in Table G.3. Those rows are ordered by increased discrepancies in the location of their center points. This order shows some correlation with the column containing RMS value of the associated discrepancies. All calculated discrepancies were plotted in Figure G.3, where it can be observed that 20% of them (32) are in the ±0.1-foot range (approximately ±1 inch. That is, most of the distances do not have a discrepancy within the inherent error of the model which is related to the geo-referenced control points.

Table G.3: Analysis of Discrepancies in 161 Measured Distances (Selected Center Points)

Selected Center Point	Employed Instrum. to acquire coords.	Coordinates of Center Point and their discrepancies			ANALYSIS of DISCREPANCIES in 161 MEASURED DISTANCES						
		Northing (ft)	Easting (ft)	Elev. (ft)	Discrepancy in Center Location, (ft)	# of Measured Distances	Min Discrep. (ft)	Max Discrep. (ft)	Mean Discrep. (ft)	Std Dev Discrep. (ft)	RMS Discrep. (ft)
GL8	UAV	885203.201	774289.125	207.522	0.014	27	-0.684	0.546	-0.178	0.345	0.414
	Total-Sta	885203.196	774289.113	207.515							
	Discrep.	0.005	0.011	0.007							
GL1	UAV	884591.216	773877.588	211.877	0.018	27	-0.691	0.303	-0.103	0.259	0.314
	Total-Sta	884591.220	773877.585	211.894							
	Discrep.	-0.004	0.003	-0.017							
GL5	UAV	885240.765	773872.217	210.230	0.018	27	-0.855	0.619	0.170	0.323	0.405
	Total-Sta	885240.769	773872.232	210.238							
	Discrep.	-0.004	-0.015	-0.009							
GL3	UAV	884908.352	773908.401	210.704	0.044	27	-0.907	0.413	-0.082	0.254	0.280
	Total-Sta	884908.389	773908.389	210.724							
	Discrep.	-0.037	0.013	-0.020							
GL2	UAV	884792.015	773822.787	210.165	0.057	27	-0.760	0.321	-0.100	0.242	0.311
	Total-Sta	884791.975	773822.799	210.126							
	Discrep.	0.040	-0.012	0.039							
N12	UAV	884935.275	773896.530	210.712	0.240	26	-1.743	1.816	-0.009	1.037	0.096
	Total-Sta	884935.354	773896.326	210.613							
	Discrep.	-0.079	0.204	0.099							

Table G.4 (a): Discrepancy Analysis of 161 Measured Distances in Georeferenced Photo-Based Model

	Distance Measured (RTS,ft)	Discrepancy (ft)	Relative Discrepancy (%)	Absolute Discrepancy (ft)
Min =	29.558	-1.743	-4.348	0.005
Max =	774.453	1.816	1.526	1.816
Mean =		-0.018	-0.044	0.335
Std Dev =		0.494	0.481	0.363
Median =		-0.040	-0.020	0.237
				Median of |Discr|

Table G.4 (b): Discrepancy Analysis of 161 Measured Distances in Georeferenced Photo-Based Model

<table>
<tr><th>Sum & %</th><th>Sum & %</th><th>Sum & %</th><th>Sum & %</th><th>Sum & %</th><th>Sum & %</th><th>Sum & %</th><th>Sum & %</th><th>Sum & %</th></tr>
<tr><td>7</td><td>18</td><td>25</td><td>27</td><td>32</td><td>50</td><td>67</td><td>80</td><td>110</td></tr>
<tr><td>4.3%</td><td>11.2%</td><td>15.5%</td><td>16.8%</td><td>19.9%</td><td>31.1%</td><td>41.6%</td><td>49.7%</td><td>68.3%</td></tr>
<tr><td>Points with |Discr|<0.02</td><td>Points with |Discr|<0.04</td><td>Points with |Discr|<0.06</td><td>Points with |Discr|<0.08</td><td>Points with |Discr|<0.10</td><td>Points with |Discr|<0.15</td><td>Points with |Discr|<0.20</td><td>Points with |Discr|<Median</td><td>Points with |Discr|<0.35</td></tr>
<tr><td>0.020 ft</td><td>0.040 ft</td><td>0.060 ft</td><td>0.080 ft</td><td>0.100 ft</td><td>0.150 ft</td><td>0.200 ft</td><td>0.237 ft</td><td>0.350 ft</td></tr>
</table>

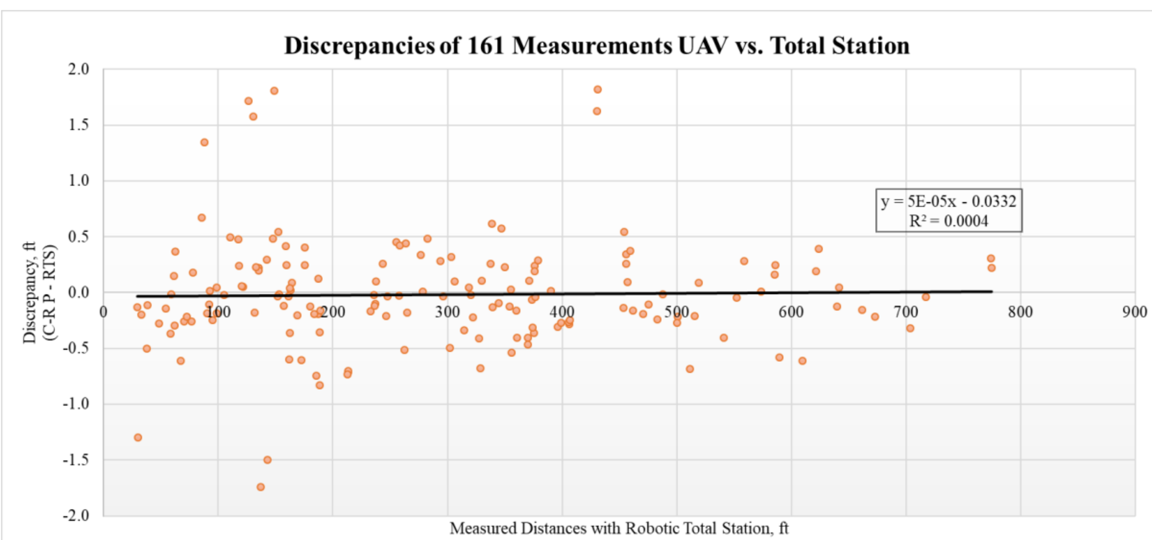

Figure G.3: Graph – Discrepancy of 161 Measurements (UAV versus Total Station)

Recommendation for Scale Bar Measurement Accuracy

By employing the new scale bar accuracy, the setting was adjusted to 0.0001 meters, which was recommended by the Cultural Heritage Imaging (2015) (Figure 26). The marker accuracy was changed to the same parameter as the scale bar accuracy, as well. After optimizing the camera alignment, the point coordinates displayed an inherent error of 7 mm (Figure G.4) and the scale bar measurements displayed an inherent error of 4 mm (Figure G.5).

Markers	X est (ft)	Y est (ft)	Z est (ft)	Accuracy (m)	Error (m)	Projections	Error (pix)
☐ E1	884877.110801	773971.057777	211.732453			15	0.124
☐ E4	884872.599528	773954.171271	183.215683			8	0.045
☐ E5	884929.085785	774027.083636	214.602916			11	0.230
☐ E9	884975.685382	773972.387082	215.885205			26	0.469
☐ E10	884897.689913	773944.677854	214.193060			24	0.201
☐ E11	885027.765122	774013.801036	216.958051			27	0.058
☐ E12	884936.467025	774023.511292	217.862677			19	0.195
☑ GL1	884591.222738	773877.591554	211.892619	0.000100	0.002214	12	0.129
☑ GL2	884792.016901	773822.817201	210.118681	0.000100	0.014123	45	0.200
☑ GL3	884908.383231	773908.382660	210.725002	0.000100	0.002601	28	0.463
☑ GL5	885240.769496	773872.231094	210.237126	0.000100	0.000513	26	0.042
☑ GL8	885203.208476	774289.128872	207.516133	0.000100	0.006115	17	0.049
☐ N1	884991.740674	773942.512742	207.316463			33	1.216
☐ N11	884989.223312	773952.927540	207.712431			26	1.536
☐ N12	884935.263680	773896.634053	210.350237			53	0.700
☐ N19	884964.737163	773894.390896	210.323381			65	0.411
☐ N20	884998.365661	773967.047028	208.874901			21	0.849
☐ N21	885085.767629	773954.165888	197.646424			22	0.036
☐ N22	885030.924474	773957.735789	203.278905			26	0.750
☐ N23	885348.083346	773973.596988	202.050897			10	0.157
☐ N24	885361.597926	773955.950459	191.554456			9	0.237
☐ N25	885245.930493	774030.571070	193.012108			4	0.022
☐ N26	885135.828277	773968.566158	199.041687			17	0.063
☐ N28	885360.392995	773965.979944	192.129421			9	0.314
☐ S2	884672.331490	773809.757456	206.643564			24	0.093
☐ S3	884687.002251	773815.951738	177.586529			10	0.029
☐ S6	884435.400378	773845.002868	172.057072			7	0.022
☐ S7	884454.181404	773774.562850	167.454466			9	0.003
☐ S8	884433.822047	773854.877461	187.598626			9	0.039
☐ S10	884760.615227	773828.610059	208.352342			14	0.123
☐ S11	884754.216154	773860.083916	211.968455			20	0.610
☐ S12	884723.497916	773891.722164	215.660283			9	0.544
☐ S12b	884623.776004	773876.152190	214.199365			14	0.317
☐ S13	884726.914512	773860.451294	214.445560			11	0.817
☐ S13b	884628.150982	773844.298411	212.849676			27	0.258
☐ W1	884885.775540	773851.533659	202.289340			41	0.087
☐ W3	884920.420554	773864.397814	196.058153			32	0.349
☐ W6	884943.232502	773761.662683	183.018625			6	0.017
☐ W11	884799.935212	773764.972495	203.968151			33	0.071
☐ W12	884835.401270	773803.453883	209.013726			47	0.274
☐ W13	884852.341532	773809.554290	208.803464			55	0.204
☐ W14	884906.047424	773758.362107	183.762043			18	0.050
Total Error							
Control points					0.007054		0.251
Check points							0.519

Figure G.4: Results of Estimated Coordinates and Overall Error Measurement in PhotoScan (from the Recommendation of the Cultural Heritage Imaging)

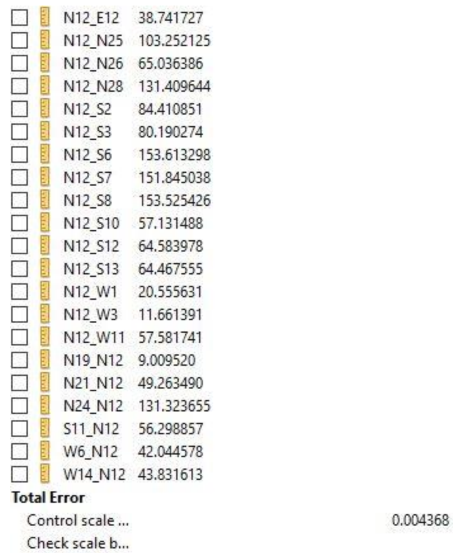

N12_E12	38.741727
N12_N25	103.252125
N12_N26	65.036386
N12_N28	131.409644
N12_S2	84.410851
N12_S3	80.190274
N12_S6	153.613298
N12_S7	151.845038
N12_S8	153.525426
N12_S10	57.131488
N12_S12	64.583978
N12_S13	64.467555
N12_W1	20.555631
N12_W3	11.661391
N12_W11	57.581741
N19_N12	9.009520
N21_N12	49.263490
N24_N12	131.323655
S11_N12	56.298857
W6_N12	42.044578
W14_N12	43.831613
Total Error	
Control scale ...	0.004368
Check scale b...	

Figure G.5: Sample of Estimated Distances and Total Error via PhotoScan Software (from the Recommendation of the Cultural Heritage Imaging)

Compared to the previously explained parameters set for the end results, the inherent errors appeared to be more accurate in point coordinates and less accurate in the scale bar measurements. Four inconsistent outliers (S3, S6, S7 and S8) were present in each distance measurement (Table G.5). They had absolute component discrepancies between 0.78 ft and 67.78 ft, respectively. It was realized that those four points represented data erroneously collected in the field. Consequently, they were removed from the present study which was completed with the remaining 26 surrounding points. A discrepancy analysis against the robotic total station was performed. The ranges of these discrepancies (max and min values), their mean values, root mean square (RMS) values and standard deviations are summarized in Table G.6. It was observed that all three RMS values and their associated standard deviations ranged in magnitude from 0.30 ft to 15.53 ft (or from 3.6 inches to 186.36 inches). That is, about 91 mm to 4734 mm each of them. This error was statistically not consistent with the inherent error in this study. From this observation, the sample size still contained more outliers within the vertical component that may need to be removed for an improved analysis.

Table G.5: Coordinate Discrepancy with Recommended Scale Bar Accuracy

Coordinate Discrepancy with Recommended Scale Bar Accuracy (UAV vs. Total Station)									
Sample Size	**Point Labels**	**Diff. in Northing (ft)**	**Diff. in Easting (ft)**	**Diff. in Elevation (ft)**	**Sample Size**	**Point Labels**	**Diff. in Northing (ft)**	**Diff. in Easting (ft)**	**Diff. in Elevation (ft)**
1	**E1**	-1.093	-0.785	-1.379	16	**N28**	0.131	0.816	-33.586
2	**E4**	-1.283	0.169	-53.108	17	**S2**	1.451	0.869	-6.824
3	**E5**	-1.096	0.491	2.383	~~18~~	~~**S3**~~	~~1.251~~	~~2.656~~	~~-60.414~~
4	**E9**	-0.458	0.544	6.571	~~19~~	~~**S6**~~	~~-0.788~~	~~2.511~~	~~-63.198~~
5	**E10**	-0.626	-0.542	4.195	~~20~~	~~**S7**~~	~~0.120~~	~~0.977~~	~~-67.784~~
6	**E11**	-0.116	0.959	7.649	~~21~~	~~**S8**~~	~~-1.584~~	~~1.559~~	~~-35.830~~
7	**E12**	-0.959	0.573	8.330	22	**S10**	0.976	0.278	-3.030
8	**N1**	-0.403	0.841	-8.046	23	**S11**	1.077	-0.177	1.703
9	**N11**	-0.402	0.889	-7.539	24	**S12**	1.497	-0.369	5.012
10	**N12**	-0.090	0.308	-0.263	25	**S13**	1.526	-0.227	4.017
11	**N19**	-0.313	0.566	-0.395	26	**W1**	-0.216	0.467	-14.082
12	**N21**	-0.106	0.559	-25.848	27	**W3**	-0.103	1.105	-25.750
13	**N24**	-0.017	0.700	-34.194	28	**W6**	0.323	1.332	-44.028
14	**N25**	-0.559	-0.195	-33.032	29	**W11**	-0.416	0.464	-7.822
15	**N26**	-0.227	0.492	-24.527	30	**W14**	-0.023	1.034	-43.274

Table G.6: Statistical Analysis of 26 Absolute Coordinate Discrepancies

	|Diff.| in Northing (ft)	**|Diff.| in Easting (ft)**	**|Diff.| in Elevation (ft)**
Min =	0.017	0.169	0.263
Max =	1.526	1.332	53.108
Mean =	**0.596**	**0.606**	**15.638**
Std Dev. =	**0.492**	**0.303**	**15.532**
RMS =	**0.773**	**0.677**	**22.040**

In comparison to the accurate one-second benchmark instrument, the photo-based model produced a minimum discrepancy of 0.001 ft with -2.52% of relative discrepancy from all 155 distance measurements. A maximum discrepancy of 1.658 ft was produced with a 2.63% of relative discrepancy of the total measurements. So, the mean discrepancy of all 155 distance measurements was 0.58 ft with a relative discrepancy of -0.04%. The result for the standard deviation for all distances measured was 0.45 ft with a relative discrepancy of 0.51% (see Table G.7). Approximately, 12% of the distances measured (19) consisted of discrepancies within the ±0.1-foot range (approximately ±1 inch). For this case study, following the recommended scale bar accuracy produced results that were less accurate in comparison the robotic total station.

Table G.7 (a): Discrepancy Analysis of 155 Measured Distances in Georeferenced Photo-Based Model

	Distance Measured (RTS, ft)	Discrepancy (ft)	Relative Discrepancy (ft)	Absolute Discrepancy (ft)
Min =	29.558	-1.658	-2.518	0.001
Max =	774.453	1.646	2.627	1.658
Mean =		-0.104	-0.038	0.581
Std Dev. =		0.731	0.512	0.455
Median =		-0.044	-0.017	0.484
				Median of |Discr|

Table G.7 (b): Discrepancy Analysis of 155 Measured Distances in Georeferenced Photo-Based Model

Sum & %	Sum & %	Sum & %	Sum & %	Sum & %	Sum & %	Sum & %	Sum & %	Sum & %
6	11	15	17	19	27	38	77	90
3.9	7.1	9.7	11.0	12.3	17.4	24.5	49.7	58.1
Points with |Discr|<0.02	**Points with |Discr|<0.04**	**Points with |Discr|<0.06**	**Points with |Discr|<0.08**	**Points with |Discr|<0.10**	**Points with |Discr|<0.15**	**Points with |Discr|<0.20**	**Points with |Discr|<Median**	**Points with |Discr|<0.60**
0.020 ft	0.040 ft	0.060 ft	0.080 ft	0.100 ft	0.150 ft	0.200 ft	0.484 ft	0.600 ft

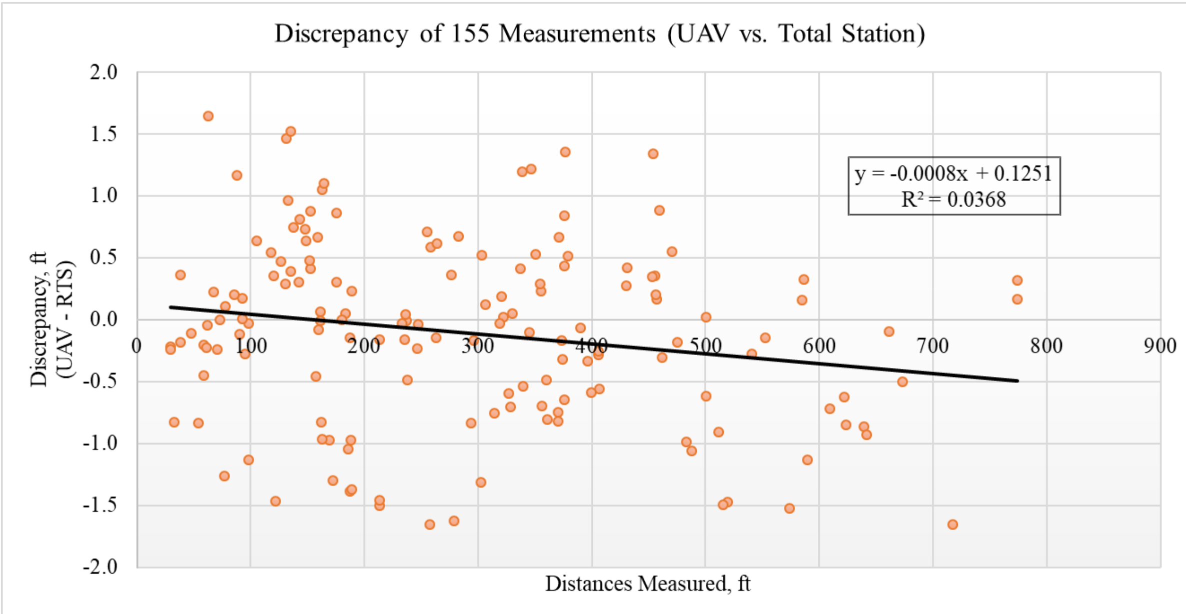

Figure G.6: Graph – Discrepancy with Recommended Accuracy Setting from Cultural Heritage Imaging (2015)

Recommendation for Camera Optimization Alignment

Another analysis was made due to a camera optimization alignment recommendation from the Agisoft PhotoScan protocol, "*Tutorial (Beginner level): Orthomosaic and DEM Generation with Agisoft PhotoScan Pro 1.3 (with Ground Control Points*)" (Appendix F). To enhance the accuracy of the estimated point coordinates and distance measurements, the protocol suggests optimizing the camera alignment as shown in Figure G.7. Yet, it suggested that the rolling shutter should be included in the optimization setting, if the personnel are using photos from a DJI drone. The rolling shutter is a setting that represents the camera acquiring neighboring images from an unmanned aerial vehicle.

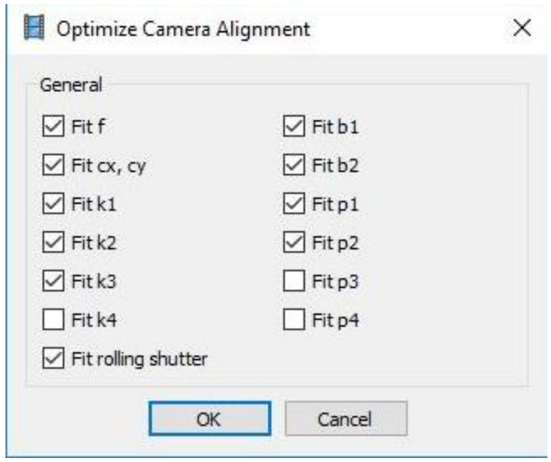

Figure G.7: Example of Optimize Camera Alignment Settings recommended by Agisoft PhotoScan (2017) for DJI Cameras

In this case study, a DJI Mavic Pro Platinum Quadcopter was employed for image acquisition. For this analysis, the rolling shutter camera alignment was optimized as suggested. Along with the recommended scale bar accuracy setting by Cultural Heritage Imaging (2015), The PhotoScan software estimated an inherent error of 142 mm for the point coordinates (Figure G.8). In addition, an inherent error of 0.40 mm was estimated for the virtual scale bar measurements (Figure G.9). Compared to the estimated inherent error from the original parameter settings, the rolling shutter camera alignment optimization increased the overall error in point coordinates. Yet, the overall error for scale bar measurements decreased to less than one millimeter. Also, an observation was made on the estimated error is pixels (Figure G.8). The pixel values had decreased and became more accurate in comparison to the default and recommended scale bar analyses. A discrepancy analysis was performed to compare these point coordinates and distance measurements against the data obtained with the accurate one-second benchmark instrument. Three inconsistent outliers (S6, S7 and S8) were present in each measurement. They had component discrepancies between 0.83 ft and 66.31 ft, respectively. It was realized that those three points represented data erroneously collected in the field and, consequently, they were removed from the present study which was completed with the remaining 27 surrounding points, as shown in Table G.8.

Markers	X est (ft)	Y est (ft)	Z est (ft)	Accuracy (m)	Error (m)	Projections	Error (pix)
E1	884876.022112	773970.102057	212.758062			15	0.000
E4	884871.122460	773953.670688	185.722899			8	0.000
E5	884926.739887	774028.066289	216.811812			11	0.002
E9	884974.312195	773973.527663	216.319946			26	0.003
E10	884896.796239	773944.343087	214.455956			24	0.000
E11	885026.877396	774015.861629	217.672278			27	0.000
E12	884934.300389	774024.547638	219.897474			19	0.002
GL1	884591.006817	773877.706602	211.806119	0.001000	0.079465	12	0.000
GL2	884792.711081	773822.522557	210.138007	0.001000	0.239671	45	0.000
GL3	884907.916229	773908.454965	210.883967	0.001000	0.153548	28	0.001
GL5	885240.553123	773872.098775	210.166296	0.001000	0.080412	26	0.000
GL8	885203.361839	774289.334931	207.502825	0.001000	0.084473	17	0.000
N1	884990.462661	773943.601189	207.420174			33	0.006
N11	884987.921640	773954.140500	207.950516			26	0.008
N12	884934.605314	773897.331398	210.359877			53	0.001
N19	884963.758501	773895.477501	210.312914			65	0.001
N20	884997.165993	773968.470263	209.125641			21	0.003
N21	885084.994974	773953.886073	196.448174			22	0.000
N22	885030.101701	773959.355084	203.772147			26	0.002
N23	885349.290011	773974.007133	201.250662			10	0.001
N24	885362.882134	773956.200223	190.859917			9	0.003
N25	885245.750653	774031.807173	192.404437			4	0.000
N26	885135.063574	773968.836807	198.558555			17	0.000
N28	885361.703584	773966.285946	191.366065			9	0.002
S2	884670.793704	773809.142007	206.723514			24	0.000
S3	884685.768557	773815.761942	177.967958			10	0.000
S6	884435.352844	773847.209517	173.263749			7	0.000
S7	884453.195893	773776.635630	168.932212			9	0.000
S8	884433.855452	773856.972723	188.242941			9	0.000
S10	884760.660967	773828.012323	209.090565			14	0.000

Figure G.8 (a): Sample of Estimated Point Coordinates via PhotoScan (from the Recommendation of Agisoft PhotoScan, 2017)

S11	884753.972874	773859.767167	212.949758			20	0.002
S12	884722.707963	773891.402673	215.885487			9	0.003
S12b	884623.119149	773875.894436	213.763981			14	0.001
S13	884726.252758	773859.929965	214.402993			11	0.002
S13b	884626.974708	773844.379687	212.423892			27	0.001
W1	884886.092298	773852.396729	202.368459			41	0.000
W3	884920.216394	773865.445472	196.376285			32	0.002
W6	884944.281480	773764.254840	182.988139			6	0.000
W11	884801.485803	773764.171934	203.667726			33	0.000
W12	884836.639417	773803.769323	208.743623			47	0.001
W13	884853.451698	773810.201226	208.441026			55	0.001
W14	884907.880555	773760.380957	183.607007			18	0.000
Total Error							
Control points					0.142081		0.000
Check points							0.002

Figure G.8 (b): Sample of Estimated Point Coordinates and Total Error via PhotoScan (from the Recommendation of Agisoft PhotoScan, 2017)

W14_N12	43.304597	
Total Error		
Control scale ...		0.000416
Check scale b...		

Figure G.9: Sample of Estimated Distance and Total Error via PhotoScan (from the Recommendation of Agisoft PhotoScan, 2017)

Table G.8: Coordinate Discrepancy with Recommended Camera Alignment Optimization

Coordinate Discrepancy with Recommended Camera Alignment Optimization (UAV vs. Total Station)									
Sample Size	**Point Labels**	**Diff. in Northing (ft)**	**Diff. in Easting (ft)**	**Diff. in Elevation (ft)**	**Sample Size**	**Point Labels**	**Diff. in Northing (ft)**	**Diff. in Easting (ft)**	**Diff. in Elevation (ft)**
1	**E1**	-2.182	-1.741	-0.353	16	**N28**	1.442	1.122	-34.349
2	**E4**	-2.761	-0.331	-50.601	17	**S2**	-0.086	0.254	-6.744
3	**E5**	-3.442	1.473	4.592	18	**S3**	0.018	2.466	-60.033
4	**E9**	-1.831	1.685	7.006	~~19~~	**~~S6~~**	~~-0.835~~	~~4.718~~	~~-61.991~~
5	**E10**	-1.520	-0.877	4.458	~~20~~	**~~S7~~**	~~-0.865~~	~~3.050~~	~~-66.306~~
6	**E11**	-1.004	3.020	8.363	~~21~~	**~~S8~~**	~~-1.551~~	~~3.655~~	~~-35.186~~
7	**E12**	-3.126	1.610	10.364	22	**S10**	1.022	-0.320	-2.291
8	**N1**	-1.681	1.929	-7.942	23	**S11**	0.834	-0.494	2.685
9	**N11**	-1.703	2.101	-7.300	24	**S12**	0.707	-0.688	5.237
10	**N12**	-0.749	1.005	-0.253	25	**S13**	0.864	-0.748	3.974
11	**N19**	-1.291	1.653	-0.405	26	**W1**	0.100	1.330	-14.003
12	**N21**	-0.879	0.279	-27.046	27	**W3**	-0.308	2.152	-25.432
13	**N24**	1.267	0.950	-34.888	28	**W6**	1.371	3.924	-44.059
14	**N25**	-0.738	1.041	-33.640	29	**W11**	1.135	-0.336	-8.122
15	**N26**	-0.991	0.763	-25.010	30	**W14**	1.811	3.053	-43.429

The ranges of these coordinate discrepancies (max and min values), their mean values, root mean square (RMS) values and standard deviations are summarized in Table G.9. For the distance discrepancies, the analysis resulted in a mean discrepancy value of 0.49 ft or 5.88 inches (relative discrepancy of -0.05%) with a standard deviation of 0.54 ft or 6.48 inches (relative discrepancy of 0.39%). Approximately, 17% of the distances measured consist of discrepancies within the ±0.1-foot range (±1 inch), as shown in Table G.10. For this case study, the recommended camera alignment optimization was more accurate than the results of the recommended scale bar accuracy for measurement. Yet, the results remained less accurate in comparison to the one-second robotic total station.

Table G.9: Statistical Analysis of 27 Coordinate Discrepancies with Recommended Camera Alignment Optimization

	|Diff.| in Northing (ft)	|Diff.| in Easting (ft)	|Diff.| in Elevation (ft)
Min =	0.018	0.254	0.253
Max =	3.442	3.924	60.033
Mean =	1.291	1.383	17.503
Std Dev. =	0.842	0.933	17.213
RMS =	1.541	1.669	24.549

Table G.10 (a): Analysis of Discrepancies in 161 Distance Measurements (Recommended Camera Alignment Optimization)

	Distance Measured (RTS,ft)	Discrepancy (ft)	Relative Discrepancy (%)	Absolute Discrepancy (ft)
Min =	29.558	-2.475	-1.977	0.006
Max =	774.453	2.334	1.074	2.475
Mean =		-0.057	-0.054	0.485
Std Dev =		0.724	0.387	0.540
Median =		-0.041	-0.020	0.278
				Median of |Discr|

Table G.10 (b): Analysis of Discrepancies in 161 Distance Measurements (Recommended Camera Alignment Optimization)

Sum & %	**Sum & %**	**Sum & %**	**Sum & %**	**Sum & %**	**Sum & %**	**Sum & %**	**Sum & %**	**Sum & %**
7	15	22	24	28	43	58	80	112
4.3	9.3	13.7	14.9	17.4	26.7	36.0	49.7	69.6
Points with |Discr|<0.02	**Points with |Discr|<0.04**	**Points with |Discr|<0.06**	**Points with |Discr|<0.08**	**Points with |Discr|<0.10**	**Points with |Discr|<0.15**	**Points with |Discr|<0.20**	**Points with |Discr|<Median**	**Points with |Discr|<0.50**
0.020 ft	0.040 ft	0.060 ft	0.080 ft	0.100 ft	0.150 ft	0.200 ft	0.278 ft	0.500 ft

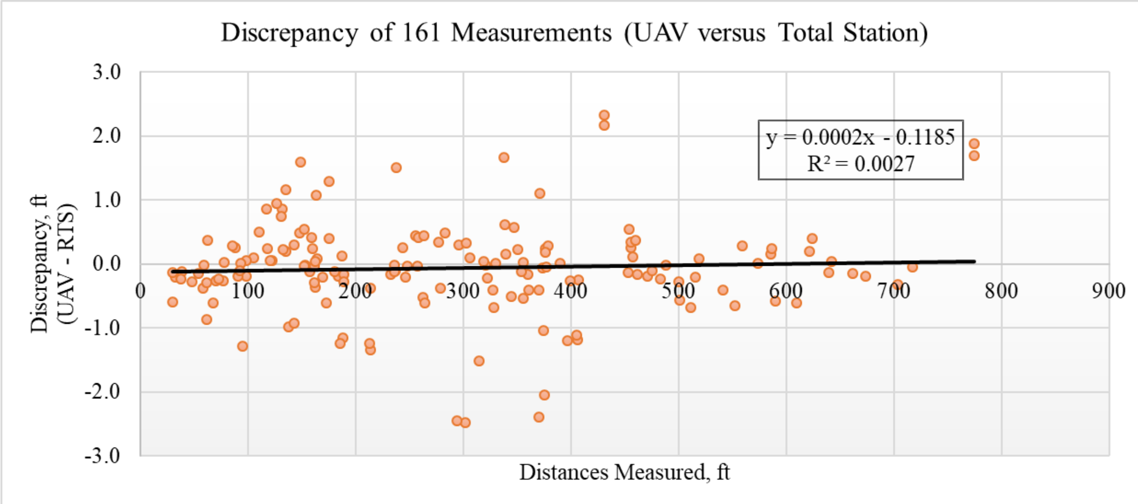

Figure G.10: Graph – Distance Discrepancy with Recommended Camera Alignment Optimization from Agisoft PhotoScan (2017)

Conclusion

Due to a limitation in point selection with the photogrammetry software, only 27 points widely distributed within the modeled area (i.e., discarding 3 outliers). The standard deviations of the discrepancies in point positions did not coincide with their associated RMS values: RMS_{North}=0.46 ft, RMS_{East}=0.60 ft, and RMS_{Elev}=3.96 ft. That is, the standard deviations of those discrepancies range from 0.152 to 16.75 ft (or from 46 to 5105 mm) in the considered intersection area. This was inconsistent with the inherent error for the 27 point coordinates which was 0.03 ft (0.42 inches) or 11 mm, as shown in Table G.11. Also, the inherent error for the 161 measured distances was 0.006 ft (0.07 inches) or 1.87 mm (Table G.11). Approximately, 7% of the discrepancies were less than 0.02 ft. Most of these discrepancies were not within the inherent error. The coordinate components were observed and most of the elevation components had erroneously large discrepancies in comparison to the point locations obtained with the accurate one-second benchmark instrument. This elevation error could be caused by human error in point acquistion within the photo-based model or in the field with the one-second robotic total station. With a comparison of the results in point position with both modern technologies, the 3D Terrestrial LiDAR is more appropriate for this particular study. To assist the Blue-Mile group and the Statesboro city engineers, the laser scanning technology produces more reliable information for redesigning a city street infrastructure with virtual surveying methods.

Table G.11: Comparison of Case Study 3 Results (Inherent Software Error versus Calculated Point and Distance Discrepancy to Robotic Total Station)

Inherent Software Error vs. Calculated Point and Distance Discrepancy to R.T.S.				
Geo-referenced (Target-to-Target) Point-Cloud Model				
		(ft)	**(in)**	**(mm)**
Inherent Software Error		0.085	1.024	**26**
Point Discrepancy	**Northing**	0.052	0.624	16
	Easting	0.039	0.468	12
	Elevation	0.042	0.504	13
Distance Discrepancy		0.053	0.636	16
Geo-referenced Photo-Based Model				
		(ft)	**(in)**	**(mm)**
Inherent Software Point Error		0.003	0.035	**11**
Point Discrepancy	**Northing**	0.208	2.495	63
	Easting	0.357	4.280	109
	Elevation	15.684	188.207	4780
Inherent Software Distance Error		0.001	0.006	**2**
Distance Discrepancy		0.335	4.020	102

APPENDIX H

PERCENT RELATIVE DISCREPANCY GRAPHS IN DISTANCES

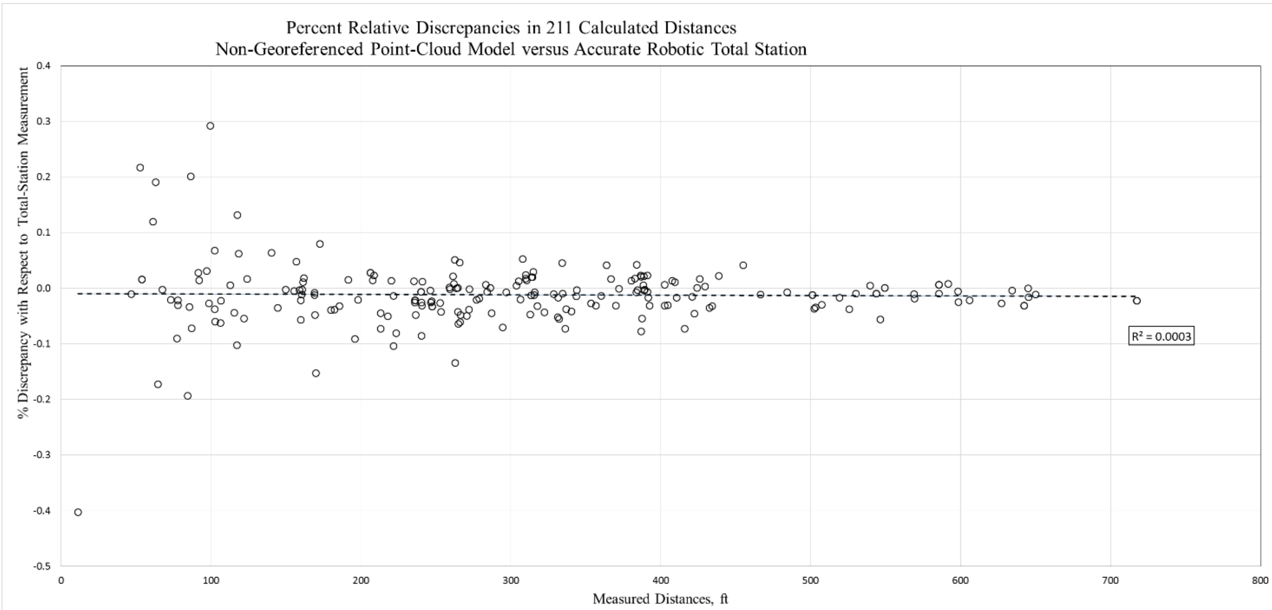

Figure H.1: Graph – Percent Relative Discrepancies in 211 Calculated Distances Non-Georeferenced Point-Cloud Model vs. Accurate-Robotic Total Station

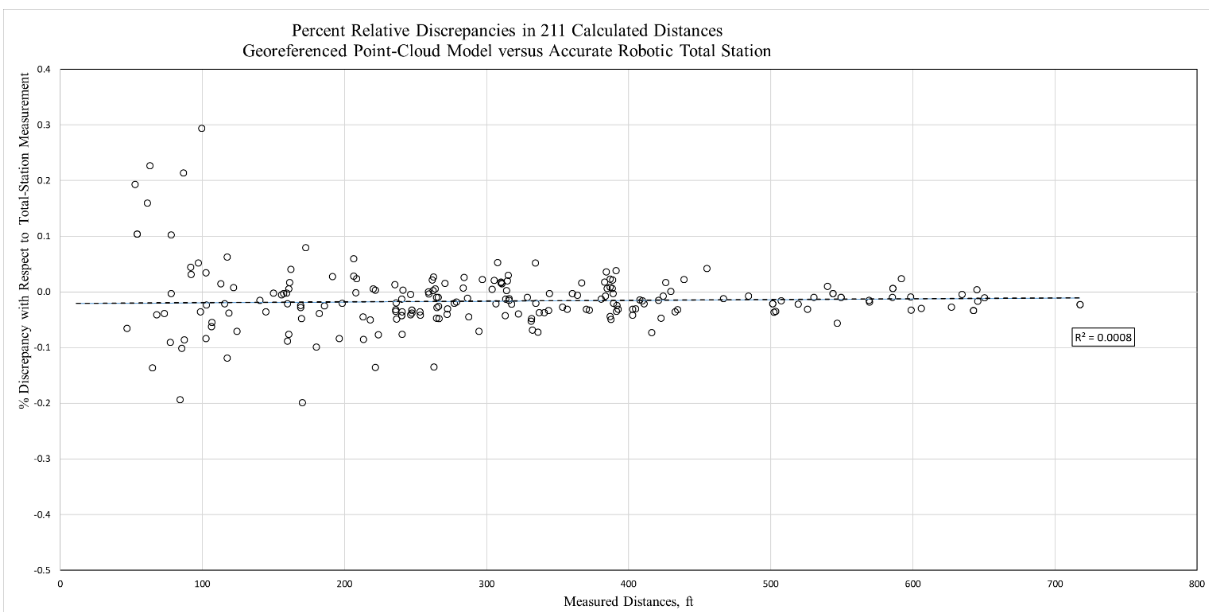

Figure H.2: Graph – Percent Relative Discrepancies in 211 Calculated Distances Georeferenced Point-Cloud Model vs. Accurate-Robotic Total Station

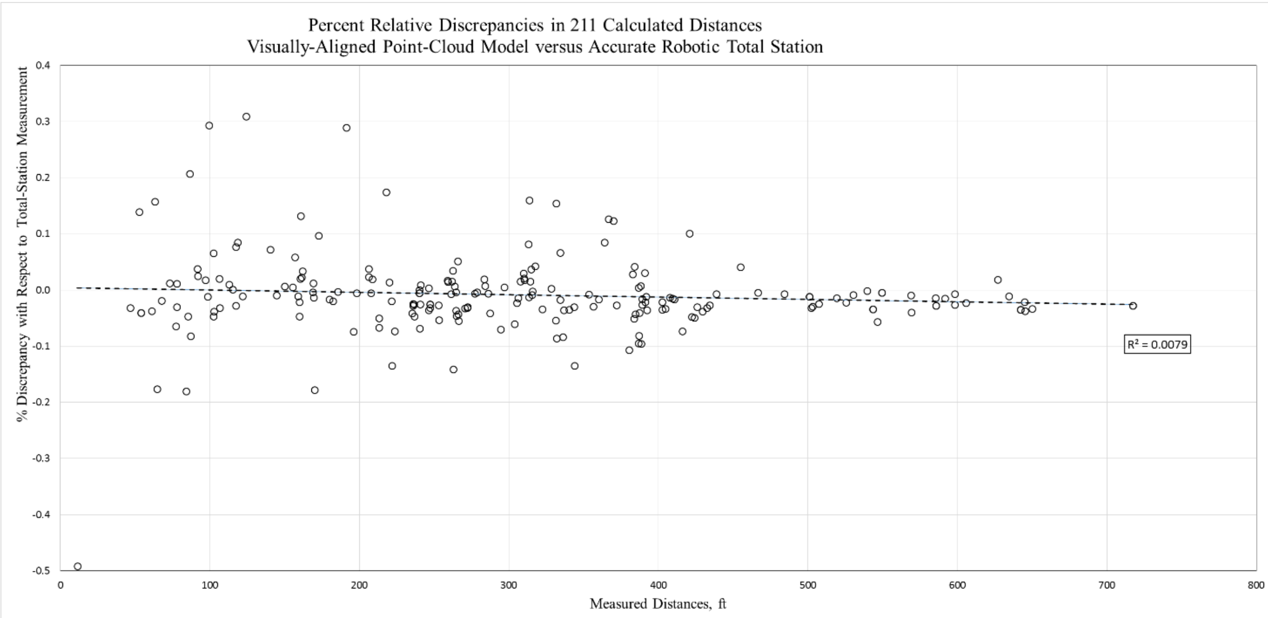

Figure H.3: Graph – Percent Relative Discrepancies in 211 Calculated Distances Visually-Aligned Point-Cloud Model vs. Accurate-Robotic Total Station

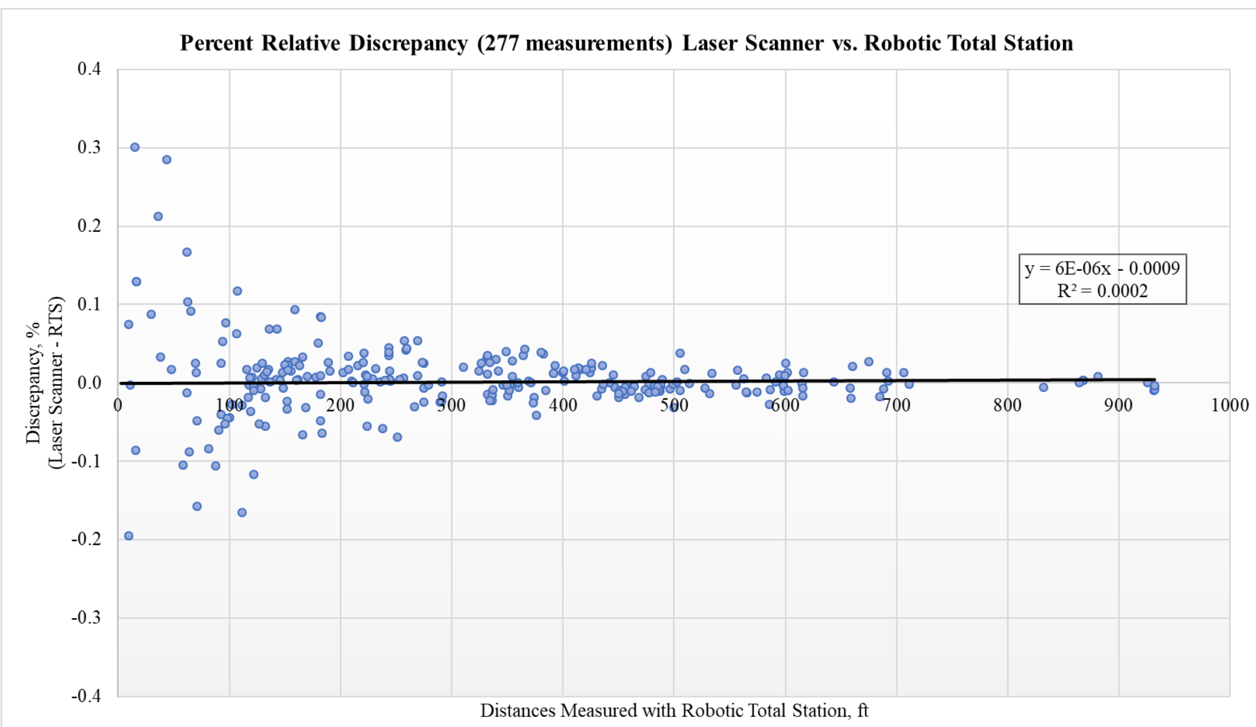

Figure H.4: Graph – Percent Relative Discrepancy of 277 Measurements (Laser Scanner versus Robotic Total Station)

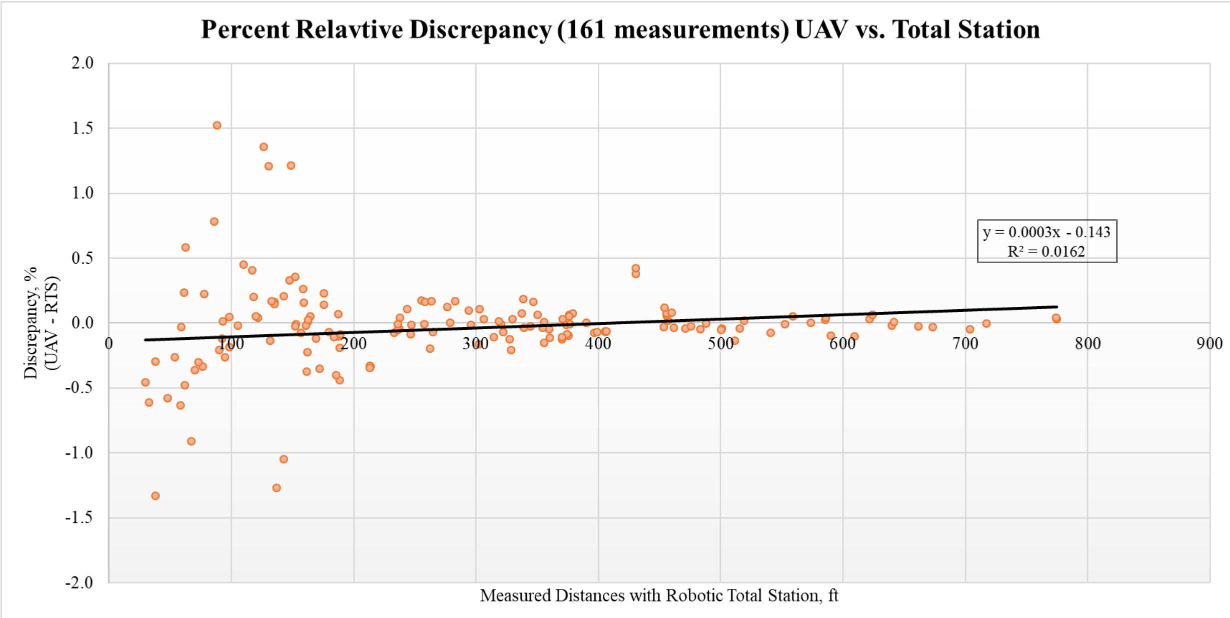

Figure H.5: Graph – Percent Relative Discrepancy of 161 Measurements (UAV versus Total Station)

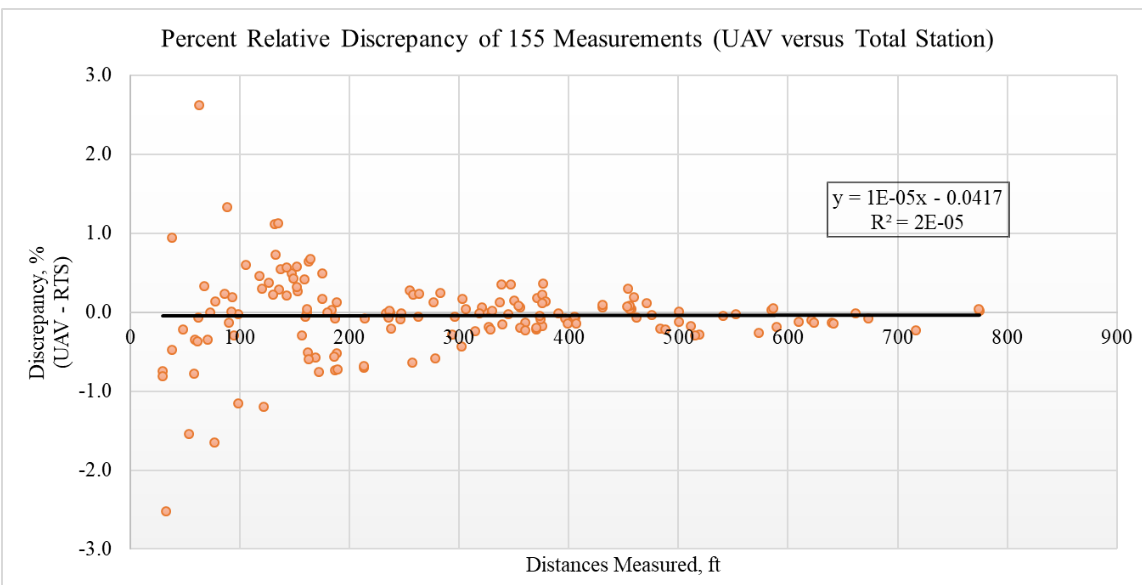

Figure H.6: Graph – Percent Relative Discrepancy with Recommended Accuracy Setting from Cultural Heritage Imaging (2015)

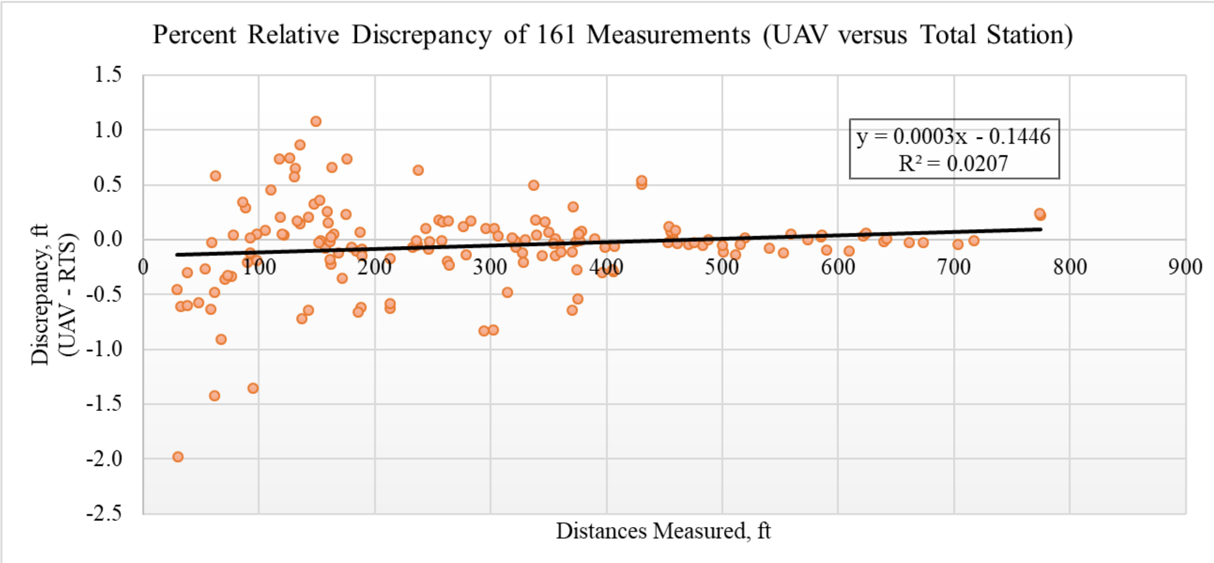

Figure H.7: Graph – Percent Relative Discrepancy with Recommended Camera Alignment Optimization from Agisoft PhotoScan (2017)

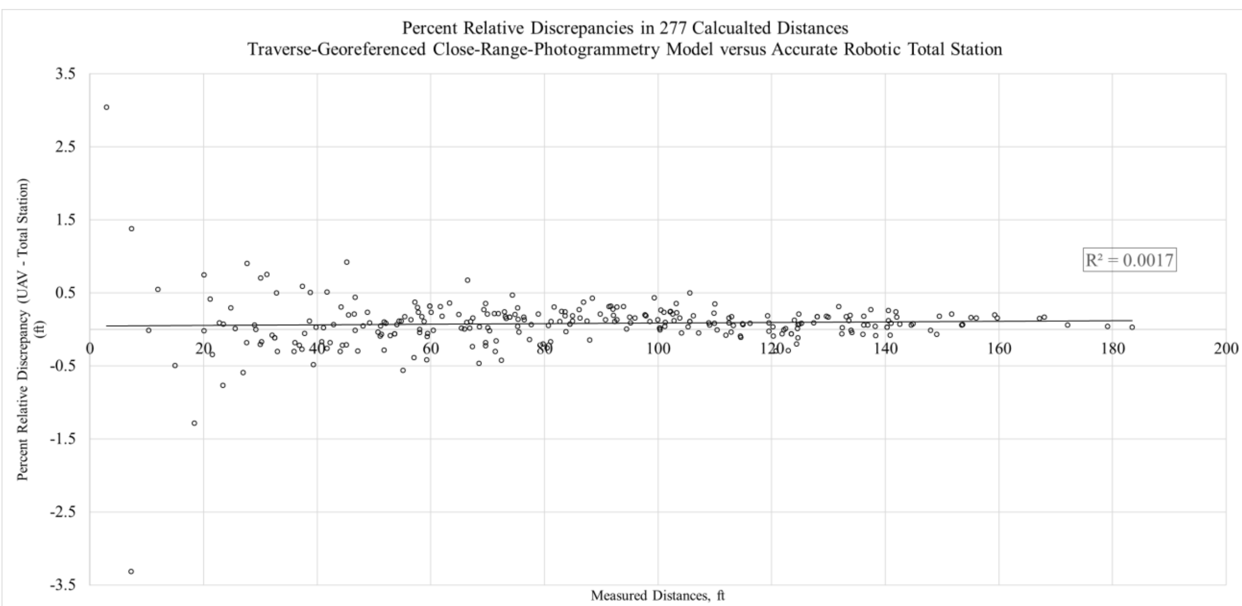

Figure H.8: Graph – Percent Relative Discrepancy in 277 Calculated Distances Traverse-Georeferenced Close-Range Photogrammetry Model versus Accurate Robotic Total Station (Building Structure with Parking Lot Infrastructure and Topography)